

NAVAL POSTGRADUATE SCHOOL Monterey, California



THESIS

DTIC QUALITY INSPECTED 4

**A SENSITIVITY STUDY OF NUMERICAL SOLUTIONS OF
THE SOUTH CHINA SEA OCEAN MODEL TO VARIOUS
GRIDS GENERATED BY GRID GENERATION
TECHNIQUE**

by

Vinh X. Tran

December 1995

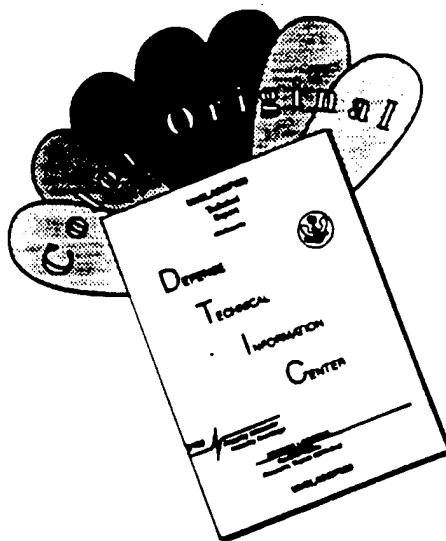
Thesis Advisor:
Second Reader:

Le N. Ly
Max F. Platzer

Approved for public release; distribution is unlimited.

19960328 049

DISCLAIMER NOTICE



THIS DOCUMENT IS BEST QUALITY AVAILABLE. THE COPY FURNISHED TO DTIC CONTAINED A SIGNIFICANT NUMBER OF COLOR PAGES WHICH DO NOT REPRODUCE LEGIBLY ON BLACK AND WHITE MICROFICHE.

REPORT DOCUMENTATION PAGE

Form Approved
OMB No. 0704-0188

Public reporting burden for this collection of information is estimated to average 1 hour per response, including the time reviewing instructions, searching existing data sources gathering and maintaining the data needed, and completing and reviewing the collection of information. Send comments regarding this burden estimate or any other aspect of this collection of information, including suggestions for reducing this burden to Washington Headquarters Services, Directorate for Information Operations and Reports, 1215 Jefferson Davis Highway, Suite 1204, Arlington, VA 22202-4302, and to the Office of Management and Budget, Paperwork Reduction Project (0704-0188), Washington, DC 20503.

1. AGENCY USE ONLY (Leave Blank)		2. REPORT DATE December 1995	3. REPORT TYPE AND DATES COVERED Master's Thesis	
4. TITLE AND SUBTITLE A SENSITIVITY STUDY OF NUMERICAL SOLUTIONS OF THE SOUTH CHINA SEA OCEAN MODEL TO VARIOUS GRIDS GENERATED BY GRID GENERATION TECHNIQUE(U)			5. FUNDING NUMBERS	
6. AUTHOR(S) Tran, Vinh X.				
7. PERFORMING ORGANIZATION NAME(S) AND ADDRESS(ES) Naval Postgraduate School Monterey, CA 93943-5000			8. PERFORMING ORGANIZATION REPORT NUMBER	
9. SPONSORING/ MONITORING AGENCY NAME(S) AND ADDRESS(ES)			10. SPONSORING/ MONITORING AGENCY REPORT NUMBER	
11. SUPPLEMENTARY NOTES The views expressed in this thesis are those of the author and do not reflect the official policy or position of the Department of Defense or the United States Government.				
12a. DISTRIBUTION / AVAILABILITY STATEMENT Approved for public release; distribution is unlimited.			12b. DISTRIBUTION CODE	
13. ABSTRACT (Maximum 200 words) The sensitivity of numerical solutions of systems of nonlinear flow equations (Navier-Stokes equations) to the grid used is investigated through the use of the South China Sea (SCS) numerical ocean model. Traditionally, rectangular coordinate grids are used in environmental modeling. The advantage of rectangular coordinate grids is their simplicity in the generation process. However, rectangular coordinate grids are not well suited for regions with complex terrain (coastlines and topography) and occasionally lead to poor accuracy in numerical solutions. The grid generation techniques are being introduced to coastal ocean modeling to study the sensitivity of numerical solutions to the grid used and to investigate the enhancement of the modeling process. Grid generation techniques are broadly used in aeronautical engineering community for solving CFD problems. One orthogonal (121x191) and two curvilinear nearly-orthogonal grids (121x191 and 151x241) are designed to couple with the SCS numerical ocean model. The grids are designed using the EAGLEView grid generation code developed by the National Science Foundation (NSF) Engineering Research Center (ERC) of Mississippi State University. EAGLEView implements a grid generation technique using mainly elliptic and algebraic generation systems. The designed grids are processed with the SCS numerical ocean model for 200 days to study the sensitivity of numerical solutions to the grid used. The solutions of the temperature and salinity fields are presented and analyzed. The advantages of curvilinear nearly-orthogonal grids are also discussed.				
14. SUBJECT TERMS Grid Generation Techniques, EAGLEView, EAGLE Grid Generation System, Sensitivity of Numerical Solutions, Coastal Ocean Modeling.			15. NUMBER OF PAGES 86	
			16. PRICE CODE	
17. SECURITY CLASSIFICATION OF REPORT Unclassified	18. SECURITY CLASSIFICATION OF THIS PAGE Unclassified	19. SECURITY CLASSIFICATION OF ABSTRACT Unclassified	20. LIMITATION OF ABSTRACT UL	

Approved for public release; distribution is unlimited

**A SENSITIVITY STUDY OF NUMERICAL SOLUTIONS OF THE SOUTH
CHINA SEA OCEAN MODEL TO VARIOUS GRIDS GENERATED BY GRID
GENERATION TECHNIQUE**

Vinh X. Tran
Lieutenant, United States Navy
B.S., University of Oklahoma, 1988

Submitted in partial fulfillment of the
requirements for the degree of

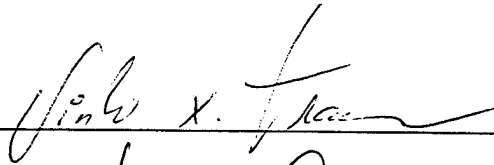
MASTER OF SCIENCE IN AERONAUTICAL ENGINEERING

from the

NAVAL POSTGRADUATE SCHOOL

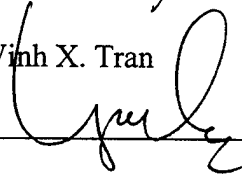
December 1995

Author:

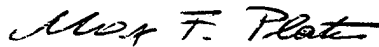


Vinh X. Tran

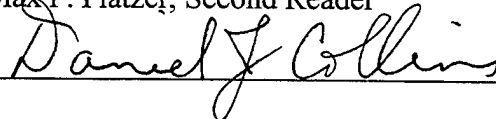
Approved by:



Le N. Ly, Thesis Advisor



Max F. Platzer, Second Reader



Daniel J. Collins, Chairman,
Department of Aeronautics and Astronautics

ABSTRACT

The sensitivity of numerical solutions of systems of nonlinear flow equations (Navier-Stokes equations) to the grid used is investigated through the use of the South China Sea (SCS) numerical ocean model. Traditionally, rectangular coordinate grids are used in environmental modeling. The advantage of rectangular coordinate grids is their simplicity in the generation process. However, rectangular coordinate grids are not well suited for regions with complex terrain (coastlines and topography) and occasionally lead to poor accuracy in numerical solutions. The grid generation techniques are being introduced to coastal ocean modeling to study the sensitivity of numerical solutions to the grid used and to investigate the enhancement of the modeling process. Grid generation techniques are broadly used in the aeronautical engineering community for solving CFD problems.

One orthogonal (121x191) and two curvilinear nearly-orthogonal grids (121x191 and 151x241) are designed to couple with the SCS numerical ocean model. The grids are designed using the EAGLEView grid generation code developed by the National Science Foundation (NSF) Engineering Research Center (ERC) of Mississippi State University. EAGLEView implements a grid generation technique using mainly elliptic and algebraic generation systems. The designed grids are processed with the SCS numerical ocean model for 200 days to study the sensitivity of numerical solutions to the grid used. The solutions of the temperature and salinity fields are presented and analyzed. The advantages of curvilinear nearly-orthogonal grids are also discussed.

TABLE OF CONTENTS

I.	INTRODUCTION	1
A.	GENERAL REMARKS.....	1
B.	GRID GENERATION	2
C.	THE STUDY OF NUMERICAL SOLUTIONS	5
II.	GRID GENERATION SYSTEM-THE EAGLEVIEW CODE.....	7
A.	GENERAL OVERVIEW.....	7
B.	ELLIPTIC GENERATION SYSTEM.....	8
III.	SCS NUMERICAL OCEAN MODEL.....	13
A.	BASIC MODEL EQUATIONS.....	13
B.	MODEL INITIALIZATION.....	17
IV.	NUMERICAL SIMULATIONS.....	19
A.	GRID DESIGN	19
B.	ANALYSIS OF NUMERICAL SOLUTIONS.....	23
1.	Salinity Field.....	24
2.	Temperature Field.....	25
V.	DISCUSSION AND CONCLUSION	27
	LIST OF REFERENCES.....	29
	APPENDIX A: SALINITY FIELD SOLUTIONS.....	31
	APPENDIX B: TEMPERATURE FIELD SOLUTIONS	53
	INITIAL DISTRIBUTION LIST	75

ACKNOWLEDGEMENTS

The author would like to express a sincere appreciation to the author's advisor Dr. Le N. Ly for his guidance and patience during the effort of performing this research. The author is also thankful to Dr. Max F. Platzer for his support and interest in the project. Special thanks to Dr. Phu Luong of NAVOCEANO, Stennis Space Center, MS for his assistance in EAGLEView and data visualizations.

I. INTRODUCTION

A. GENERAL REMARKS

The advent of supercomputers with high computing speed and large core memories has allowed the majority of unsolved problems in Fluid Dynamics to be treated numerically. Complex problems can now be solved in a few seconds of computer time with very little cost which would have taken years of work with computational methods and computers available twenty years ago. As a consequence, a new method termed computational fluid dynamics (CFD) has become available for attacking complicated problems in systems of non-linear partial differential equations. This method has permitted advanced simulations of flow phenomena for a variety of applications. The areas range from aircraft and missile design to large-scale simulations of the atmosphere and the ocean. The numerical solutions of the fluid flow equations have progressed to the point of finite-difference (or finite-volume) approximation about arbitrary and complex geometries with reliable and predictable accuracy. Similar advances are also emerging in hydrodynamics, electromagnetism, magnetohydrodynamics, heat and mass transfer and, to some degree, in all field problems.

The traditional experimental and theoretical approaches remain important in engineering design for systems involving fluid and heat flow equations. However, the trend is clearly toward greater reliance on computer based predictions in the design process. This trend can be largely explained by the effect of a rapidly developing digital computer industry and a relatively low cost of utilizing these machines. The cost of performing a

given calculation has been significantly reduced in the last decade and is expected to be steadily declining for some time into the future.

Contrarily, the experimentation costs have been significantly increased in recent years. The construction of complex models and wind tunnel facilities to match realistic flow conditions has elevated the cost every day. The increasing energy cost to operate the wind tunnels is also contributing to the mounting expense of the experimental approach. However, the experimental approach still remains the best method of representing the most realistic solutions for many complex flow problems.

On the other hand, the theoretical approach is the most inexpensive method to solve flow problems. The difficulty with the theoretical approach is that simplifying assumptions are made and the problems are restricted to simple geometries and physics. One significant advantage of the theoretical approach is that reasonable answers can be obtained in a minimum amount of time and this is quite useful in preliminary design work. In closing, the computational approach is judged to be the most efficient method for treating systems of non-linear flow equations (Navier-Stokes equations) at the present time.

B. GRID GENERATION

A vital element of computing numerical solutions for systems of non-linear flow equations is the discretization of the physical field into a collection of points or elemental volumes (cells) on which to represent the flow equations in finite form. The application of finite mathematical techniques to acquire this essential measure is called grid generation. A grid which is not well suited to the problem can lead to unsatisfactory results. In some

applications, improper choice of grid point locations can also lead to model instability or lack of convergence in numerical solutions [1]. A well constructed grid can greatly simplify solutions of systems of non-linear fluid flow equations and subsequently reduce computing time and the cost of performing the calculation.

Grid generation is a construction process which must accommodate the characteristic of the governing equations and the geometry of the physical domain. The governing equations are defined in a physical coordinate system and are then transformed to an idealized rectangular computational domain. This situation is illustrated in Figure 1. In simple terms, grid generation is a procedure for the orderly distribution of observers over a physical field in such a way that efficient communication between observers is possible and all physical phenomena on the entire continuous field may be represented with sufficient accuracy by this finite collection of observations [2]. Hence, the representation of the physical phenomena on the continuous field is strongly dependent on the distribution of these observers. This implies that numerical solutions of nonlinear flow equations is heavily affected by the distribution of the grid points.

Grid generation about complex configurations is considered as a major pacing factor for the ability to obtain numerical solutions of non-linear partial differential equations. There are generally three available methods to generate numerical grids: (1) complex variable method, (2) algebraic method, and (3) differential equation method based on the solution of a set of partial differential equations [1]. The first method has the advantage of analyzing or partially analyzing the transformations that are being used as

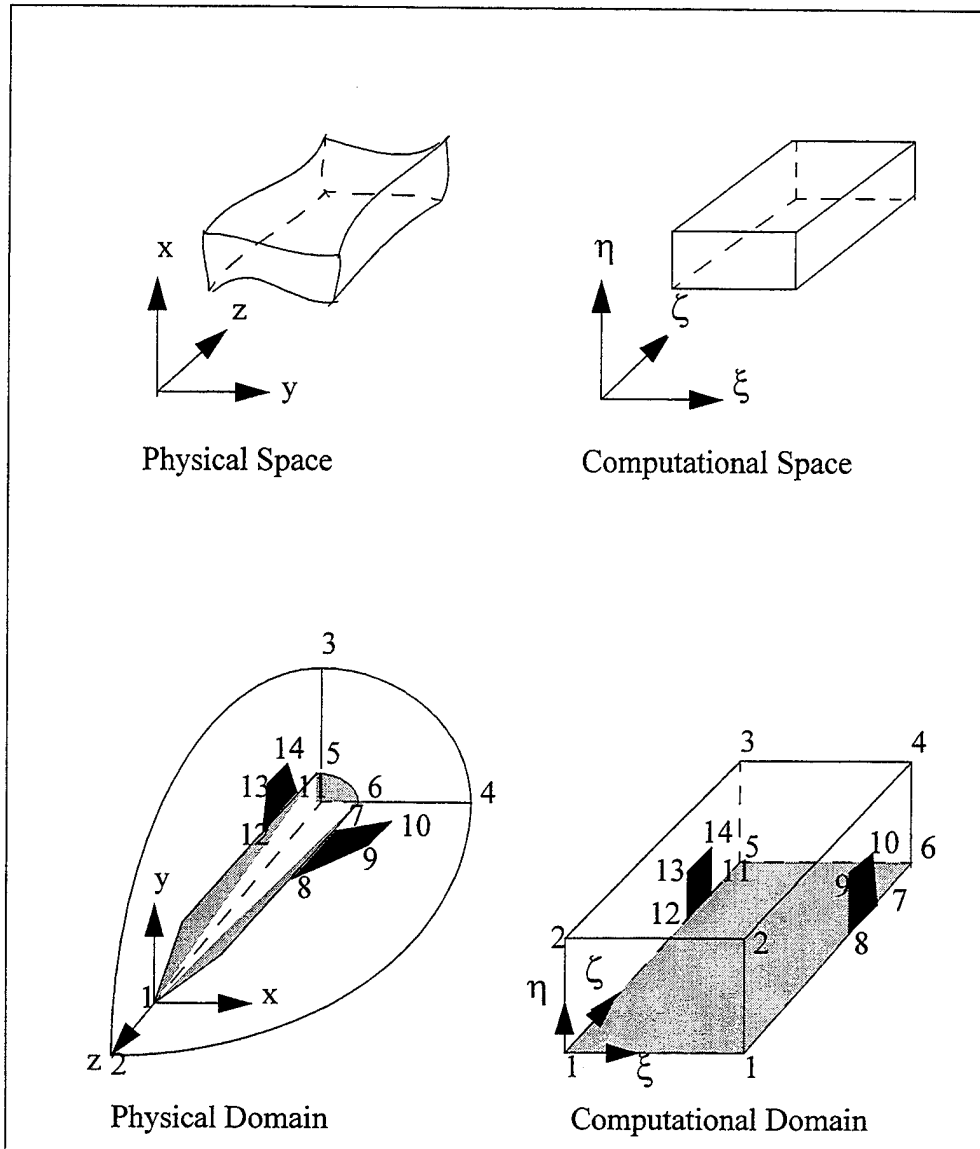


Figure 1: Physical domain and computational domain [3]

opposed to the other two methods that are entirely numerical. Unfortunately, this method is restricted solely to two dimensions and therefore, it is uncommonly used. The second method is based on the interpolation or approximation among boundaries and intermediate surfaces in the field. The last method, in which the coordinates are the solution of partial

differential equations, may be elliptic, parabolic, or hyperbolic. Several major grid generation codes, such as EAGLEView, GENIE ++, INGRID, GRAPE, and GRIDGEN, are presently available for use to generate grids on complex configurations. The techniques of numerical grid generation and its applications are thoroughly covered in reference [4].

C. THE STUDY OF NUMERICAL SOLUTIONS

The intent of this thesis is to study the sensitivity of numerical solutions of systems of nonlinear flow equations due to grid utilization. The study involved the design of an orthogonal and two curvilinear nearly-orthogonal grids which were used in conjunction with the South China Sea (SCS) numerical ocean model. The grids were designed using the EAGLEView code which was developed by the National Science Foundation (NSF) Engineering Research Center (ERC) for Computational Field Simulation of Mississippi State University. The SCS numerical ocean model was developed at the Naval Postgraduate School (NPS) based on the Princeton Ocean Model (POM) [5]. The sensitivity of numerical solutions of the SCS model due to the design of the three grids is the scope of this study. The advantages and disadvantages of orthogonal and curvilinear grids will also be discussed.

Traditionally, rectangular coordinate grids have been commonly used in environmental modeling. The advantage of rectangular coordinate grids is their simplicity in the generation process. However, open boundary conditions are poorly represented numerically with rectangular coordinate grids. This is especially true for regions with complex terrain even when treated with very high resolution. Rectangular coordinate grids

also lack the ability to follow the coastlines and eliminate apathetic regions of the domain. This has resulted in an unnecessary expense of computing resources in regions of apathy and inaccurate numerical solutions in regions of interest. On the other hand, the curvilinear nearly-orthogonal grids have the ability to enhance the numerical solutions by better treatment of coastlines and boundary conditions and still remain within realistic computational resources. The curvilinear grids also have the ability to increase resolution in the subregion of the model domain without increasing computational expenses. The grid generation technique has been widely used in the aerospace community and the introduction of its application to the oceanography community has created a new direction in coastal ocean modeling [6,7].

II. GRID GENERATION SYSTEM-THE EAGLEVIEW CODE

A. GENERAL OVERVIEW

The EAGLEView grid code is a general three-dimensional grid generation code based on a composite block structure. The code was developed by the NSF Engineering Research Center for Computational Field Simulation of Mississippi State University. The code can be operated either as an algebraic generation system or as an elliptic generation system. The code can also be operated in two or three dimensions on a plane or on a curved surface. In the case of a curved surface, the surface is splined and the generation is done in terms of surface parametric coordinates. The input of the code is structured to be user-friendly oriented and arbitrary block configurations can be treated. The EAGLEView code was developed with the intention of reducing the time expended to generate the grids for engineering designs and analysis in computational field simulation.

The EAGLEView grid code permits an arbitrary three-dimensional region to be filled with a number of blocks. The number of blocks can be varied depending on the discretion of the user. The blocks are linked to each other with continuity across the interfaces. The code uses an elliptic generation system with automatic evaluation of the control functions. The evaluation of the control functions is completed either directly from the initial algebraic grid and then smoothed, or by interpolation from the boundary-point distributions. In the former case, the relative spacing of the grids is done by the algebraic system and the smoothing of the grid is done by the elliptic system. In the latter case, the arc length and the curvature contributions to the control functions are evaluated and

interpolated separately into the field from the appropriate boundaries. The control function at each point in the field is then formed by combining the interpolated elements.

The control functions can also be automatically determined to provide orthogonality at boundaries with specified normal spacing. In this case, the iterative adjustments in the control functions are made by increments radiated from boundary points where orthogonality has not yet been attained. This allows the basic control function structure evaluated from the algebraic grid, or from the boundary-point distributions, to be retained and thus relieves the iterative process from the need to establish this basic form of the control functions.

The generation of the initial solution to start the iterative process of the elliptic generation system is done by the three-dimensional algebraic system which is based on transfinite interpolation (using either Lagrange or Hermite interpolation) [4]. This feature permits the code to be run as an algebraic generation system if desired. The interpolation is defaulted to complete transfinite interpolation from all boundaries; however, it can be restricted by input to any combination of directions or lesser degree of interpolation. The mathematical techniques of grid generation that are applicable to the EAGLEView grid code are discussed in detail in references [4,8].

B. ELLIPTIC GENERATION SYSTEM

The properties of the elliptic generation system is based on the derivation of the Laplace or Poisson equations. The Laplace system is the most simple elliptic partial differential system and one that produces the smoothest possible grid; however, the

coordinate lines in the interior of the field tend to be equally spaced regardless of how the boundary points are spaced. This is caused by the strong smoothing effect of the Laplacian system. On the other hand, the Poisson system can provide control of the coordinate line spacing in the field to match with that of the boundaries.

The elliptic grid generation technique used in the EAGLEView grid code is derived from the Poisson equations

$$\nabla^2 \xi^i = P^i \quad (i = 1, 2, 3) \quad \text{Eq 1}$$

where the functions, P^i are the “control functions” which can be fashioned to control the spacing and orientation of coordinate lines.

Reference [4] reveals that if a curvilinear coordinate system, $\xi^i (i = 1, 2, 3)$, which satisfies the Laplace system, $\nabla^2 \xi^i = 0 (i = 1, 2, 3)$, is transformed to another coordinate system, $\xi^i (i = 1, 2, 3)$, then the new curvilinear coordinates, ξ^i , will satisfy the inhomogeneous elliptic system as defined by (Eq 1) with the control functions

$$P^i = \sum_{j=1}^3 \sum_{k=1}^3 g^{jk} P_{jk}^i \quad (i = 1, 2, 3) \quad \text{Eq 2}$$

where P_{jk}^i defined the transformation from ξ^i to ξ^i ,

$$P_{jk}^i = \sum_{m=1}^3 \sum_{n=1}^3 \frac{\partial \xi^m}{\partial \xi^j} \frac{\partial \xi^n}{\partial \xi^k} \frac{\partial^2 \xi^i}{\partial \xi^m \partial \xi^n} \quad \text{Eq 3}$$

and

$$g^{jk} = \nabla_{\xi^j} \cdot \nabla_{\xi^k} = \frac{1}{g} (g_{jm} g_{kn} - g_{jn} g_{km}) \quad \text{Eq 4}$$

with $(i, j, h), (k, m, n)$ cyclic, is the contravariant metric tensor.

$g = \det|g_{ij}| = \hat{r}_{\xi^1} \cdot (\hat{r}_{\xi^2} \times \hat{r}_{\xi^3})$ is the square of the Jacobian of the transformation, and

$g_{ij} = \hat{r}_{\xi^i} \cdot \hat{r}_{\xi^j}$ are the elements of the covariant metric tensor. In these relations,

$\hat{r} = x\hat{i} + y\hat{j} + z\hat{k}$ is the position vector of the grid point in the Cartesian coordinates, and

$\xi^i (i = 1, 2, 3)$ are the three new curvilinear coordinates.

These results reveal that a coordinate system obtained by subsequent transformation (often called “stretching” transformation) from one generated as the solution of the Laplace system can be solved directly as the solution of the Poisson system, (Eq 1), with appropriate control functions, P_{jk}^i , as defined by (Eq 3). Therefore, the Poisson system can be adopted as the appropriate generation system with the control functions specified directly rather than through a subsequent transformation. Thus, the appropriate generation system can be defined by the combination of (Eq 1) and (Eq 2)

$$\nabla^2 \xi^i = \sum_{j=1}^3 \sum_{k=1}^3 g^{jk} P_{jk}^i \quad (i = 1, 2, 3) \quad \text{Eq 5}$$

The basis of (Eq 5) is that it produces a coordinate system that corresponds to the subsequent application of a stretching transformation from a coordinate system generated for maximum smoothness. In (Eq 3), the three control functions, $P_{ii}^i (i = 1, 2, 3)$, correspond to one-dimensional stretching in each coordinate direction and are the most

important of the control functions. The other control functions are taken to be zero, i.e.

$P_{jk}^i = \delta_j^i \delta_k^i P_i$. Thus, the generation system becomes

$$\nabla_{\xi}^2 g^{ii} P_i \quad (i = 1, 2, 3) \quad \text{Eq 6}$$

Further transformation of (Eq 6) yields

$$\sum_{i=1}^3 \sum_{j=1}^3 g^{ij} \ddot{P}_{\xi^i \xi^j} + \sum_{k=1}^3 g^{kk} P_k \ddot{P}_{\xi^k} = 0 \quad \text{Eq 7}$$

which is the elliptic generation system equation that is used in the EAGLEView grid code.

The control functions P_k are used to control the spacing and orientation of gridlines in the interior of the field. Procedures for the determination of these control functions such that (Eq 7) reflects the spacing of an algebraic grid or the boundary point spacing in the field are specifically discussed in reference [8].

III. SCS NUMERICAL OCEAN MODEL

A. BASIC MODEL EQUATIONS

The South China Sea (SCS) numerical ocean model was developed at the Naval Postgraduate School (NPS) based on the Princeton Ocean Model (POM) [5]. The POM was originally created at Princeton University in 1977 for application to oceanographic problems. Many subsequent contributions to the model were made throughout the years by various scientists and researchers from the Atmospheric and Oceanic Sciences community [9].

The model is a three-dimensional, primitive equation, ocean circulation numerical model with realistic coastlines, topography and complete thermodynamics. The model also includes an upper free surface and 16 vertical levels of sigma coordinate. A detailed description of the model is given in reference [10]. The sigma coordinate system is illustrated in Figure 2 and is defined by the equation

$$\sigma = \frac{z - \eta(x, y, t)}{H(x, y) + \eta(x, y, t)} \quad \text{Eq 8}$$

where $H(x, y)$ is the bottom topography and $\eta(x, y, t)$ is the free surface elevation. Thus, σ ranges from $\sigma = 0$ at $z = \eta$ to $\sigma = -1$ at $z = -H$. The coordinates (x, y, z) represent the conventional cartesian coordinates with x in the easterly direction, y in the northerly direction and z is normal to the surface pointing upward.

References [11,12,13] indicate that the velocity, surface elevation, salinity and temperature fields of the ocean are described by the following equations

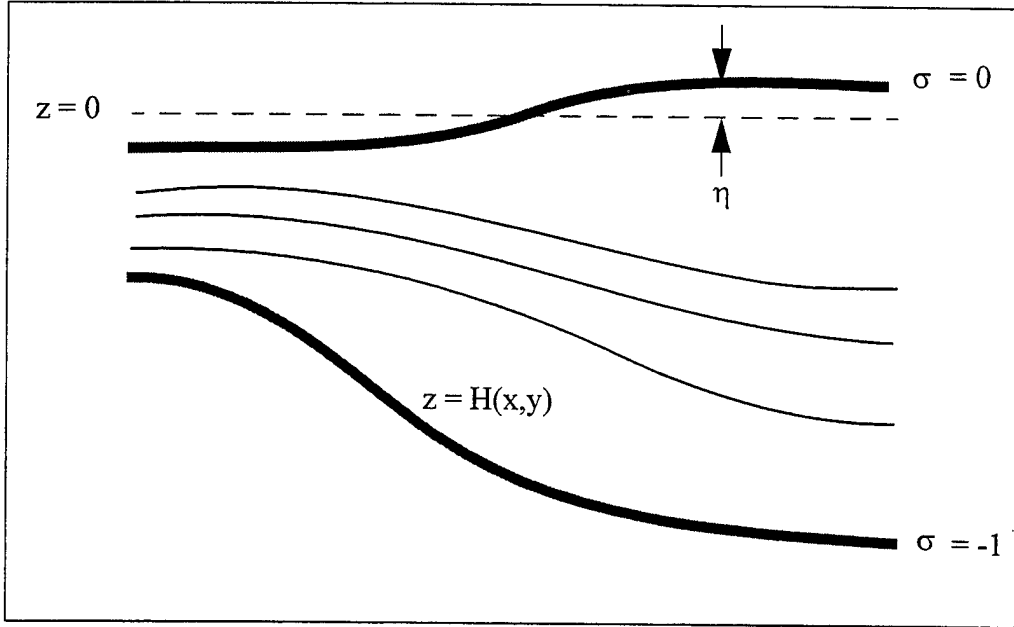


Figure 2: The sigma coordinate system [9]

$$\frac{\partial \vec{V}}{\partial t} + \vec{V} \cdot \nabla \vec{V} + W \frac{\partial \vec{V}}{\partial z} + 2\vec{\Omega} \times \vec{V} = -\frac{1}{\rho_o} \nabla P + \frac{\partial}{\partial z} \left(K_m \frac{\partial \vec{V}}{\partial z} \right) + \vec{F} \quad \text{Eq 9}$$

$$\frac{\partial P}{\partial z} = -\rho g \quad \text{Eq 10}$$

$$\nabla \cdot \vec{V} + \frac{\partial W}{\partial z} = 0 \quad \text{Eq 11}$$

$$\frac{\partial \theta_i}{\partial t} + \vec{V} \cdot \nabla \theta_i + W \frac{\partial \theta_i}{\partial z} = \frac{\partial}{\partial z} \left(K_h \frac{\partial \theta_i}{\partial z} \right) + F_{\theta_i} \quad \text{Eq 12}$$

where

\vec{V} : horizontal velocity vector with components (U, V)

W : vertical velocity

∇ : horizontal gradient operator

P : pressure

ρ_o : reference density

g : gravitational acceleration

$\rho = \rho_\theta(\theta, S)$: in situ density in general form computed by using the equation of state

$2\vec{\Omega} \times \vec{V}$: Coriolis force with $\vec{\Omega}$ as the earth rotation vector

K_m, K_h : vertical turbulence exchange coefficients for momentum, heat & salt

θ_i : mean potential temperature

\vec{F}, F_{θ_i} : horizontal mixing terms

The horizontal mixing terms $\vec{F}(F_x, F_y)$ in (Eq 9) and F_{θ_i} in (Eq 12) can be written

as follow

$$F_x = \frac{\partial}{\partial x} \left(2A_m \frac{\partial U}{\partial x} \right) + \frac{\partial}{\partial y} \left[A_m \left(\frac{\partial U}{\partial y} + \frac{\partial V}{\partial x} \right) \right] \quad \text{Eq 13}$$

$$F_y = \frac{\partial}{\partial y} \left(2A_m \frac{\partial V}{\partial y} \right) + \frac{\partial}{\partial x} \left[A_m \left(\frac{\partial U}{\partial y} + \frac{\partial V}{\partial x} \right) \right] \quad \text{Eq 14}$$

$$F_{\theta_i} = \frac{\partial}{\partial x} \left(A_h \frac{\partial \theta_i}{\partial x} \right) + \frac{\partial}{\partial y} \left(A_h \frac{\partial \theta_i}{\partial y} \right) \quad \text{Eq 15}$$

where A_m, A_h are the horizontal turbulent exchange coefficients for momentum and heat, respectively [10].

The vertical turbulent mixing terms, K_m, K_h , in the momentum conservation equation (Eq 9) and the diffusion equation (Eq 12) are determined by a second order

turbulence closure scheme. The turbulent closure scheme is characterized by the turbulent kinetic energy (TKE), $q^2/2$, and the turbulent mixing length, l . Thus, both of the turbulent equations can be written in the same form by the following equation

$$\frac{\partial Q_i}{\partial t} + \vec{V} \cdot \nabla Q_i + \tilde{W} \frac{\partial Q_i}{\partial z} = \frac{\partial}{\partial z} \left(K_q \frac{\partial Q_i}{\partial z} \right) + K_{mQ} \left[\left(\frac{\partial U}{\partial z} \right)^2 + \left(\frac{\partial V}{\partial z} \right)^2 \right] + K_{hQ} \frac{g}{\rho_o} \frac{\partial \rho}{\partial z} - K_{hQ} \frac{q^3}{B_1} + F_Q \quad \text{Eq 16}$$

where Q_i is either $q^2/2$ for TKE or $q^2 l$ for the turbulent mixing length. When

$$Q_i = q^2/2,$$

$$K_{mQ} = 2K_m; K_{hQ} = 2K_h; K_Q = 2/l; F_Q = F_q \quad \text{Eq 17}$$

and when $Q_i = q^2 l$,

$$K_{mQ} = lE_1 K_m; K_{hQ} = lE_1 K_h; K_Q = \tilde{W}; F_Q = F_l \quad \text{Eq 18}$$

The term \tilde{W} in (Eq 18) is the “wall proximity” function. In (Eq 16), the first term on the right hand side represents diffusion, the second two terms are shear production, followed by buoyancy, dissipation, and the last term models horizontal mixing [11,13]. The vertical turbulent exchange coefficients (TEC) K_m, K_h, K_q in the above equations are defined as follows

$$K_m = lqS_m; K_h = lqS_h; K_q = lqS_q \quad \text{Eq 19}$$

where S_m, S_h, S_q are the stability functions and are given in reference [14].

The model assumed that the ocean is hydrostatic and incompressible (Boussinesq approximation). Wind stress, heat, and salinity fluxes are prescribed at the free surface where $z = \eta(x, y)$. Zero heat and salinity fluxes are designated at the bottom where $z = -H(x, y)$. The condition of no diffusive fluxes of any property across the interface is used at land boundaries. The condition of mode splitting of the external (barotropic) and internal (baroclinic) modes is imposed in the model to enhance computer resources [11,13].

B. MODEL INITIALIZATION

The model is initialized with 10 seconds time step for the external (barotropic) mode and 400 seconds time step for the internal (baroclinic) mode to satisfy the Courant-Friedrichs-Levy (CFL) computational stability criterion. The bathymetry is obtained from the global ETOPO5 bathymetry dataset with 5' x 5' resolution and is interpolated to the grid of the model. The bathymetry is filtered to remove high frequency noise. The SCS model is simulated with close boundaries in order to simplify the modeling process and to strictly focus on the sensitivity study of numerical solutions due to grid usage. The model is also initialized with Levitus salinity and temperature climatology [15]. The annual salinity and temperature fields from the Levitus dataset are interpolated into the model grids and spun up 30 days diagnostically (salinity and temperature fields held constant) prior to making the prognostic run.

IV. NUMERICAL SIMULATIONS

A. GRID DESIGN

One orthogonal grid (grid1) and two curvilinear nearly-orthogonal grids (grid2 and grid3) are designed to cover the entire domain of SCS. Grid1 (Figure 3) and grid2 (Figure 4) are created to have the same number of grid points ($121 \times 191 = 23,111$ points). Grid3 (Figure 5) is designed to have a much higher resolution of grid points ($151 \times 241 = 36,391$ points). The traditional rectangular grid, grid1, is completely overlaid on the SCS domain from $99^\circ - 121^\circ$ *East* longitude and from $0^\circ - 25^\circ$ *North* latitude. This produces a range resolution of approximately 20 km x 15 km for grid1. Grid2 and grid3 are designed to eliminate apathetic regions of the SCS domain as much as possible without causing the effect of skewness to the grids (grids are ineffective to model the flow equations if the level of skewness is too high). The average range resolution for grid2 is approximately 12 km x 15 km and for grid3 is approximately 10 km x 12 km. The subregions near the northern boundary, 25° *North* latitude, and the southern boundary, 0° latitude (the equator), of grid2 and grid3 have a higher horizontal resolution from east to west than the central part of the domain. The average range resolution for these subregions is approximately 7 km x 15 km for grid2 and 5 km x 12 km for grid3. This is one advantage of the curvilinear nearly-orthogonal grids, which allows the resolution of the subregions of the domain to be increased without increasing the matrix size of the whole domain.

The above designed grids are processed with the SCS numerical ocean model for 200 days to analyze the sensitivity of numerical solutions due to grid used. The temperature

South China Sea
Orthogonal Grid Model (121X191)
Coastlines

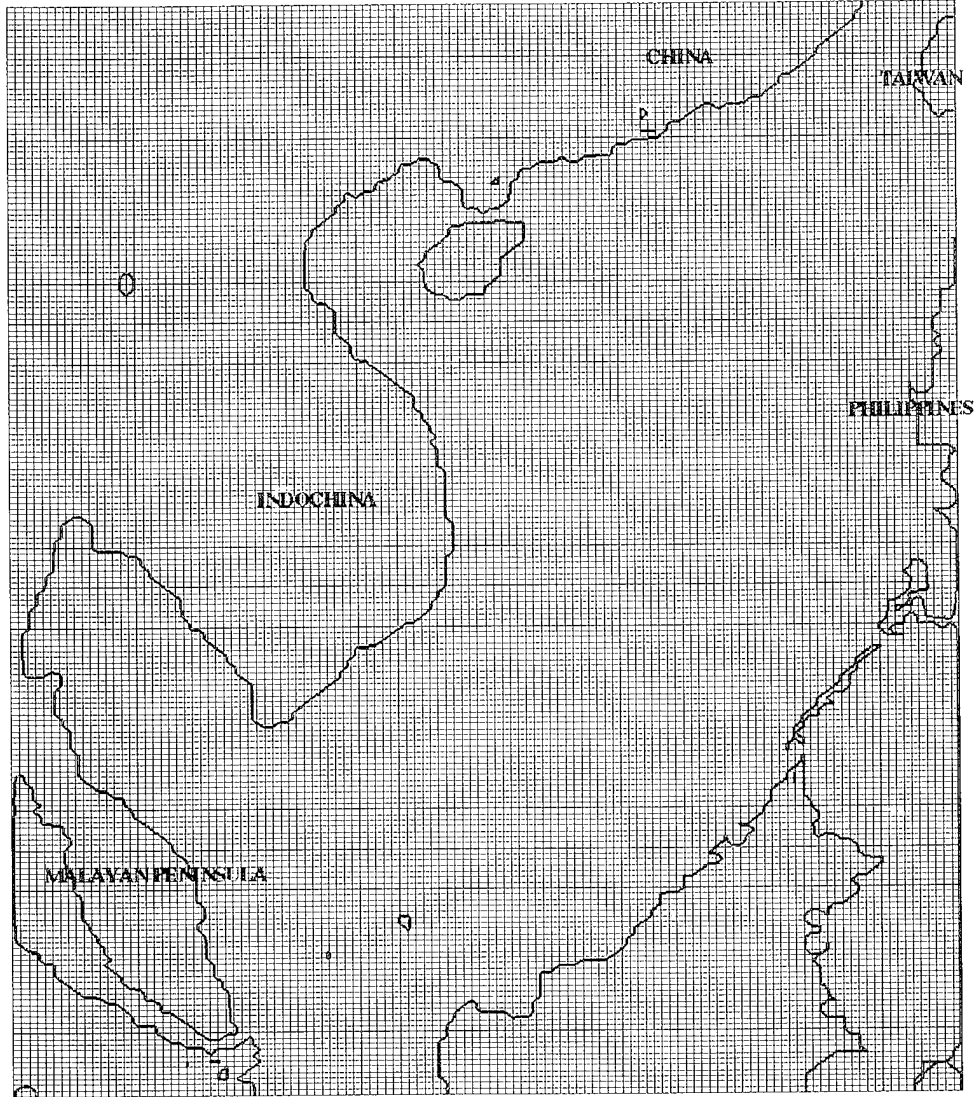


Figure 3: Grid 1

South China Sea

Nearly-orthogonal Grid Model (121X191)

Coastlines

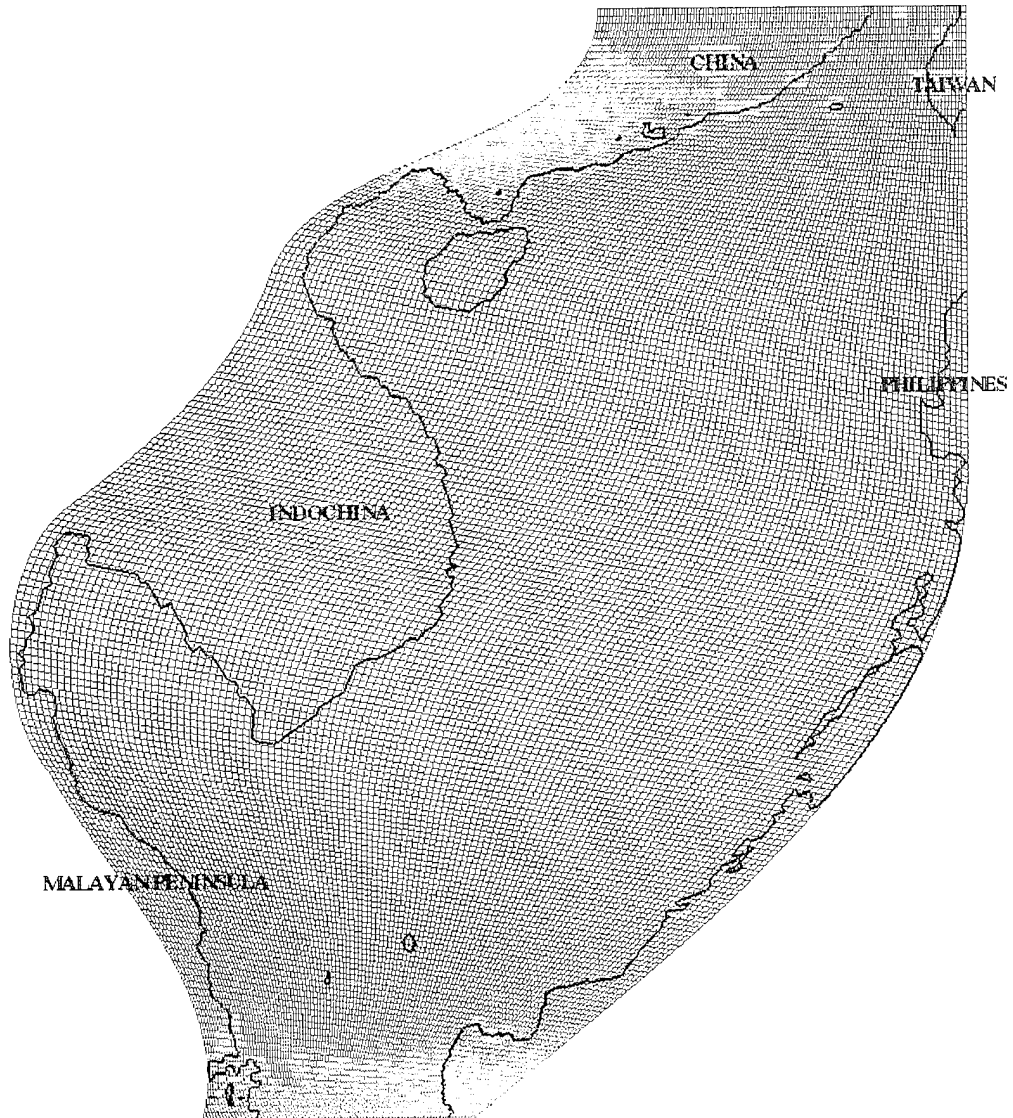


Figure 4: Grid2

South China Sea
Nearly-orthogonal Grid Model (151X241)
Coastlines

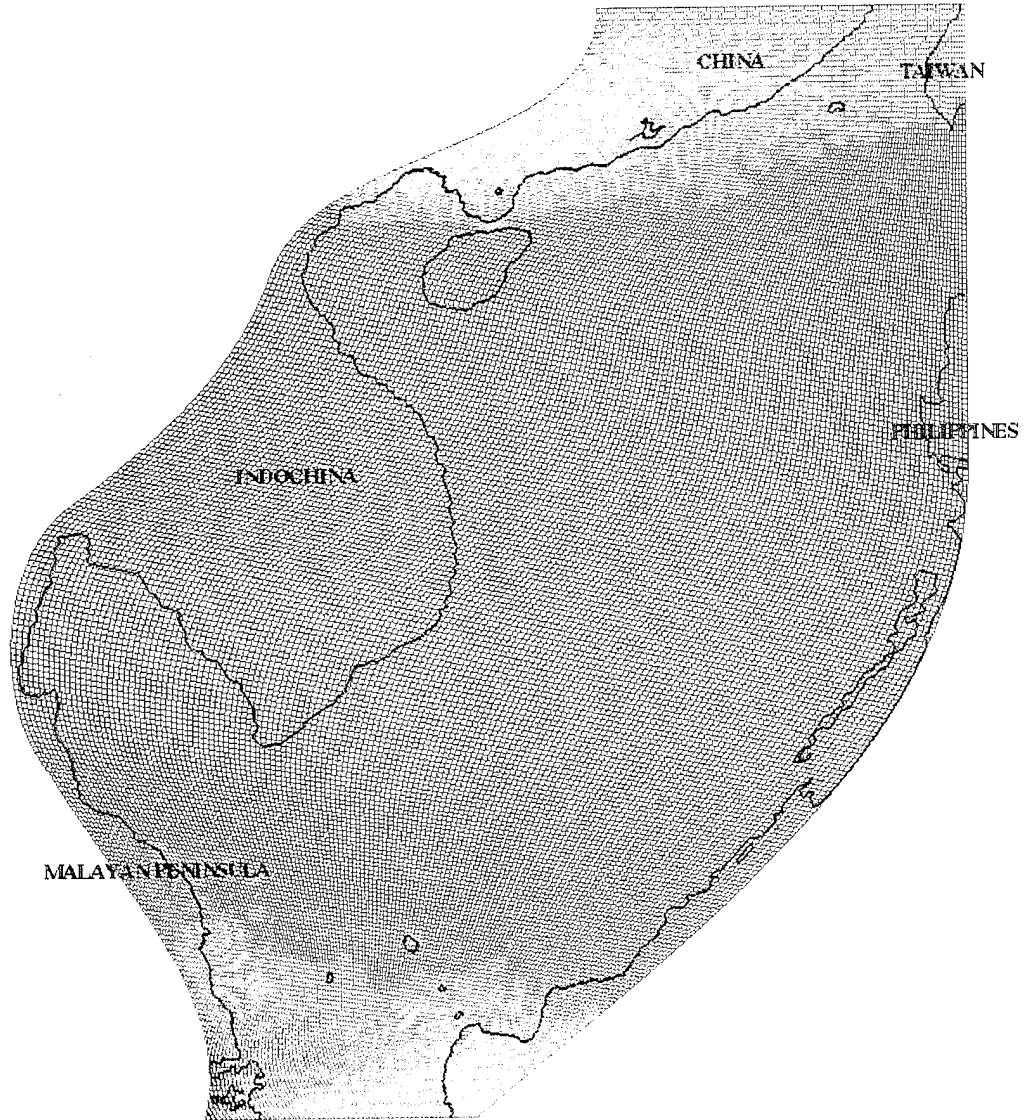


Figure 5: Grid3

and salinity fields of the model are initialized by reference [15]. The model is spun up for 30 days to obtain the initial solutions of temperature and salinity fields (0 days simulations). Subsequent solutions are obtained for 30 days, 50 days, 100 days, 150 days and 200 days respectively. The simulations are computed on the NPS CRAY-YMP supercomputer using multitasking modes with 8 CPU operated correspondingly. The numerical solutions of the higher resolution grid, grid3, are used as a reference for the true solutions. The numerical solutions of the surface temperature (sigma level 1) and salinity fields of the three grids (grid1, grid2 and grid3) are compared and analyzed. The solutions of sigma level 10 and level 15 are also obtained and compared for all three grids. The solutions of grid2 are expected to be closely related to the true solutions (i.e. solutions of grid3).

B. ANALYSIS OF NUMERICAL SOLUTIONS

The numerical solutions of the salinity and temperature fields are visualized by using the Flow Analysis Software Toolkit (FAST). FAST is a graphic software package developed at NASA Ames Research Center, Moffett Field, CA and is specifically designed for scientific visualization in computational field simulation. In the near future, a modified version of EAGLEView will be included as an integrated module in FAST to provide the researcher with a fully integrated system from the design process to system simulation and visualization [17,18,19,20]. The visualizations of the salinity and temperature fields for sigma level 1, 10 and 15 of the three grids are shown in Appendix A and B. Appendix A contains the simulations of the salinity field and Appendix B contains the simulations of the temperature field for 0 days, 100 days and 200 days respectively.

1. Salinity Field

The numerical solutions of the three grids (grid1, grid2 and grid3) for sigma level 1 (surface level), level 10 and level 15 are plotted to allow the visualization of the salinity field. The initial solutions (0 days simulations) of the surface level for all three grids are closely related (Figures A1, A2, A3). However, there are distinct differences in the flow pattern between the 200 day simulations of the three grids (Figures A4, A5, A6). The differences are more noticeable in the subregions near the northern boundary of the SCS domain where the salt density is high (~ 34.1 part per thousand - ppt) compared to other parts of the domain. The solution of grid2 is likely to resemble the solution of grid3 (Figures A5, A6). Contrarily, the solution of the traditional rectangular grid1 (Figure A4), is distinguished from the solutions of grid2 and grid3. The flow pattern of high salt density (~ 34.1 ppt) of grid1 falls short of the Hainan island while the same flow pattern of grid2 and grid3 extends beyond the island into the Gulf of Tonkin. The salinity flow patterns of the SCS central and southern region of the domain are also different. The magnifications of the northern region of the SCS domain for 0 days, 100 days and 200 days simulations are presented in Figures A7 to A15. Notice that the flow pattern of grid2 for the 100 day simulation also more closely resembles the true solution (solution of grid3) compared to the solution of grid1 (Figures A10, A11, A12).

The differences in these flow patterns between the solutions of the three grids are caused by the differences in the spatial distribution of the grid points (i.e. $\Delta x, \Delta y$). The curvilinear grids (grid2 and grid3) have a higher range resolutions ($\Delta x, \Delta y$) in regions of

interest than the traditional rectangular grid1 and this subsequently causes the sensitivities in numerical solutions between the three grids as discussed above.

The 200 day simulations of level 10 (Figures A16 to A18) and level 15 (Figures A19 to A21) are also magnified in the northwestern region of the domain to analyze the sensitivity of the salinity field below the sea surface. The solutions of grid1 are the most different from the solutions of grid2 and grid3 for both level 10 and level 15 as expected since grid1 has a much smaller range resolution than grid2 and grid3. The density of salinity along the coast of southeastern China is smaller for grid1(Figures A16, A19) compared to grid2 (Figures A17, A20) and grid3 (Figures A18, A21). The flow patterns inside the Gulf of Tonkin similar between grid2 and grid3. The density of the salinity field for this same flow pattern of grid1 is also smaller than for grid2 and grid3. These sensitivities in numerical solutions can also be explained by the differences in grid point distributions between the three grids as in the case of the surface level.

2. Temperature Field

The solutions of the temperature field are similarly plotted for all three sigma levels (level 1, 10 and 15). The initial surface temperatures (0 days simulations) for all three grids are very closely related as in the case of the salinity field (Figures B1, B2, B3). The simulations of the 200 day surface temperature field clearly show cold water mass (~ 22° C) flowing from the north into SCS (Figures B4, B5, B6). Similar to the salinity field, the flow pattern of these cold water masses extends deep into the domain of the SCS from east to west for grid2 and grid3 and falls short for grid1. The northern region of the domain is magnified for the solutions of 0 days, 100 days and 200 days respectively (Figures B7 to

B15). The flow pattern of the cold water mass ($\sim 22^{\circ}\text{C}$) for the 100 day simulation of grid2 is more closely related to the simulation of grid3. The flow of the cold water mass of grid1 also falls short for the 100 day simulation similar to the 200 day simulation as discussed above.

The 200 day simulations of the northeastern region of the SCS domain is magnified for level 10 (Figures B16 to B18) and level 15 (Figures B19 to B21) to investigate the temperature field deep below the sea surface level. The features of the temperature field at these two levels are difficult to distinguish. However, cold water ($\sim 16^{\circ}\text{C}$ for level 10 and $\sim 12^{\circ}\text{C}$ for level 15) appears at the northern boundary between China and Taiwan for solutions of grid1, where the temperature at this region for grid2 and grid3 is $\sim 22^{\circ}\text{C}$ for level 10 and 20°C for level 15. Similar to the salinity field, the solutions of grid2 are more closely related to the reference solutions of grid3.

V. DISCUSSION AND CONCLUSION

The numerical solutions of the system of non-linear flow equations (Navier-Stokes equations) are very sensitive to grid designs. This is notably true in coastal ocean modeling where large domains of the ocean are simulated. Poorly designed grids can lead to inaccurate representations of the physical field and an unnecessary expense of computing resources. Grid1 and grid2 have the same number of grid points ($121 \times 191 = 23,111$ points); however, the rectangular grid1 has only 13,005 effective grid points (i.e. the number of grid points over the water region of the domain), 56% of 23,111 points, that are useful in the calculation of numerical solutions. Grid2 has 16,252 effective grid points, 70% of 23,111 points, that are used in the simulation of the fluid flow. Notice that a certain part of the apathetic water regions has been eliminated from grid1 when grid2 is designed (i.e. the water regions of the Strait of Malacca and the Zulu Sea). This implies that the number of effective grid points for the rectangular grid1 (Figure 3) is much less than 13,005 points ($\ll 56\%$) for the region of interest (i.e. the SCS domain as shown in the curvilinear grid2, Figure 4). The curvilinear nearly-orthogonal grid has more useful grid points for the simulation than the traditional rectangular grid of the same matrix size. The curvilinear grid also has the capability to enhance the numerical solutions by increasing the horizontal resolution of the interested subregions of the domain without increasing the matrix size of the grid points (the subregions near the northern and southern boundary of the SCS domain have a much higher horizontal range resolution compared to the same regions of grid1). The CPU time for grid2 is slightly higher than grid1; however, numerical solutions are

greatly enhanced as compared to the solutions of a much higher resolution grid³. This also directly results in the achievement of reduced computational expenses.

The study produces some important elements in numerical simulations, especially in coastal ocean modeling. The interpretation of the physical fields is strongly affected by grid point distributions (i.e. grid resolutions). The study also reveals that the grid generation technique has some advantages over the traditional rectangular grid. The range resolutions (Δx , Δy) can be increased in regions of interest without increasing the expense of computing resources for the case of curvilinear nearly-orthogonal grid². For the traditional rectangular grid¹, the horizontal range resolution has to be increased from 121 to at least 350 grid points in order to obtain similar numerical solutions of the curvilinear grid². This results in a matrix size of $350 \times 191 = 66,877$ grid points vice $121 \times 191 = 23,111$ grid points which brings the amount of computing expense to almost three times higher than the computing expense of the curvilinear grid² for a similar solution. The grid generation technique also has the capability of producing multi-block grids which is not the scope of this study. However, the applications and relative advantages of this capability can greatly enhance the methods of solving systems of fluid flow equations in coastal ocean modeling and are a subject for further exploration.

LIST OF REFERENCES

- [1] Anderson, D. A., Tannehill, J. C. and Pletcher, R. H., *Computational Fluid Mechanics and Heat Transfer*, Hemisphere Publishing Corporation, New York, NY, 1984.
- [2] Thompson, J. F., "A Survey of Grid Generation Techniques in Computational Fluid Dynamics," *AIAA-83-0447*, AIAA 21st Aerospace Sciences Meeting, Reno, Nevada, January 1983.
- [3] Yoon, Y-H., "Enhancements and Extensions of EAGLE Grid Generation System," Ph.D. Dissertation, Mississippi State University, May 1991.
- [4] Thompson, J. F., Warsi, Z. U. A. and Mastin, C. W., *Numerical Grid Generation: Foundations and Applications*, North-Holland, Elsevier Science Publishing Co., Inc., New York, NY, 1985.
- [5] Ly, L. N., Chiu, C-S. and Miller, J., "A Three-Dimensional Coastal Ocean Model for the South China Sea Using the Grid Generation and Multi-block Grid Techniques," *AGU-032A-2*, **45**, Western Pacific Geophysics Meeting, Hong-Kong, 1994.
- [6] Ly, L. N. and Luong, P., "Application of Grid Generation Techniques to the Yellow Sea Simulations," High Performance Computing (HPC) Proceedings, HPC.-Asia, 1995.
- [7] Ly, L. N., Luong, P. and Chiu, C-S., "Application of Grid Generation Technique in Coastal Ocean Modeling for the Mediterranean Sea," *AGU--12B-4*, American Geophysical Union Fall Meeting, San Francisco, CA, 1993.
- [8] Thompson, J. F., "Composite Grid Generation Code for General 3-D Regions," *AIAA-87-0275*, AIAA 25th Aerospace Sciences Meeting, Reno, Nevada, January 1987.
- [9] Mellor, G. L., "User's Guide for A Three-Dimensional, Primitive Equation, Numerical Ocean Model," Atmospheric and Oceanic Sciences Program, Princeton University, Princeton, NJ, March 1993.
- [10] Blumberg, A. F. and Mellor, G. L., "A Description of a Three Dimensional Coastal Ocean Circulation Model," *Three Dimensional Coastal Models*, Coastal and Estuarine Sciences, **4**, N. S. Heaps, editor, AGU Geophysical Monograph Board, pp. 1-16, 1987.

- [11] Ly, L. N., "The Gulf of Mexico Response to Hurricane Frederic Simulated with the Princeton Numerical Ocean Circulation Model," *Institute for Naval Oceanography*, Technical Report, **TR-2**, May 1992.
- [12] Ly, L. N. and Kantha, L. H., "A Numerical Study of the Nonlinear Interaction of Hurricane Camille with the Gulf of Mexico Loop Current," *Oceanologica Acta*, Vol. 16, No. 4, pp. 341-348, 1993.
- [13] Ly, L. N., "A Numerical Study of Sea Level and Current Responses to Hurricane Frederic Using a Coastal Ocean Model for the Gulf of Mexico," *Journal of Oceanography*, Vol. 50, pp. 599-616, 1994.
- [14] Mellor, G. L. and Yamada, T., "A Hierarchy of Turbulence Closure Models for Planetary Boundary Layers," *Journal of Atmospheric Science*, **31**, pp. 1791-1806, 1982.
- [15] Levitus, S., "Climatology Atlas of the World Ocean," NOAA, *Professional Paper No. 13*, U.S. Government Printing Office, Washington D.C., pp. 173, 1982.
- [16] Ly, N. L., Kindle, J. C., Thompson, D. J. and Youtsey, W. J., "Wind Stress Analysis Over the Western Equatorial Pacific and North Atlantic Oceans based on ECMWF Operational Wind Products 1985-1989," *Institute for Naval Oceanography*, Technical Report, **TR-3**, pp. 110, 1992.
- [17] Bankcroft, G. V., Merritt, F. J., Plessel, T. C., Kelaita, P. G., McCabe, R. K. and Globus, A., "FAST: A Multi-Processed Environment for Visualization of Computational Fluid Dynamics," *Proceeding of the IEEE Visualization '90 Conference*, October 1990.
- [18] FAST, The Flow Analysis Software Toolkit, Sterling Software, Moffett Field, CA.
- [19] The NAS Panel Library, NASA Ames Research Center, Moffett Field, CA.
- [20] Soni, B. K., Thompson, J. F., Stokes, M. and Shih, M. H., "GENIE++, EAGLEView and TIGER: General and Special Purpose Graphically Interactive Grid Systems," *AIAA-92-0071*, AIAA 30th Aerospace Sciences Meeting, Reno, Nevada, January 1992.

APPENDIX A: SALINITY FIELD SOLUTIONS

Appendix A contains the simulations of salinity field numerical solutions. The simulations are numbered from Figure A1 to A21 and are being referred to as such in the text.

South China Sea
Orthogonal Grid Model (121X191)
Surface Salinity - 0 days

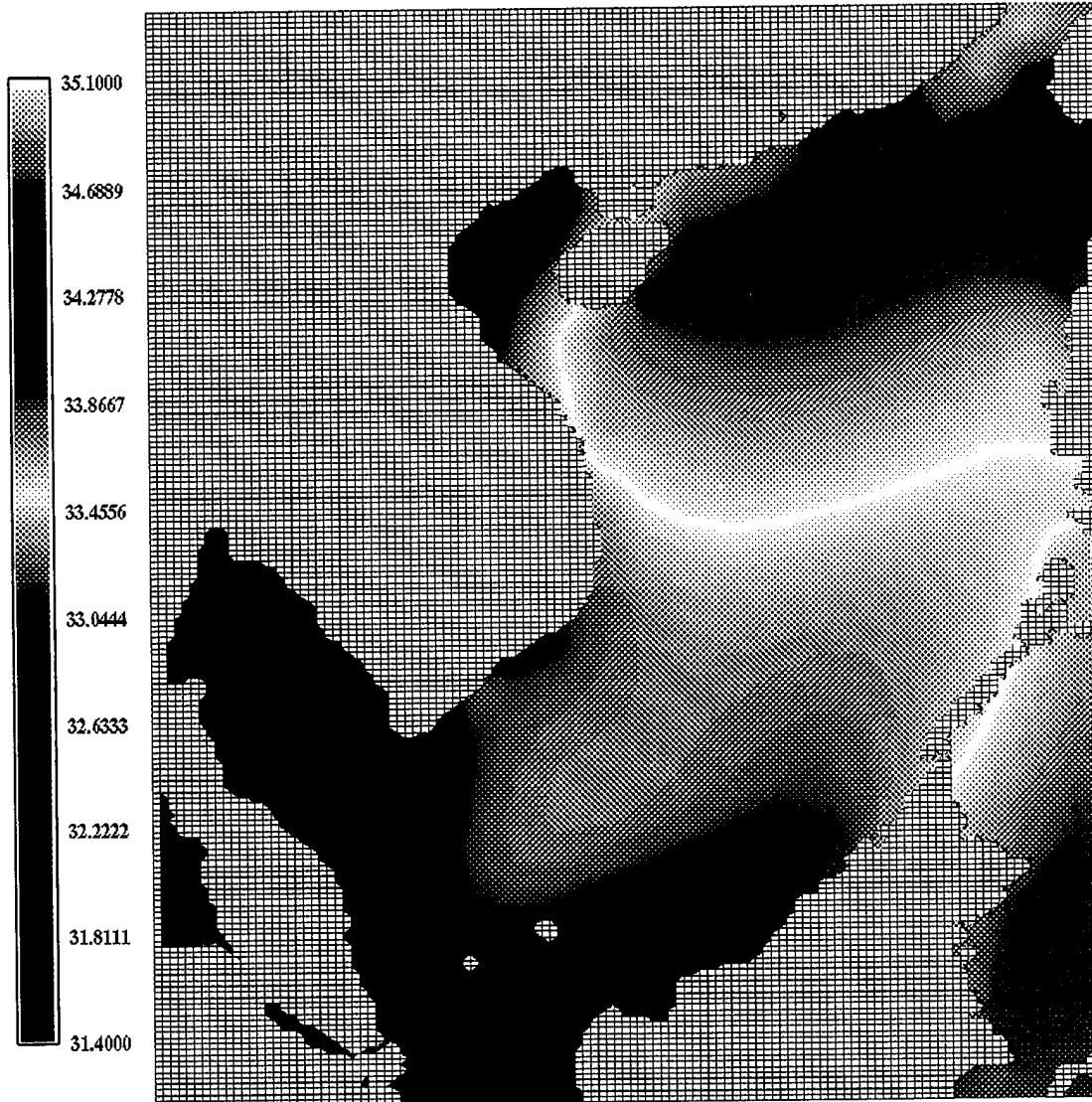


Figure A1: Grid1 - Initial Surface Salinity

South China Sea
Nearly-orthogonal Grid Model (121X191)
Surface Salinity - 0 days

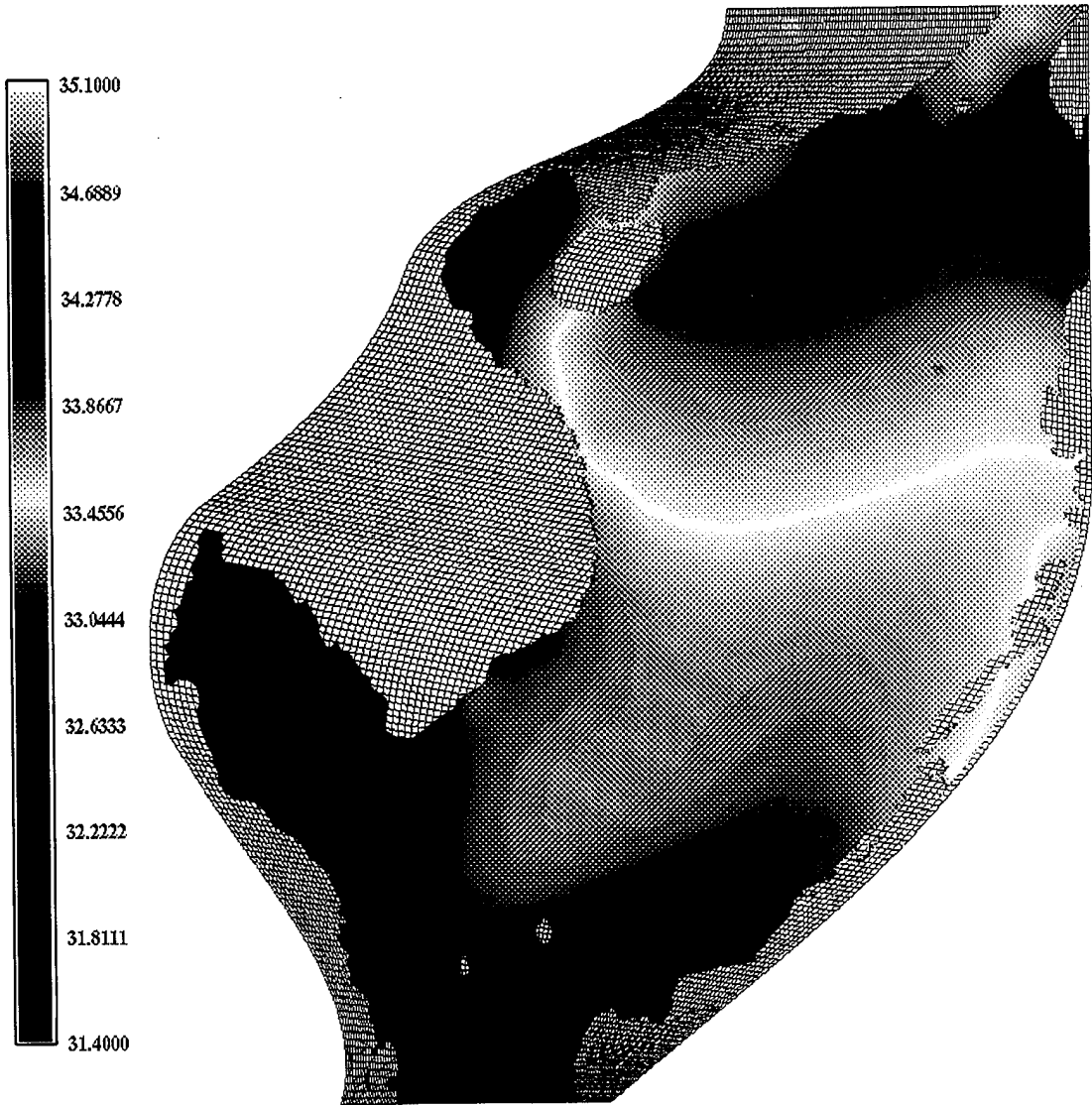


Figure A2: Grid2 - Initial Surface Salinity

South China Sea
Nearly-orthogonal Grid Model (151X241)
Surface Salinity - 0 days

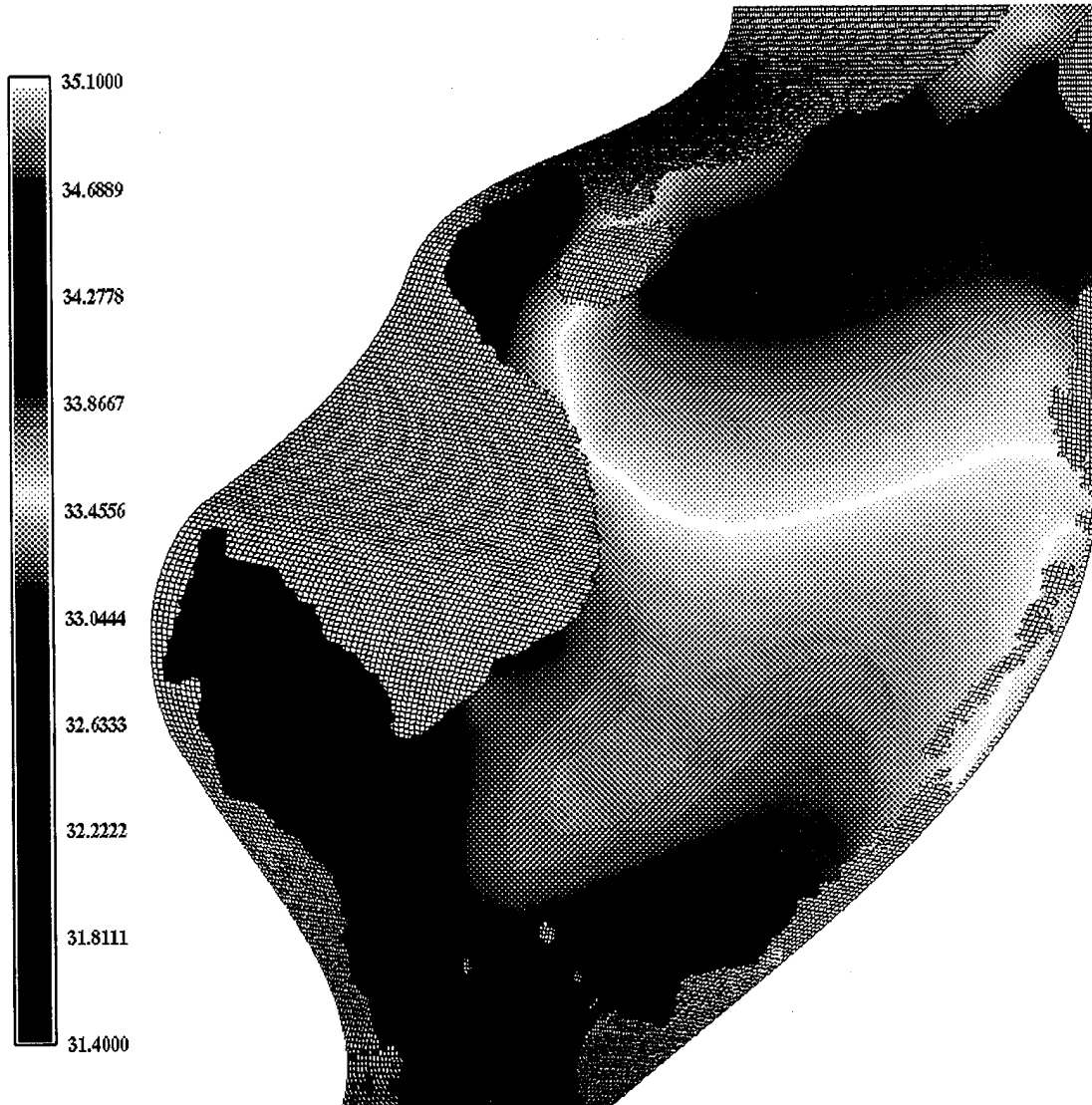


Figure A3: Grid3 - Initial Surface Salinity

South China Sea
Orthogonal Grid Model (121X191)
Surface Salinity - 200 days

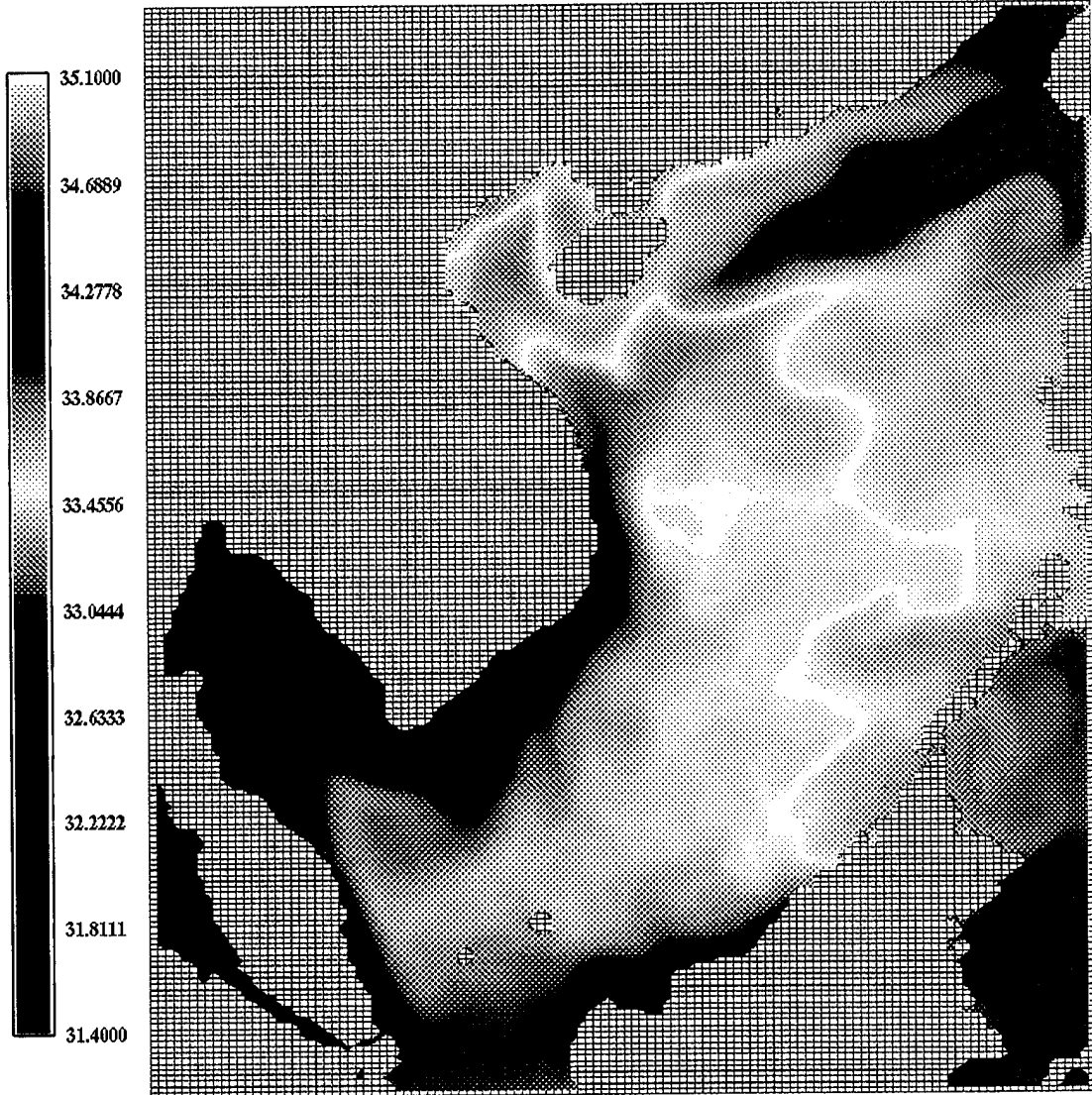


Figure A4: Grid1 - 200 days Surface Salinity

South China Sea
Nearly-orthogonal Grid Model (121X191)
Surface Salinity - 200 days

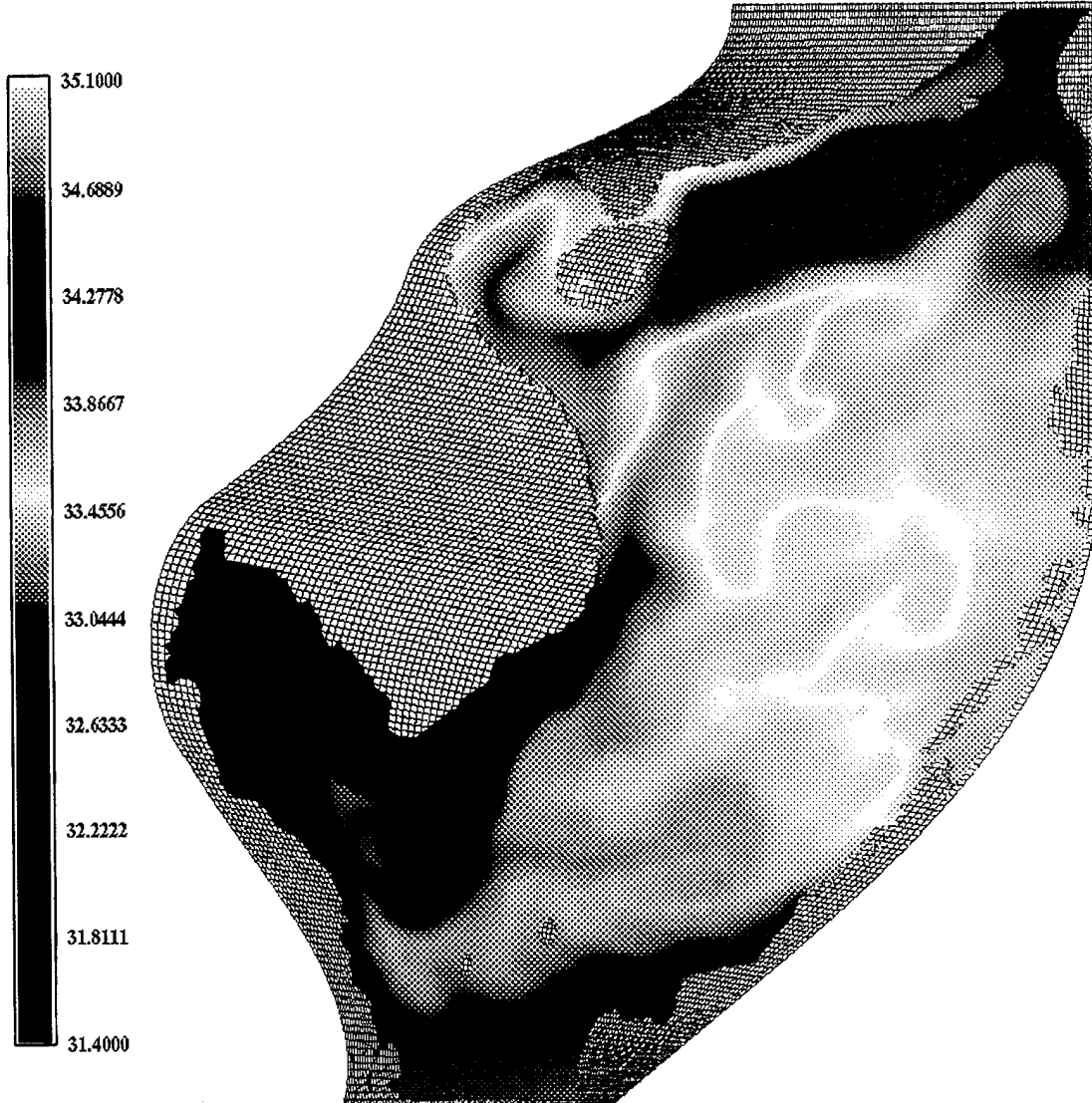


Figure A5: Grid2 - 200 days Surface Salinity

South China Sea
Nearly-orthogonal Grid Model (151X241)
Surface Salinity - 200 days

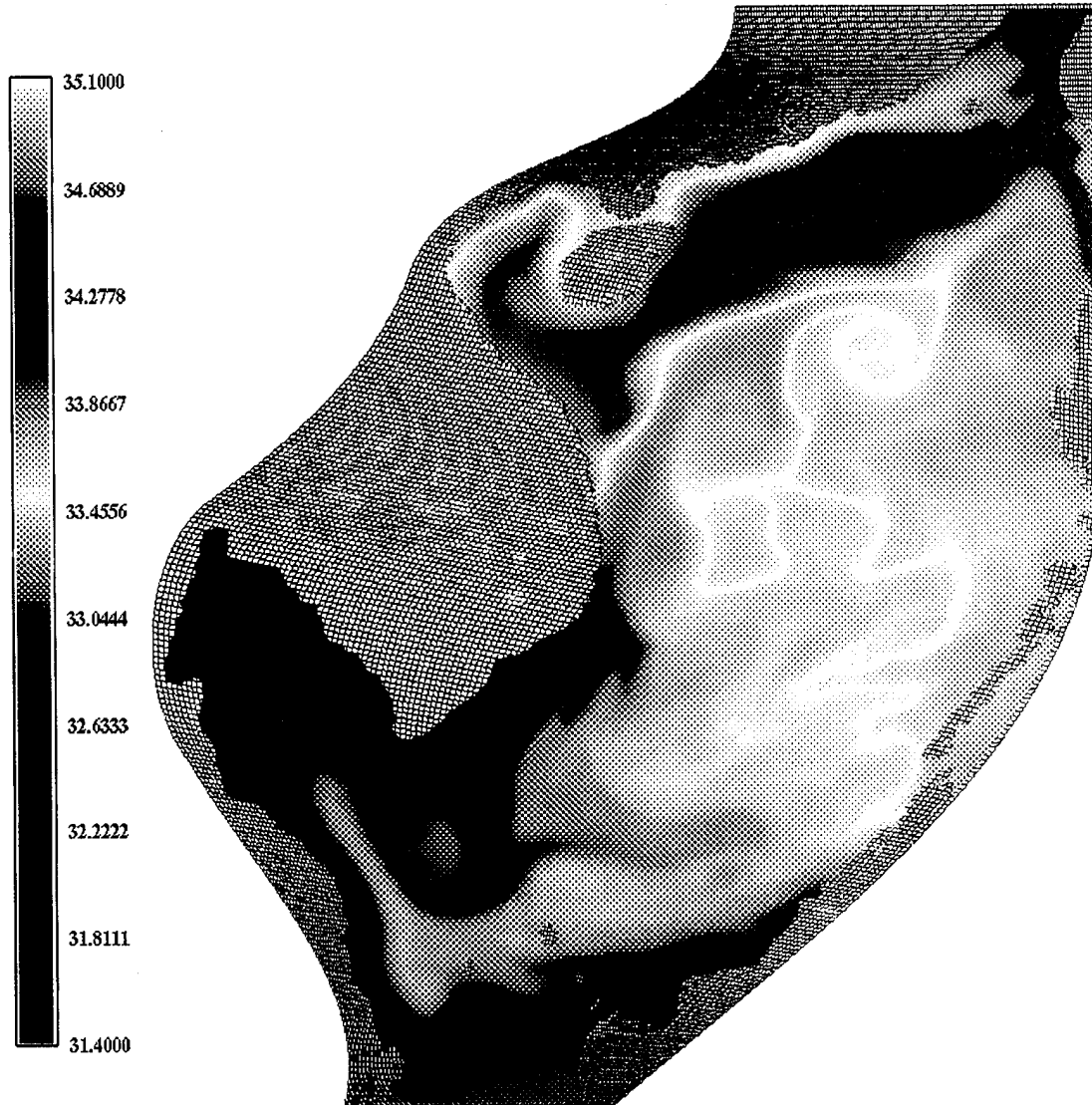


Figure A6: Grid3 - 200 days Surface Salinity

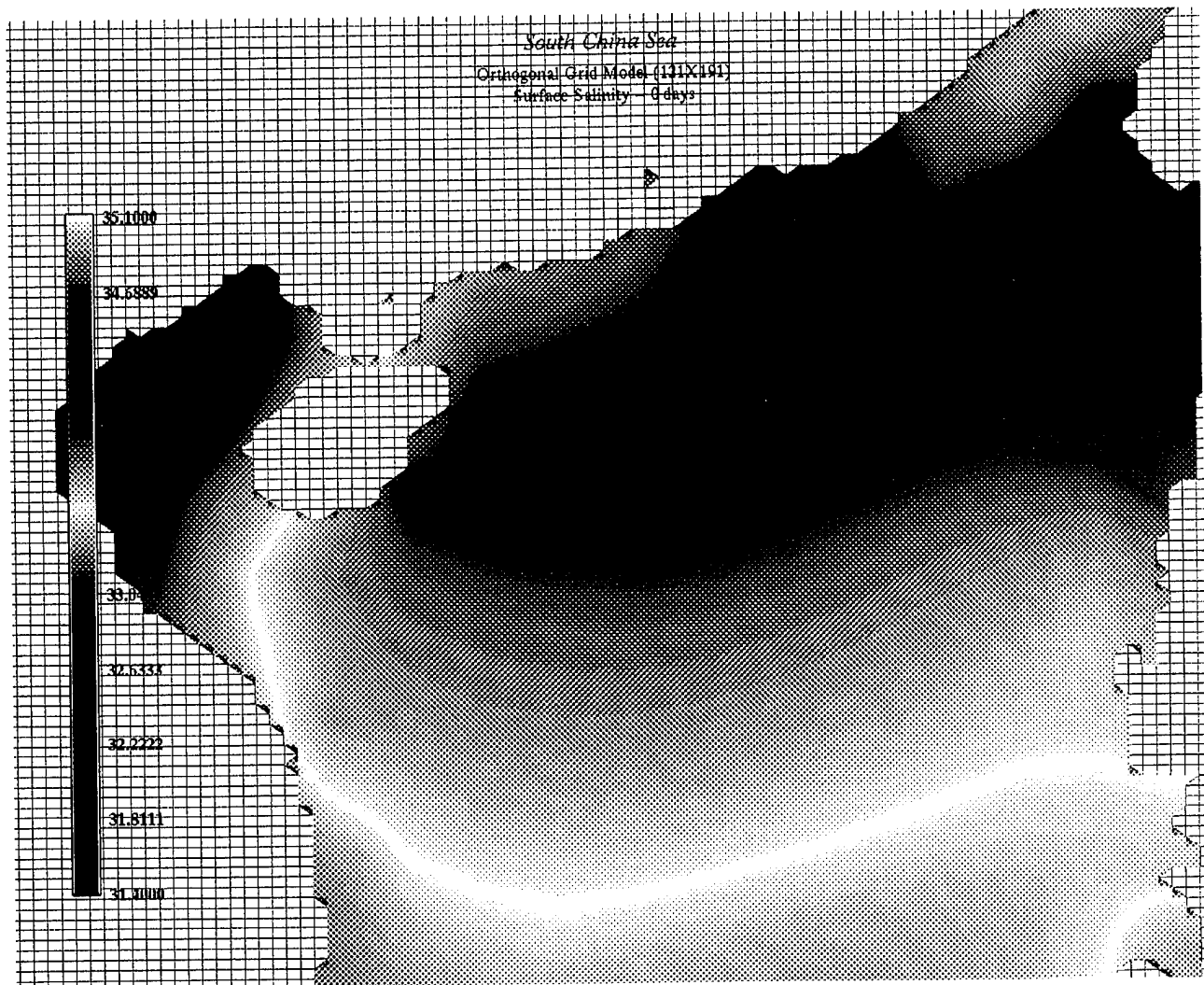


Figure A7: Grid1 - Initial Surface Salinity

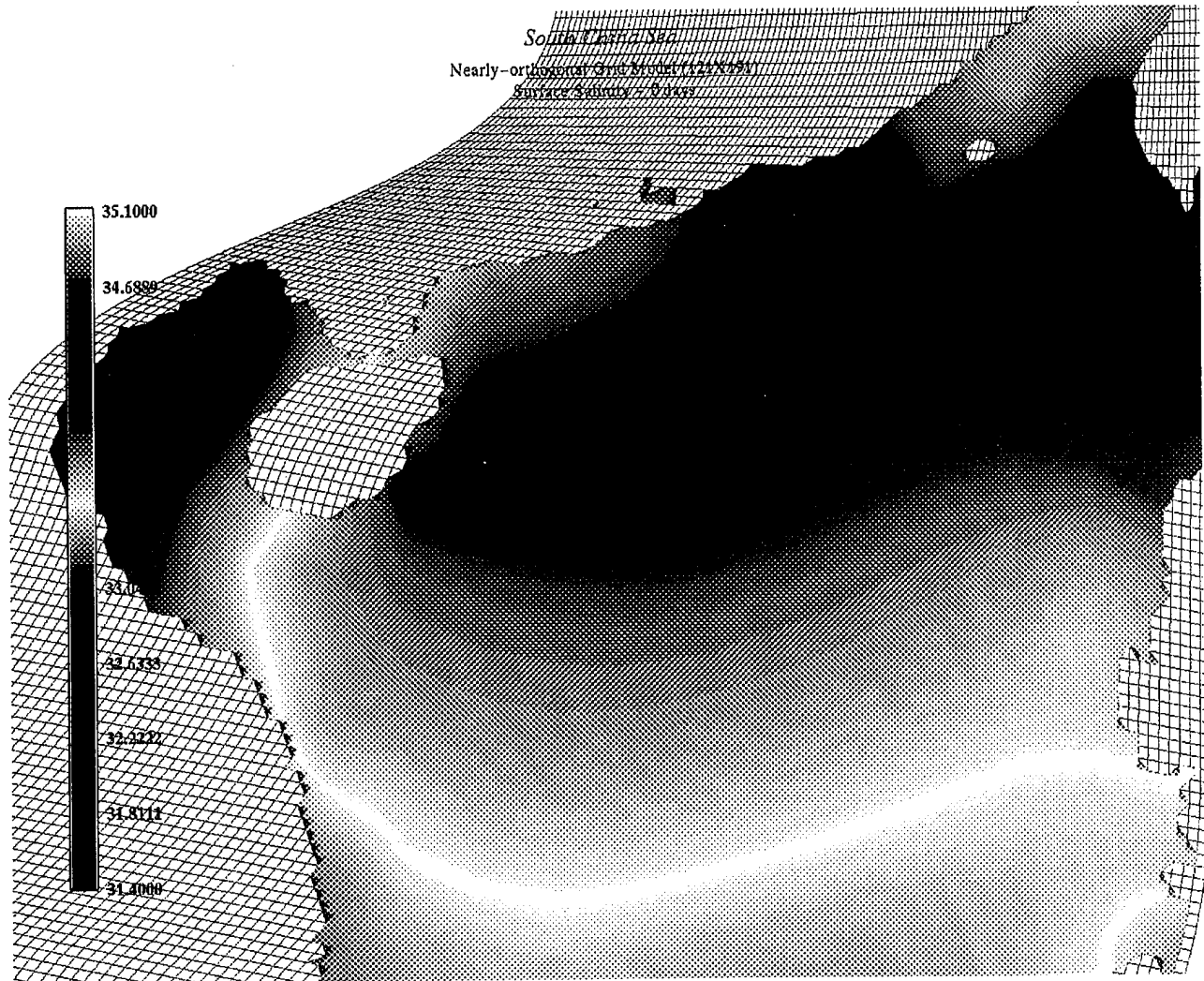


Figure A8: Grid2 - Initial Surface Salinity

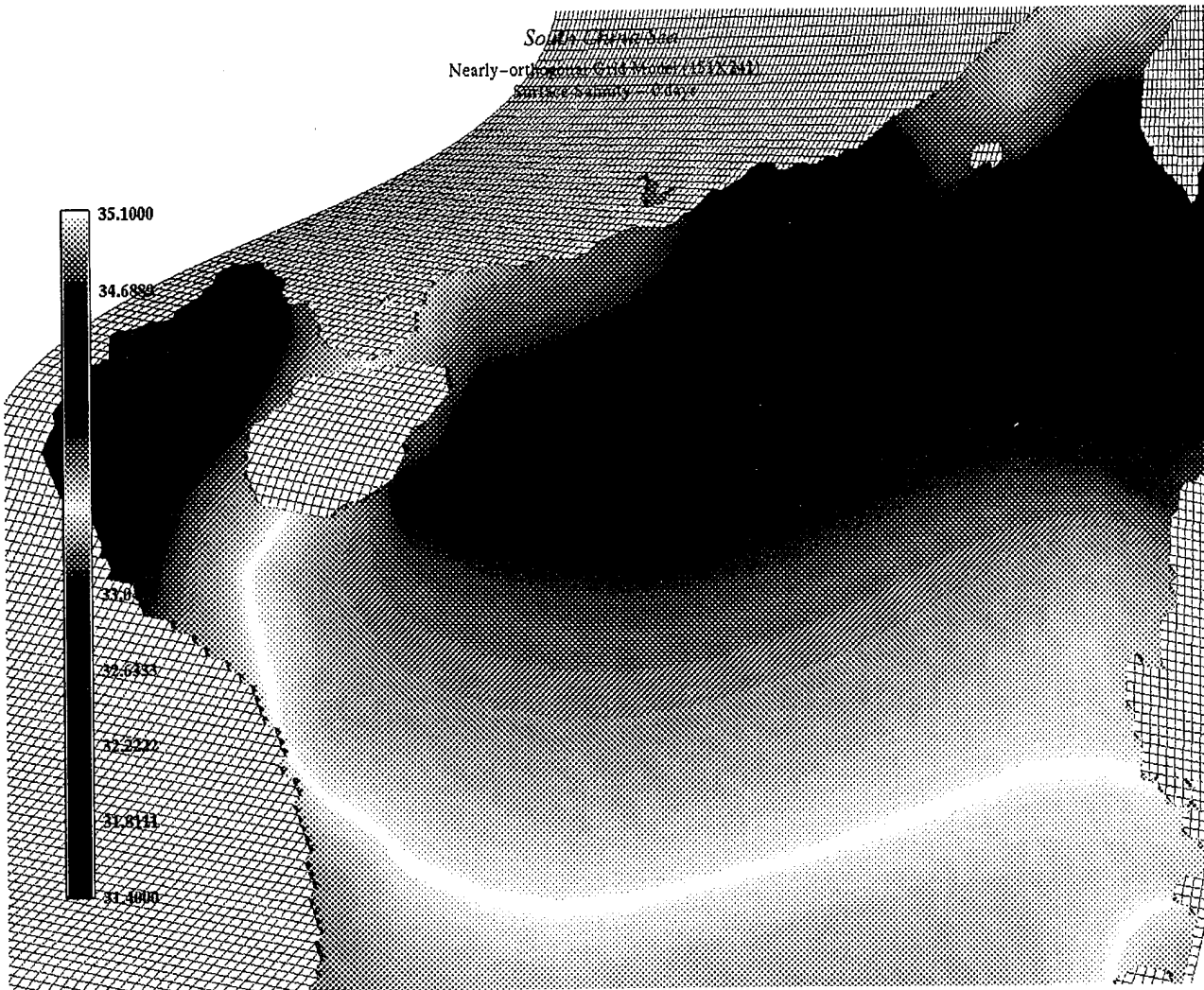


Figure A9: Grid3 - Initial Surface Salinity

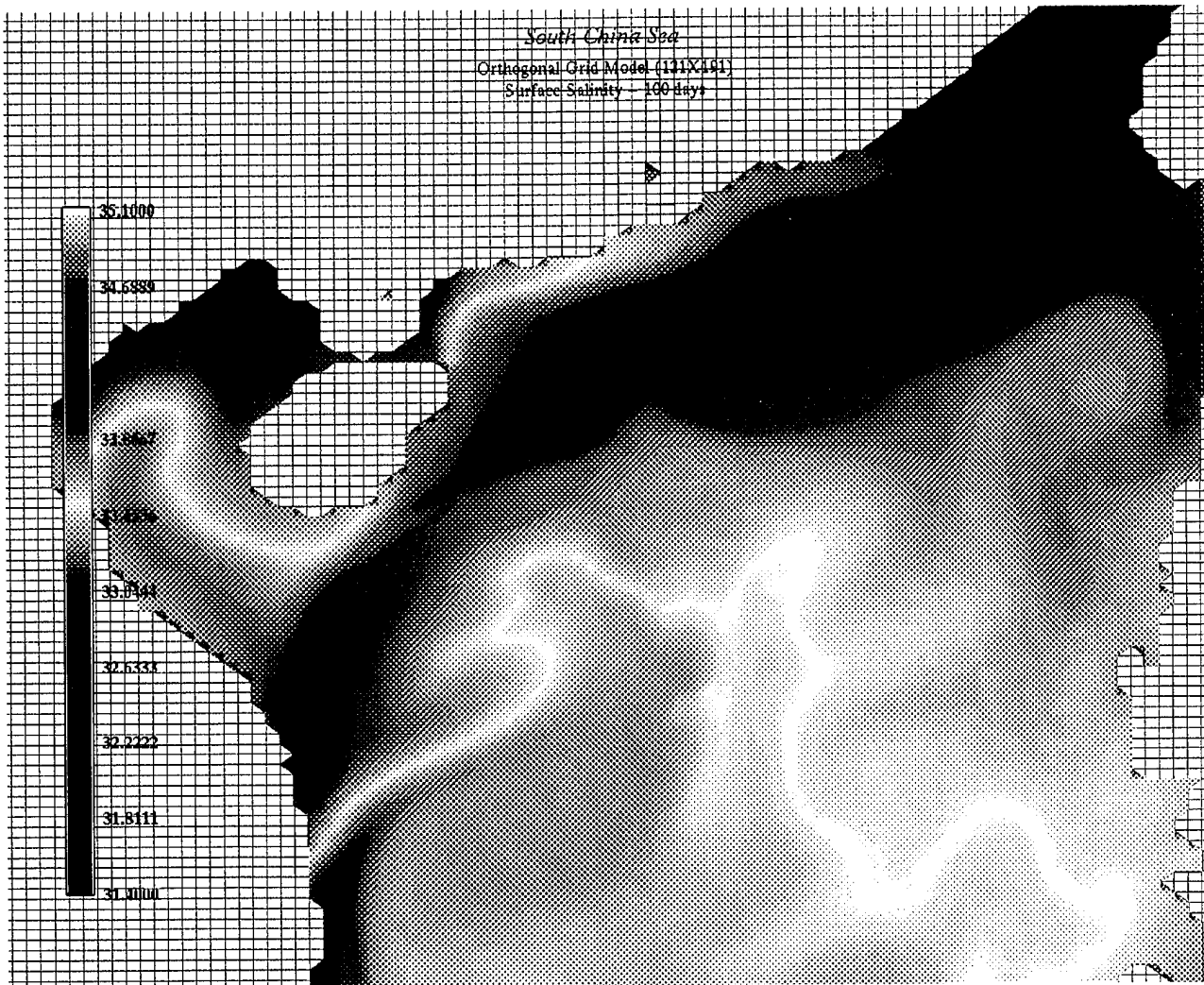


Figure A10: Grid1 - 100 days Surface Salinity

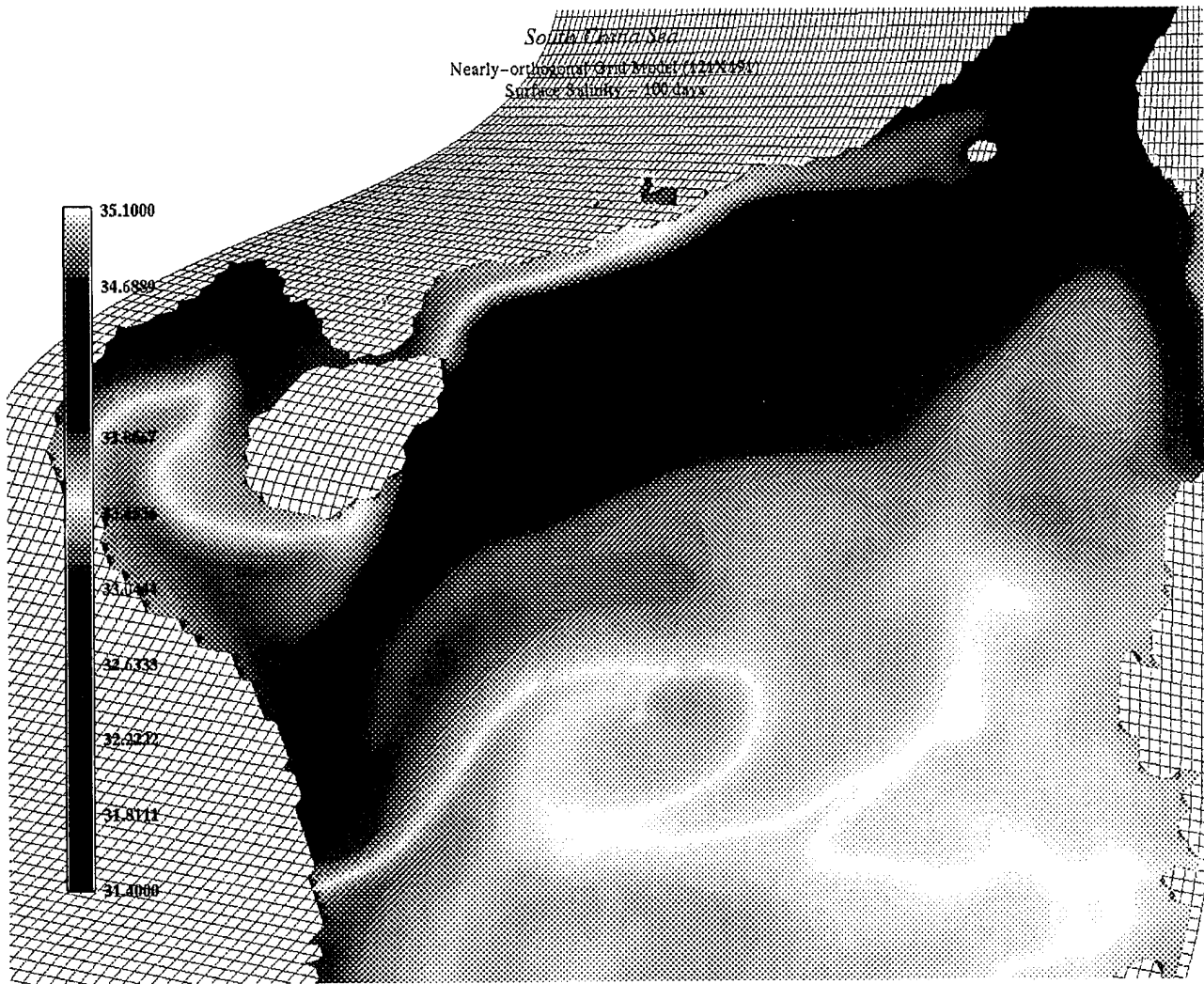


Figure A11: Grid2 - 100 days Surface Salinity

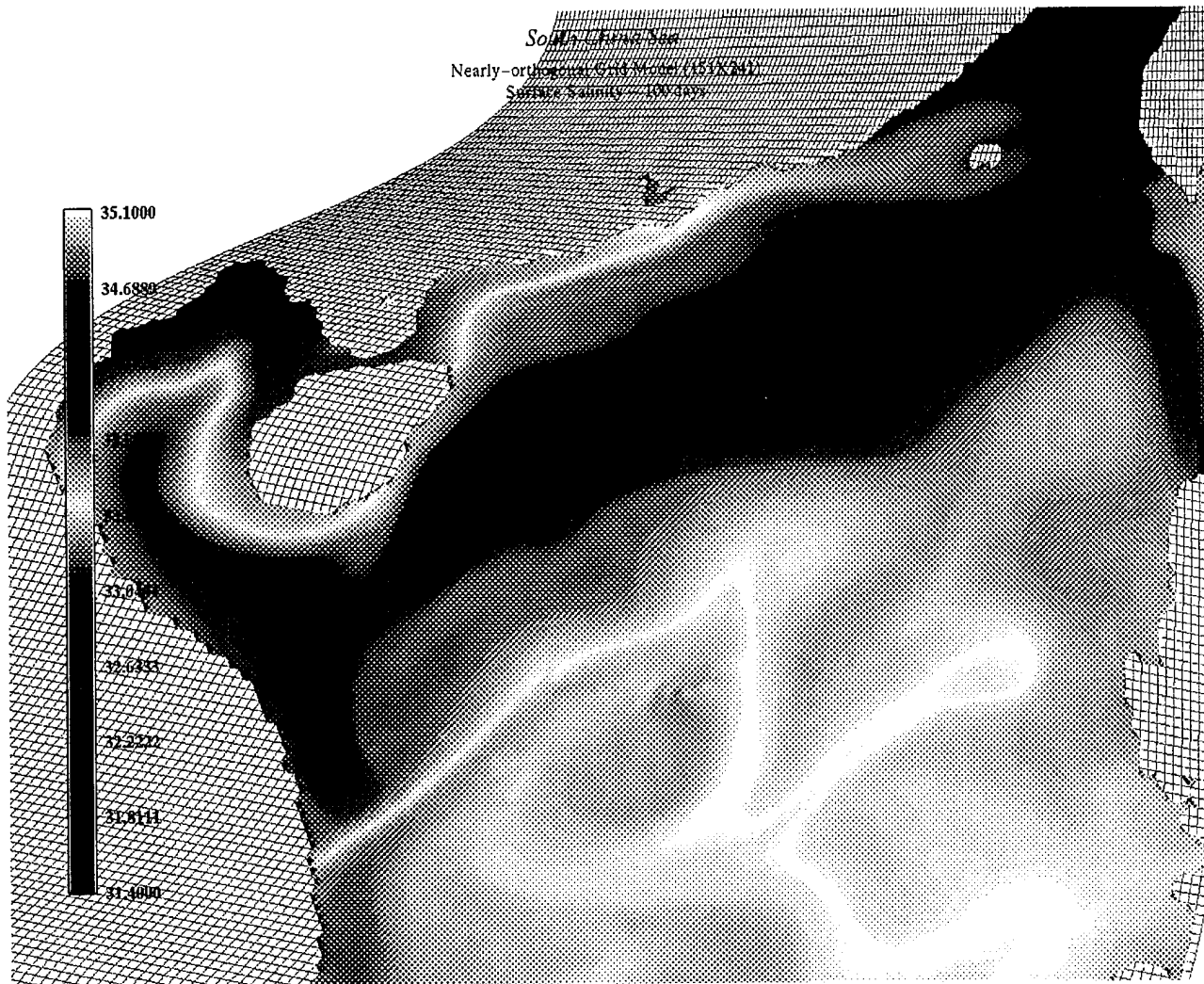


Figure A12: Grid3 - 100 days Surface Salinity

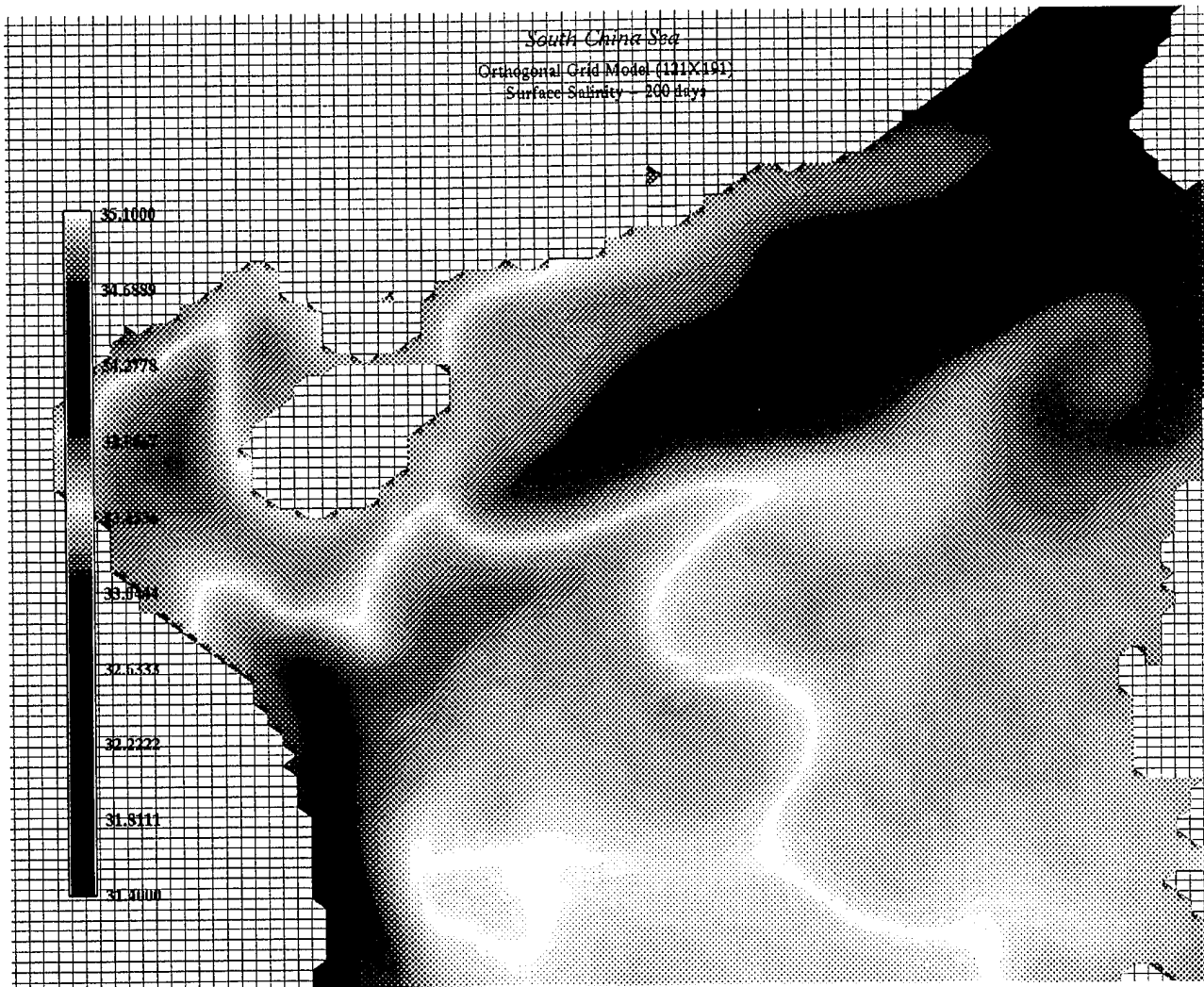


Figure A13: Grid1 - 200 days Surface Salinity

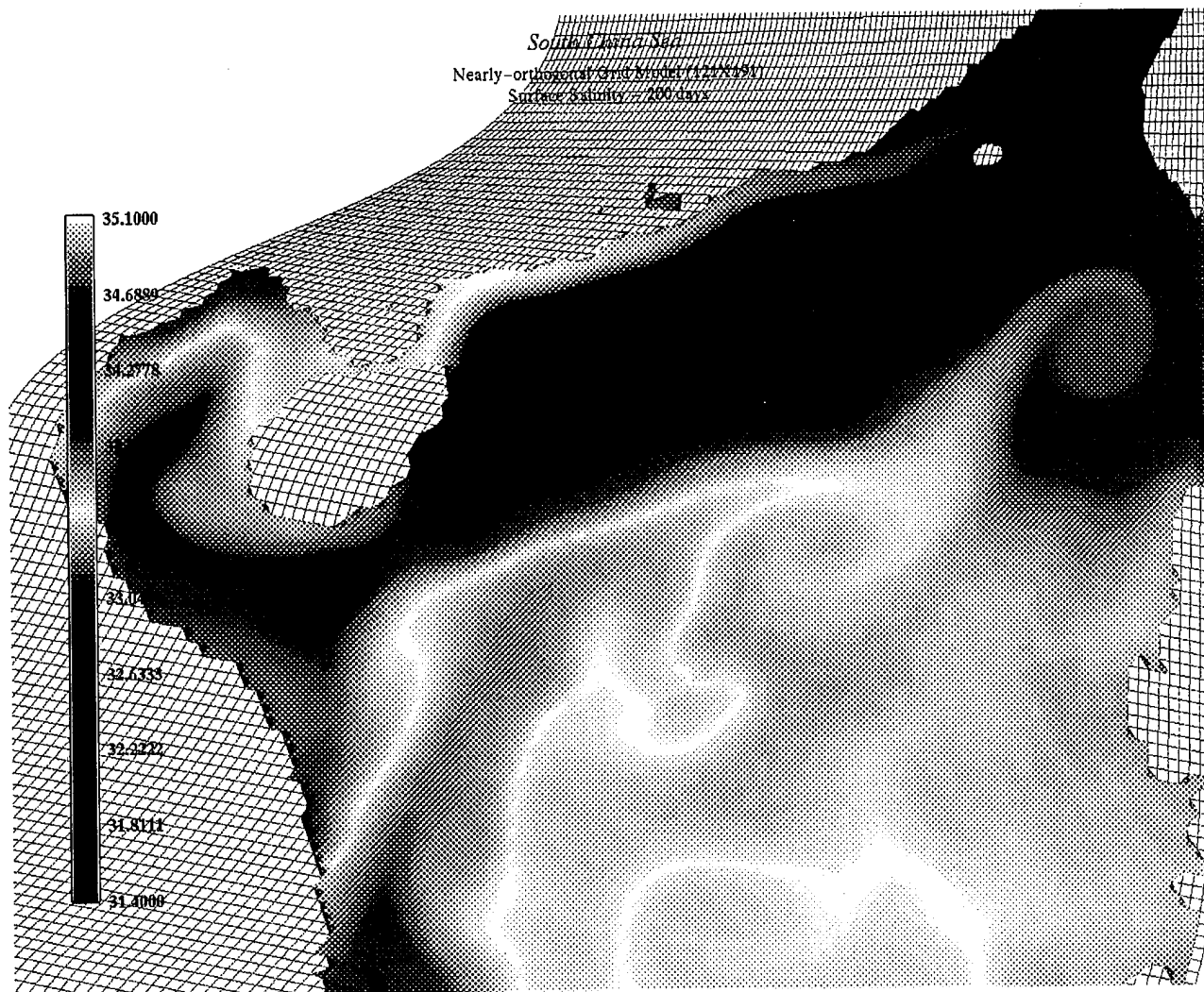


Figure A14: Grid2 - 200 days Surface Salinity

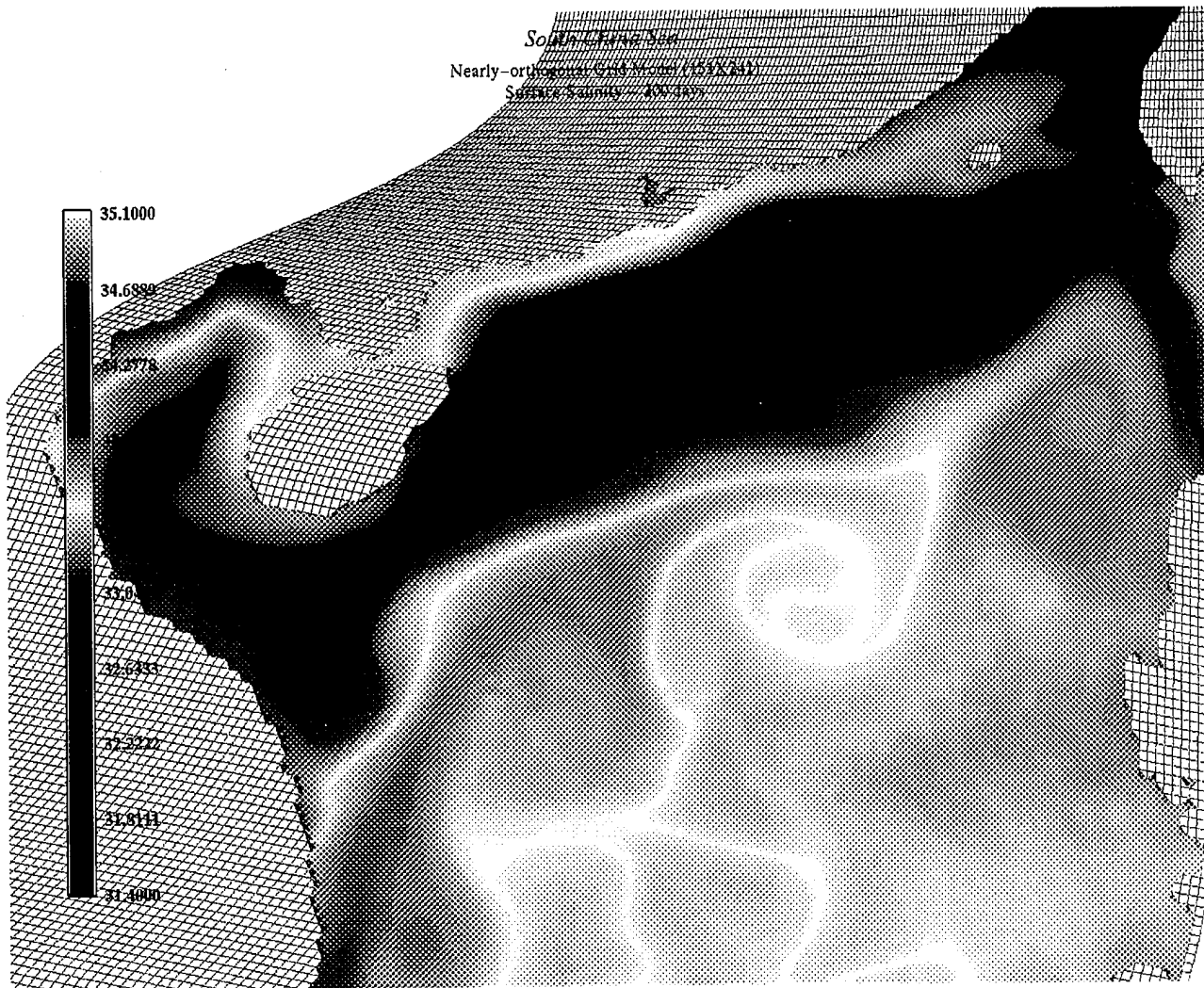


Figure A15: Grid3 - 200 days Surface Salinity

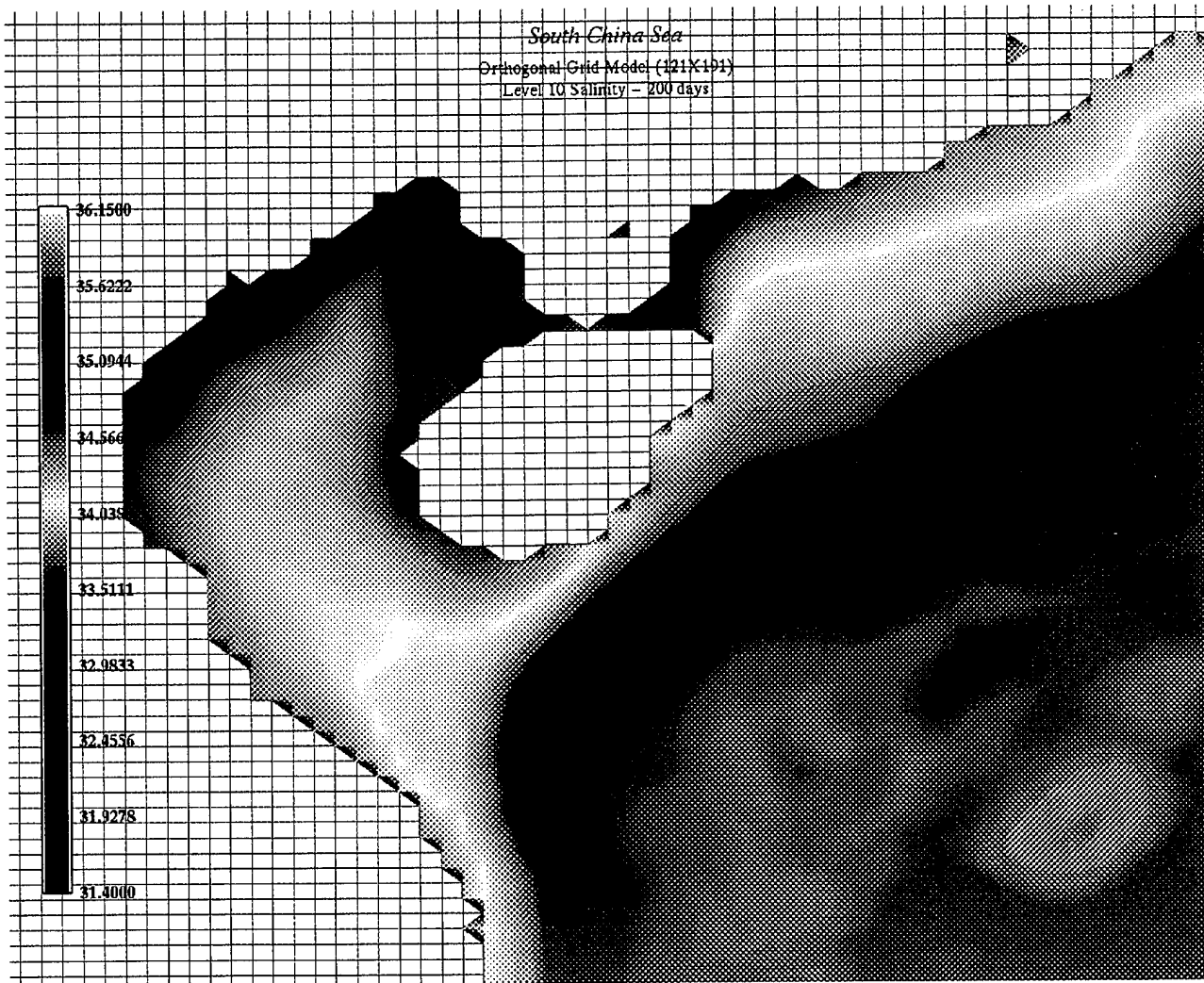


Figure A16: Grid1 - 200 days Level 10 Salinity

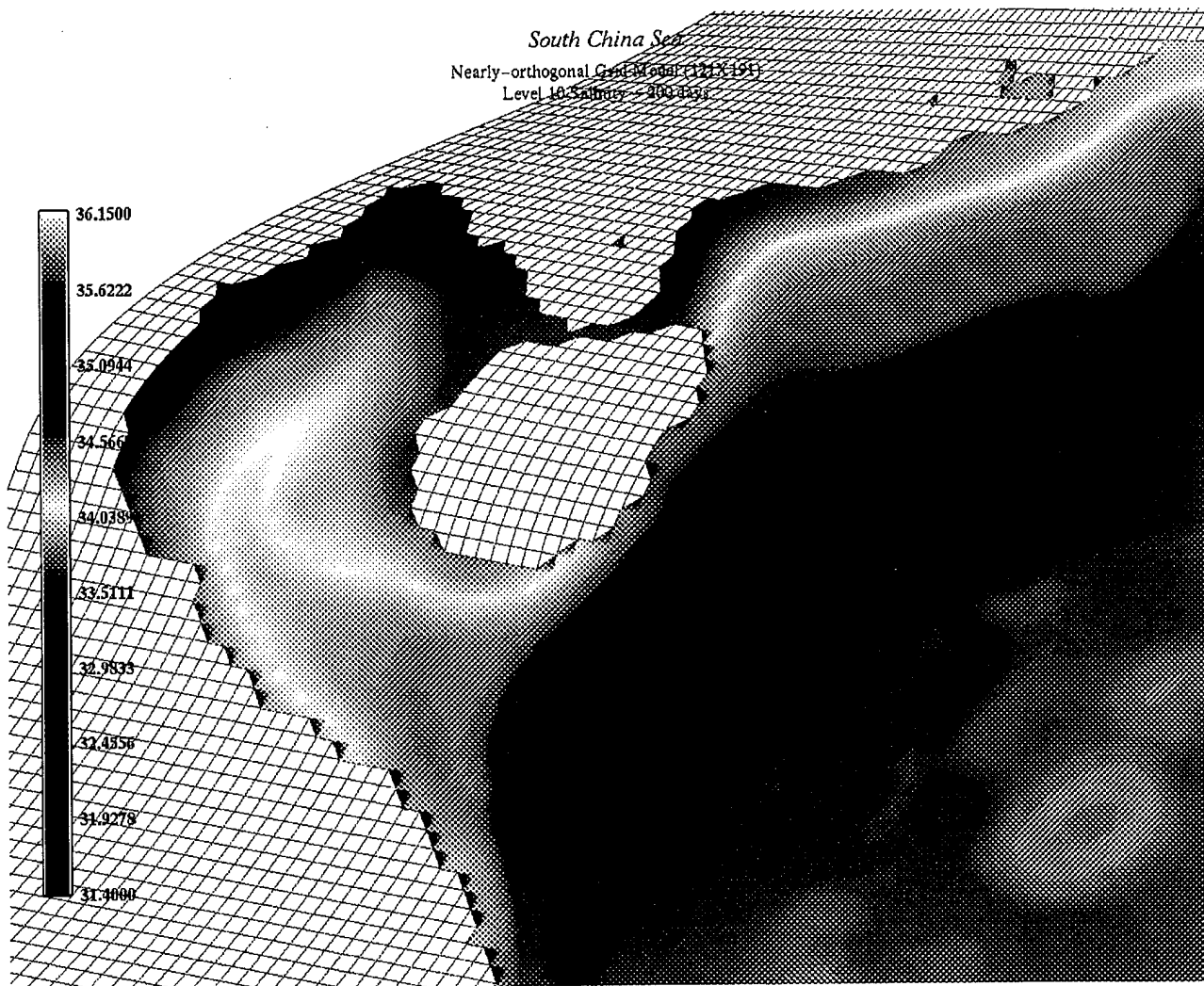


Figure A17: Grid2 - 200 days Level 10 Salinity

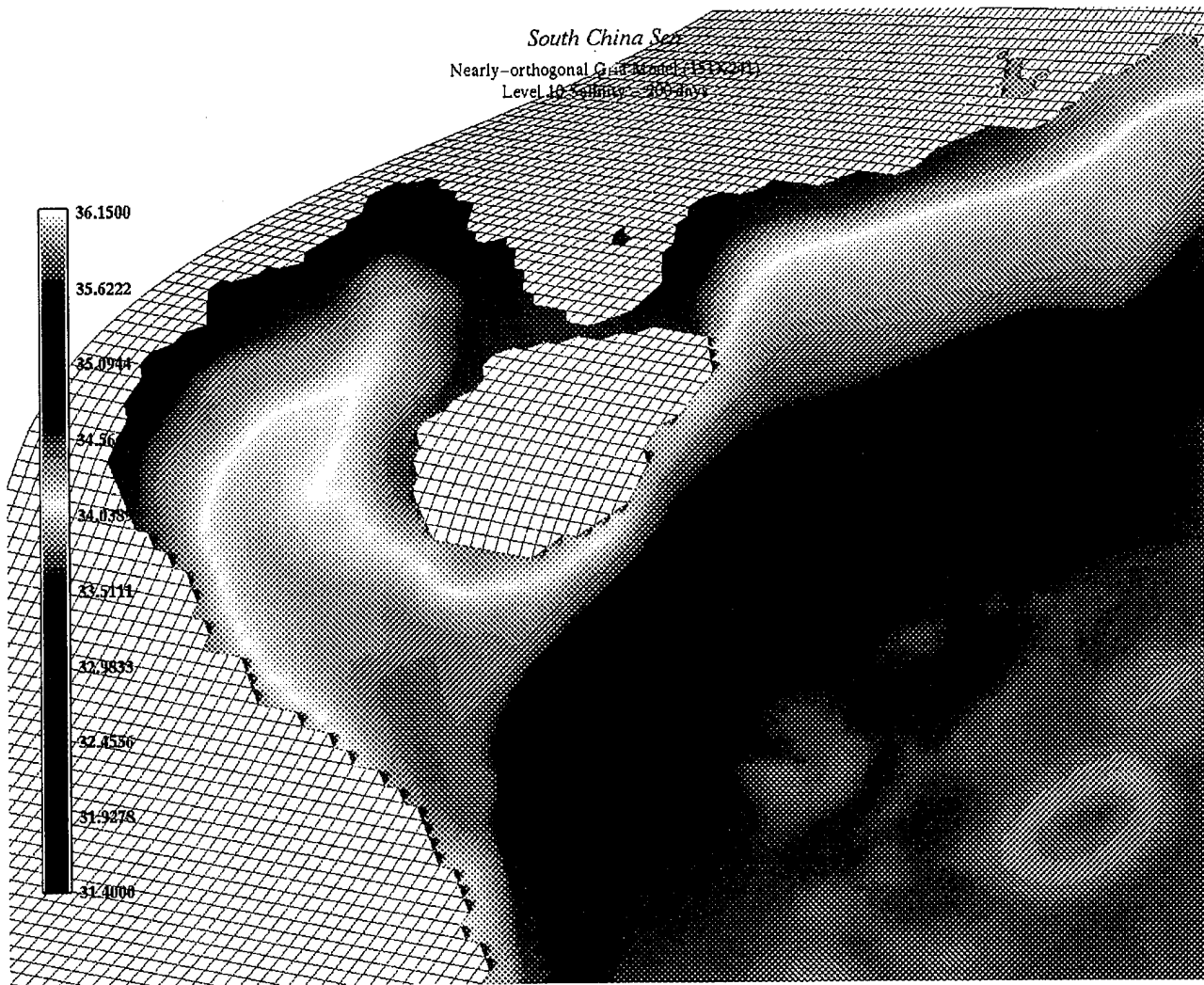


Figure A18: Grid3 - 200 days Level 10 Salinity

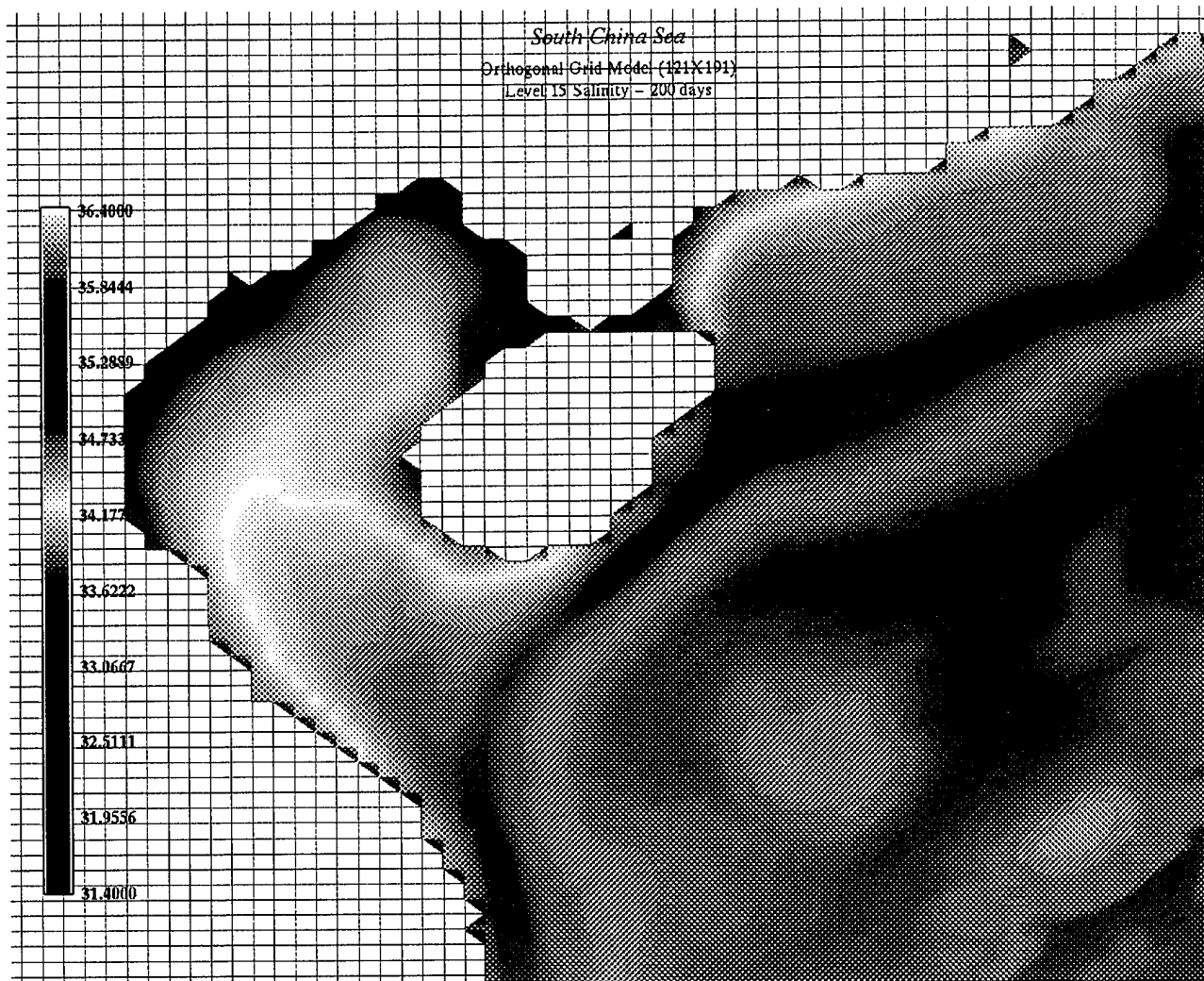


Figure A19: Grid1 - 200 days Level 15 Salinity

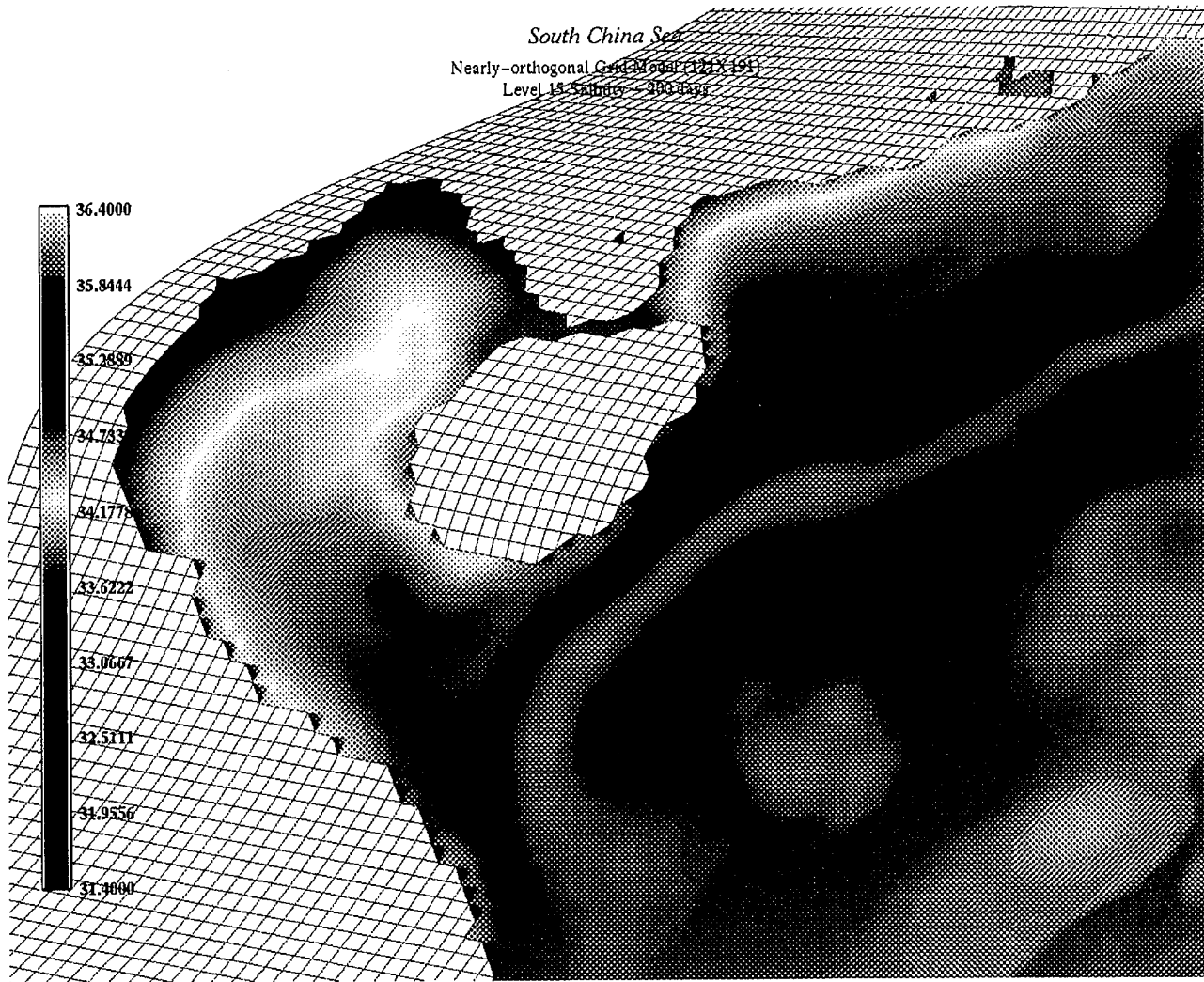


Figure A20: Grid2 - 200 days Level 15 Salinity

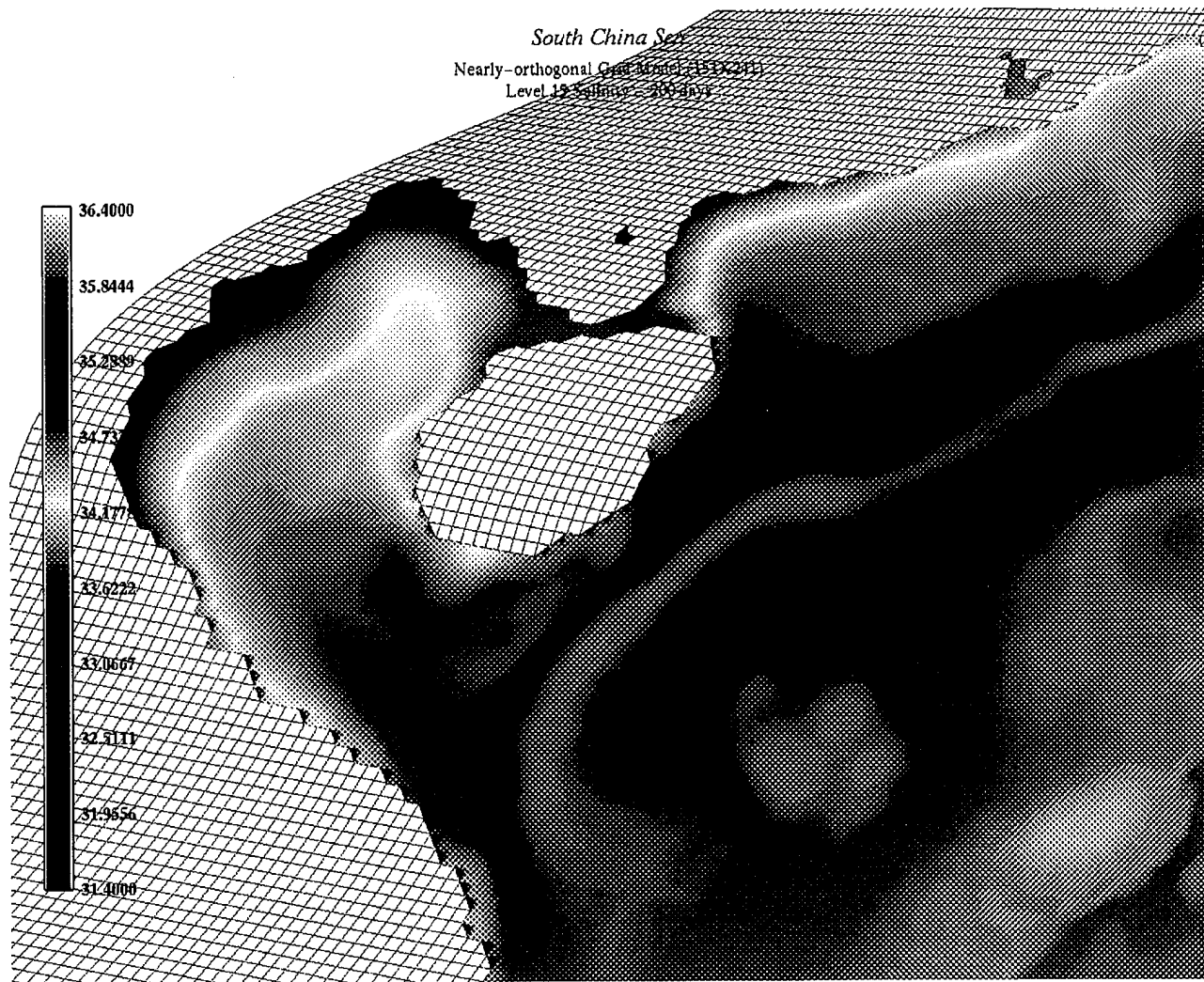


Figure A21: Grid3 - 200 days Level 15 Salinity

APPENDIX B: TEMPERATURE FIELD SOLUTIONS

Appendix B contains the simulations of temperature field numerical solutions. The simulations are numbered from Figure B1 to B21 and are being referred to as such in the text.

South China Sea
Orthogonal Grid Model (121X191)
Surface Temperature - 0 days

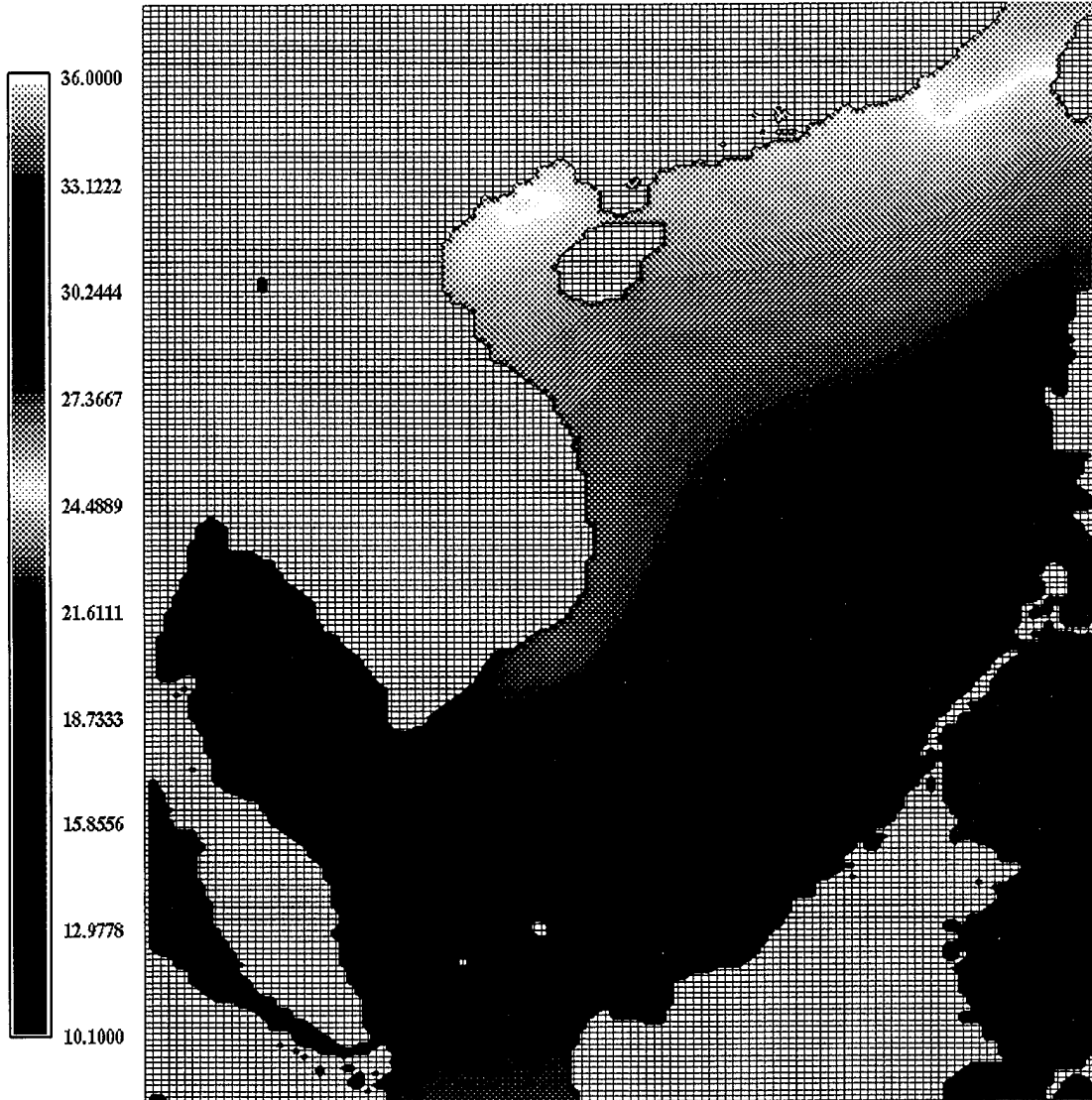


Figure B1: Grid1 - Initial Surface Temperature

South China Sea
Nearly-orthogonal Grid Model (121X191)
Surface Temperature - 0 days

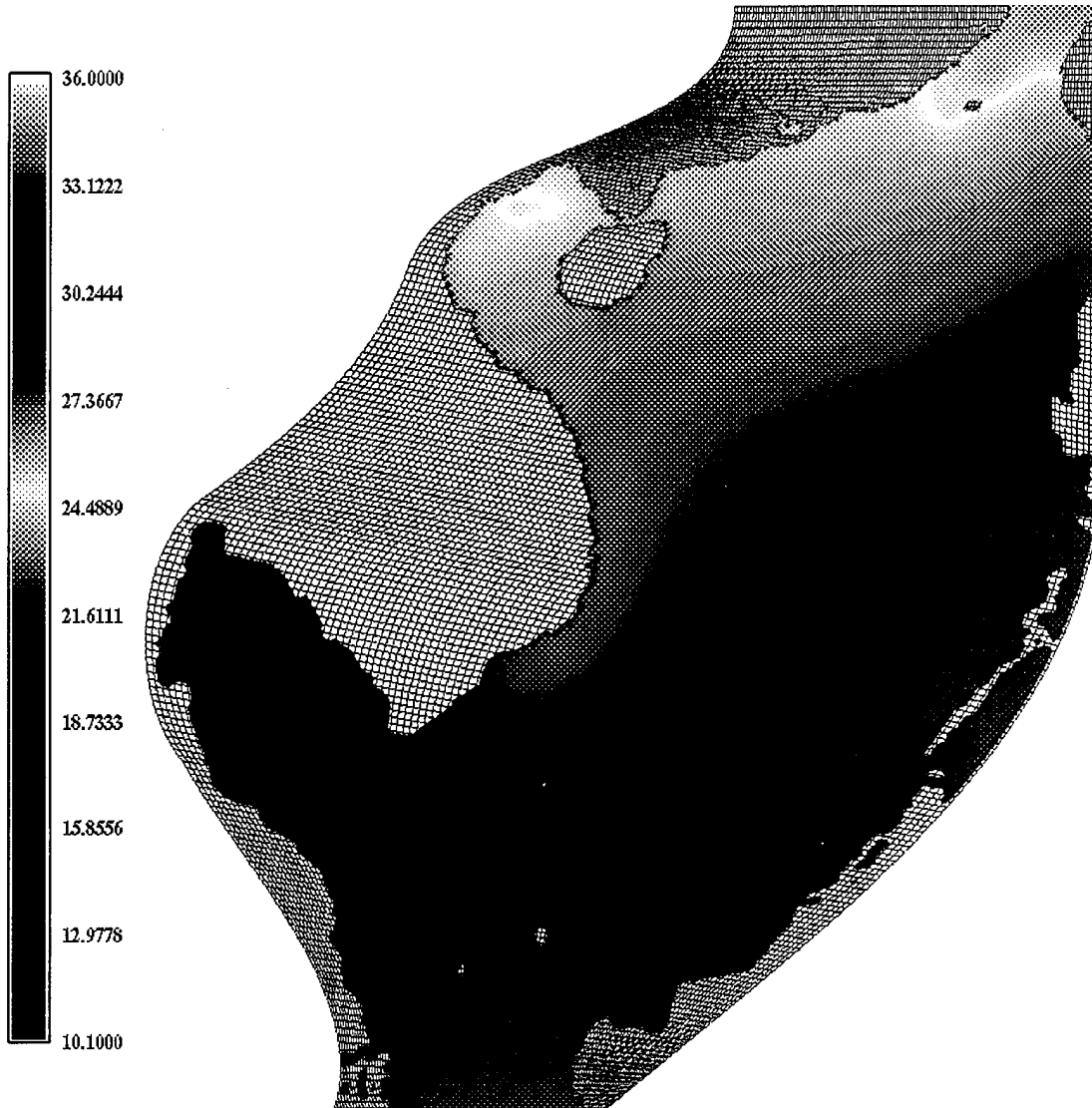


Figure B2: Grid2 - Initial Surface Temperature

South China Sea
Nearly-orthogonal Grid Model (151X241)
Surface Temperature - 0 days

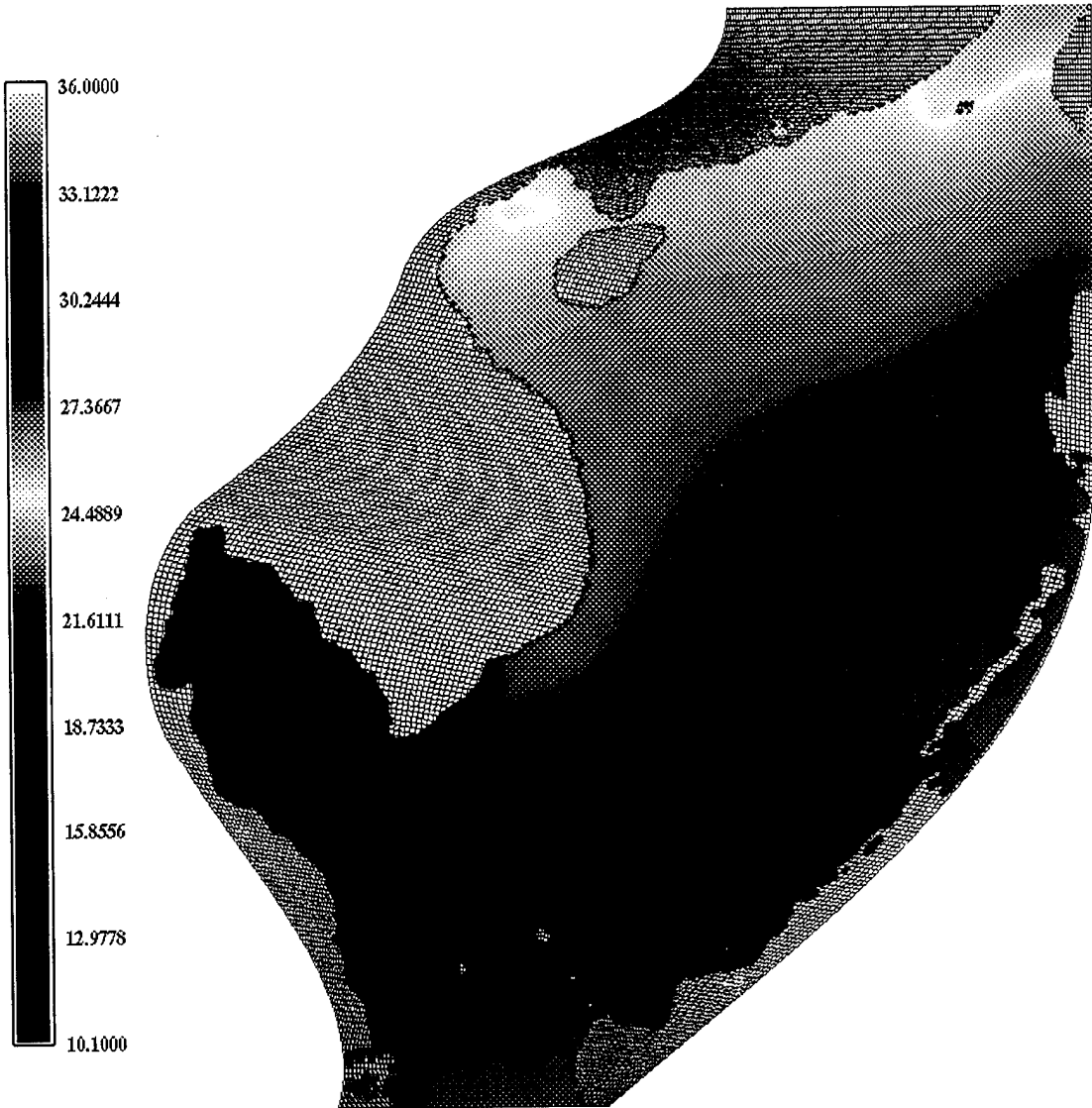


Figure B3: Grid3 - Initial Surface Temperature

South China Sea
Orthogonal Grid Model (121X191)
Surface Temperature – 200 days

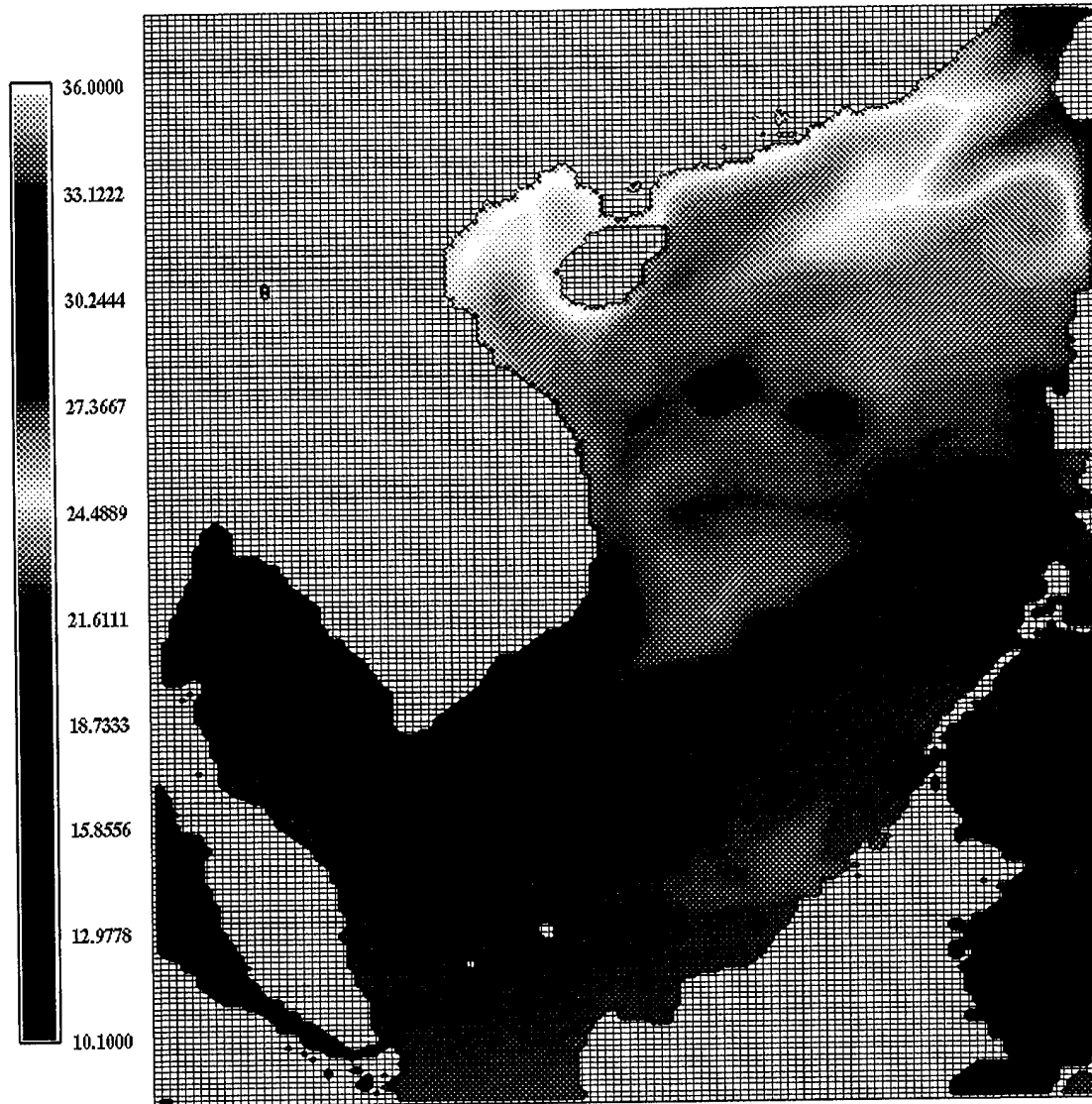


Figure B4: Grid1 - 200 days Surface Temperature

South China Sea
Nearly-orthogonal Grid Model (121X191)
Surface Temperature - 200 days

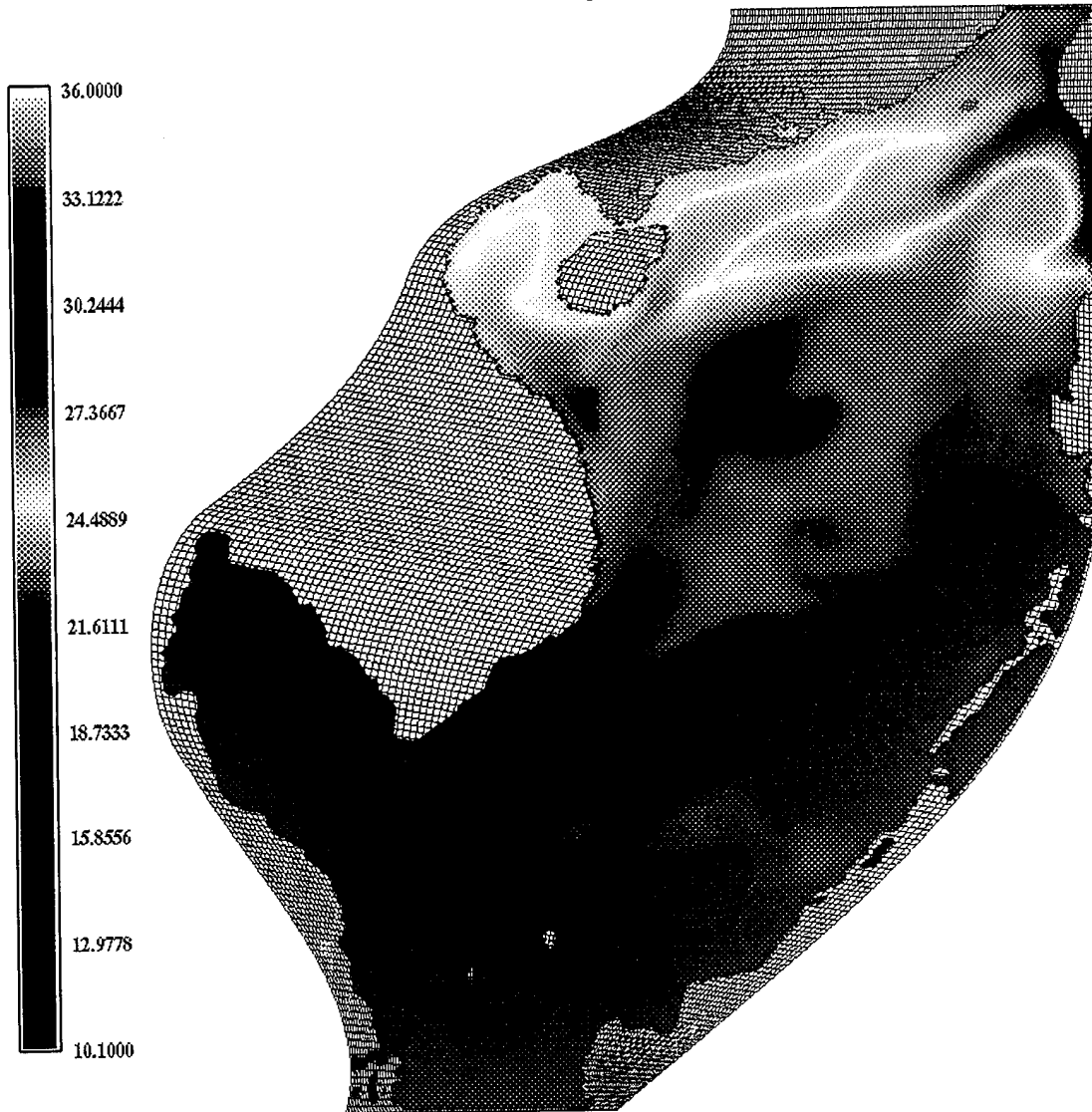


Figure B5: Grid2 - 200 days Surface Temperature

South China Sea
Nearly-orthogonal Grid Model (151X241)
Surface Temperature - 200 days

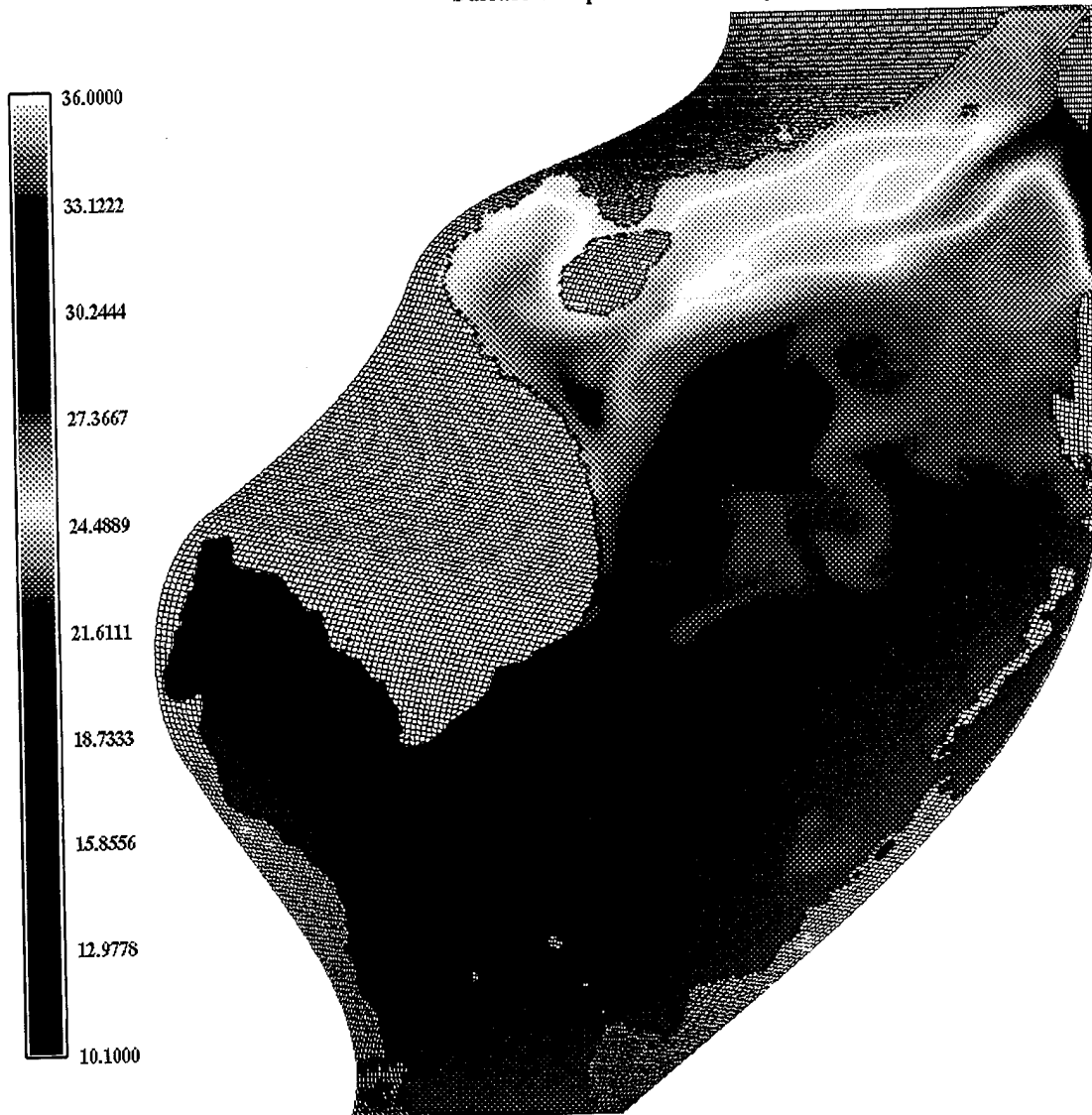


Figure B6: Grid3 - 200 days Surface Temperature

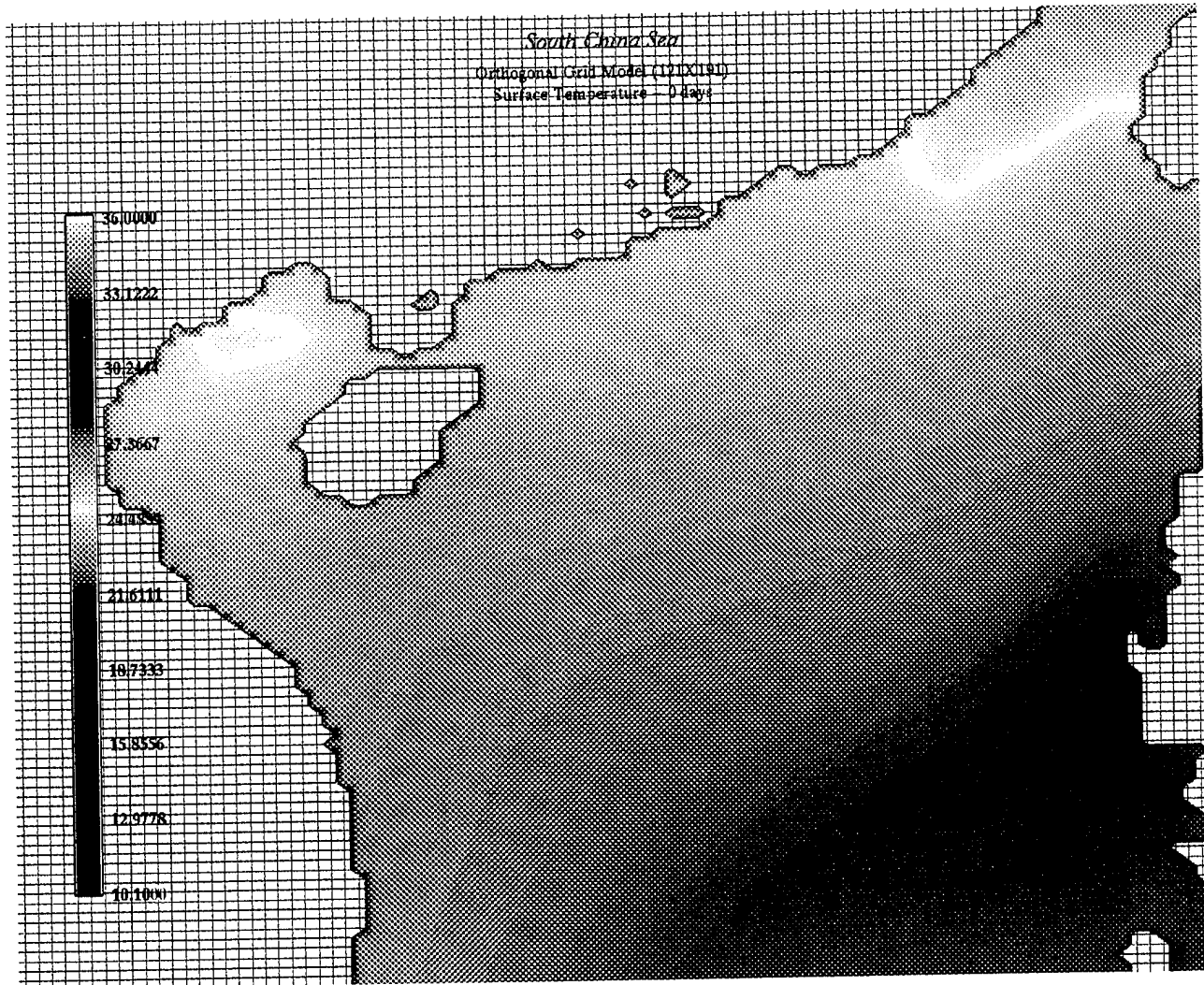


Figure B7: Grid1 - Initial Surface Temperature

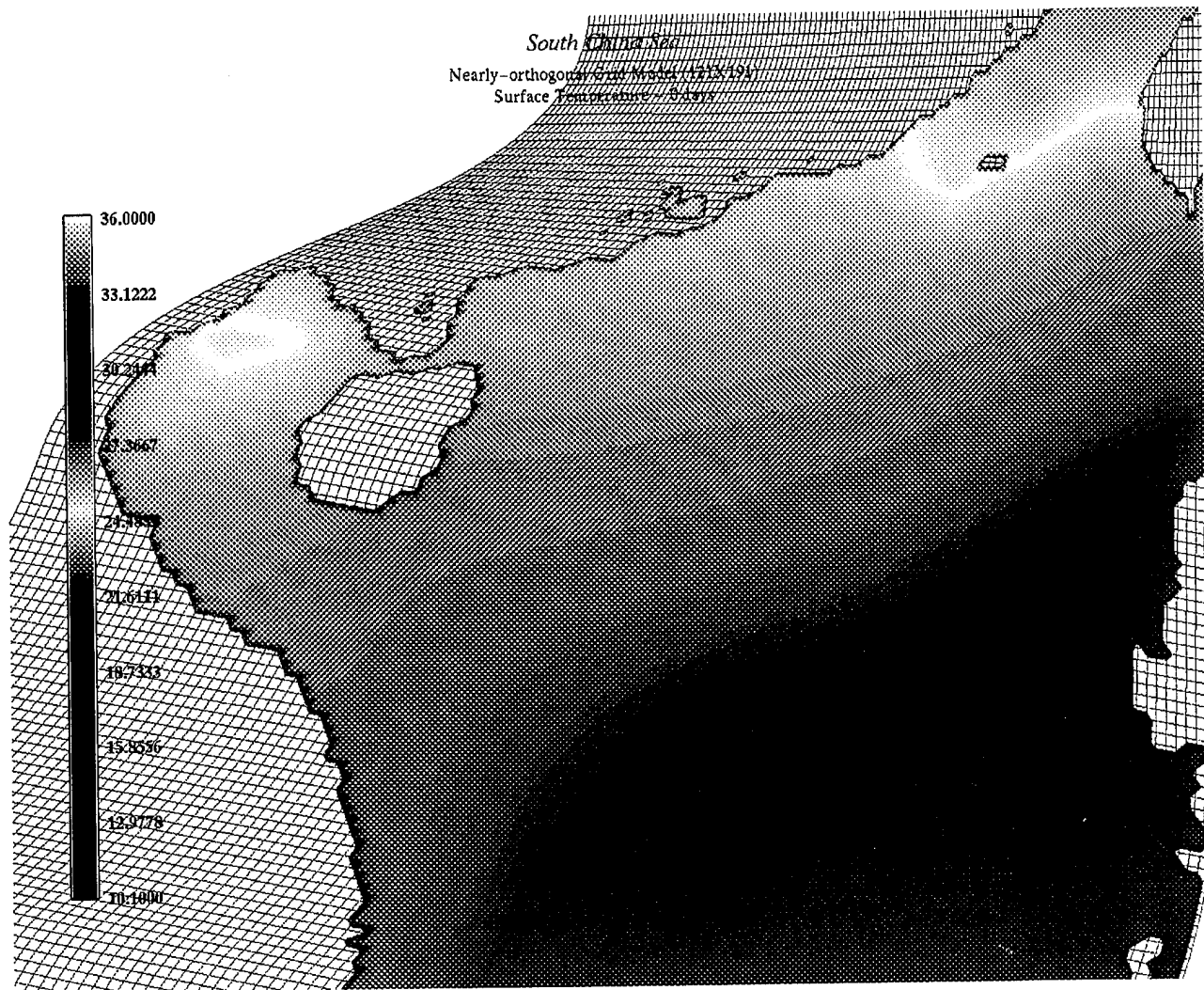


Figure B8: Grid2 - Initial Surface Temperature

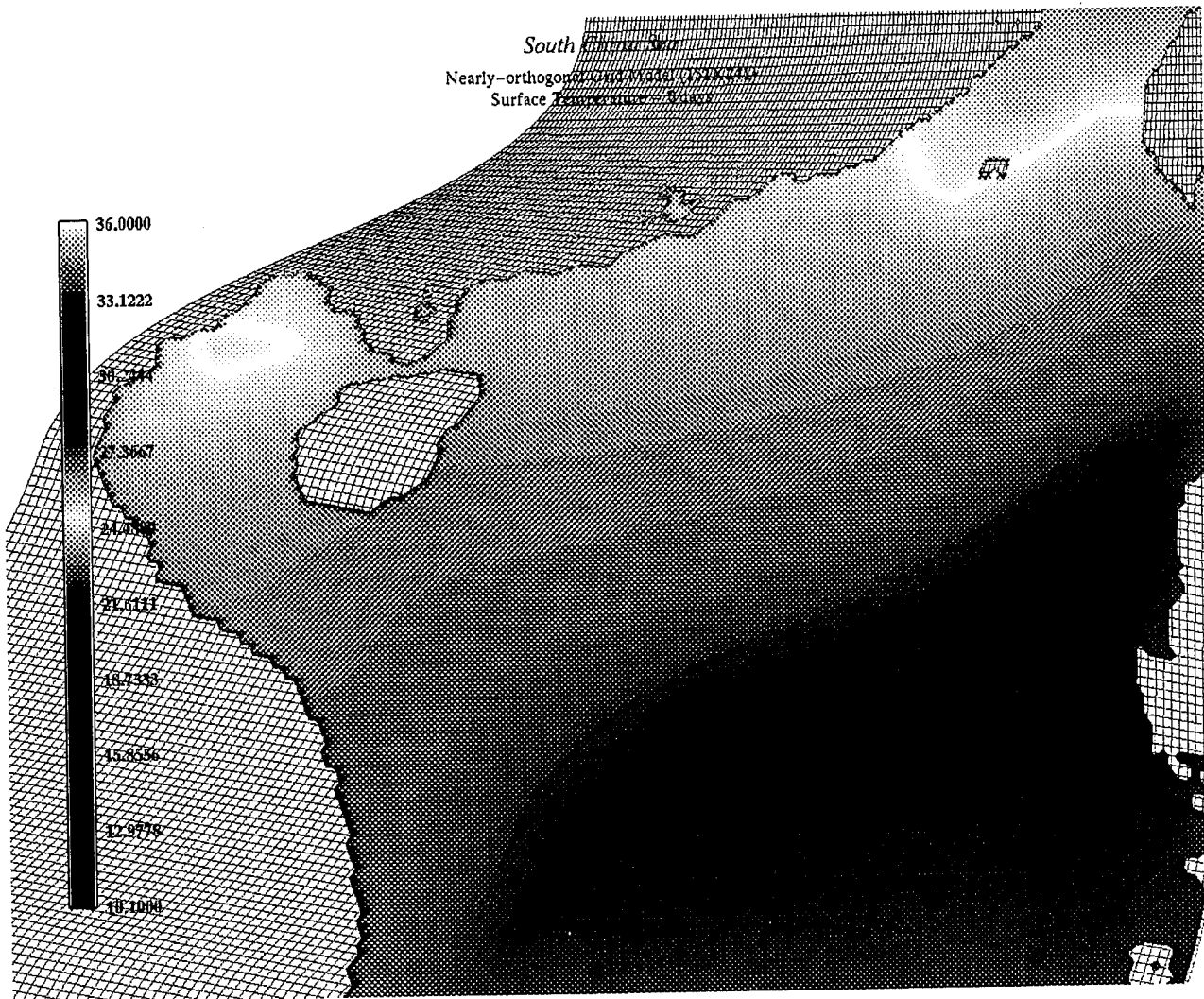


Figure B9: Grid3 - Initial Surface Temperature

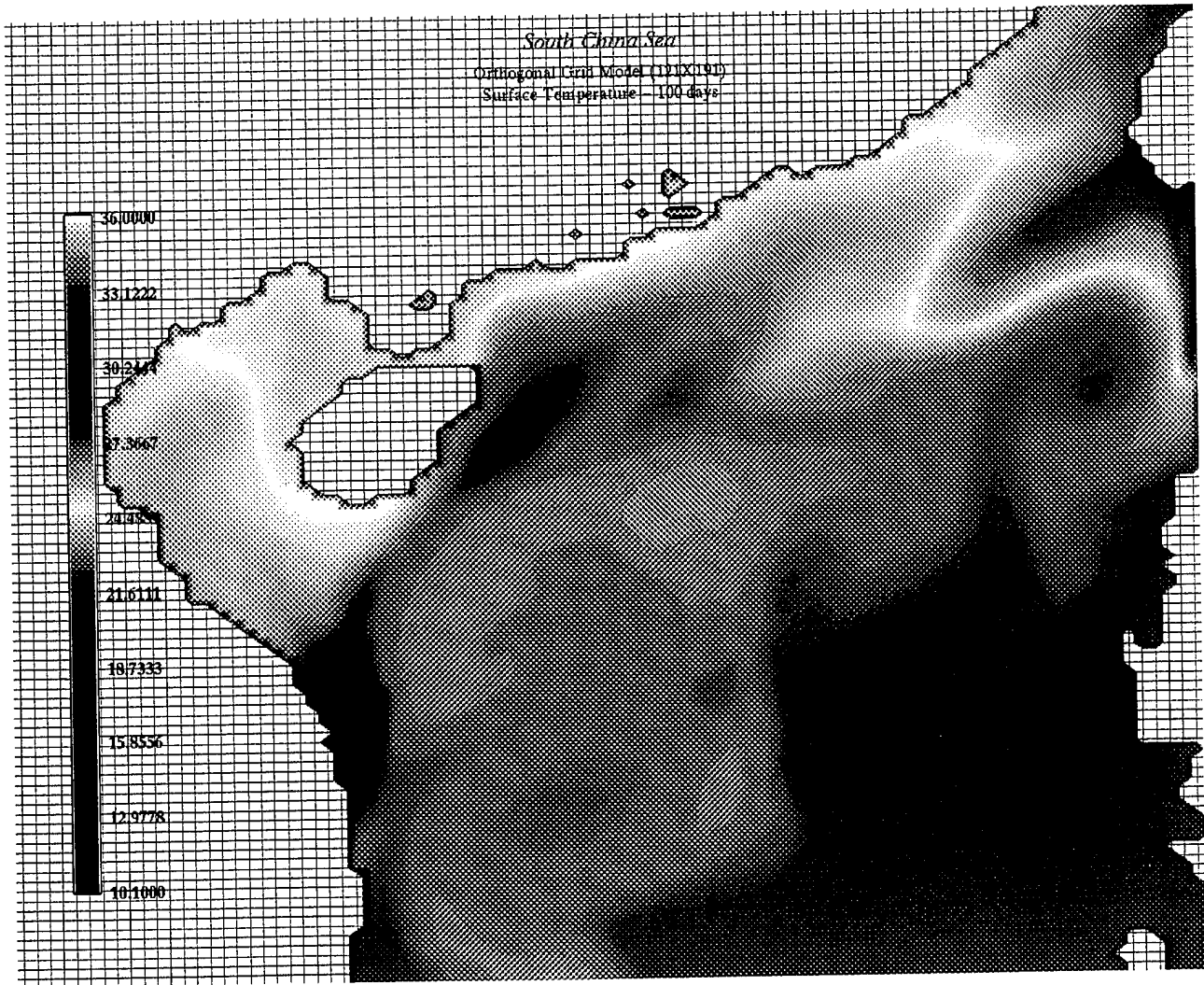


Figure B10: Grid1 - 100 days Surface Temperature

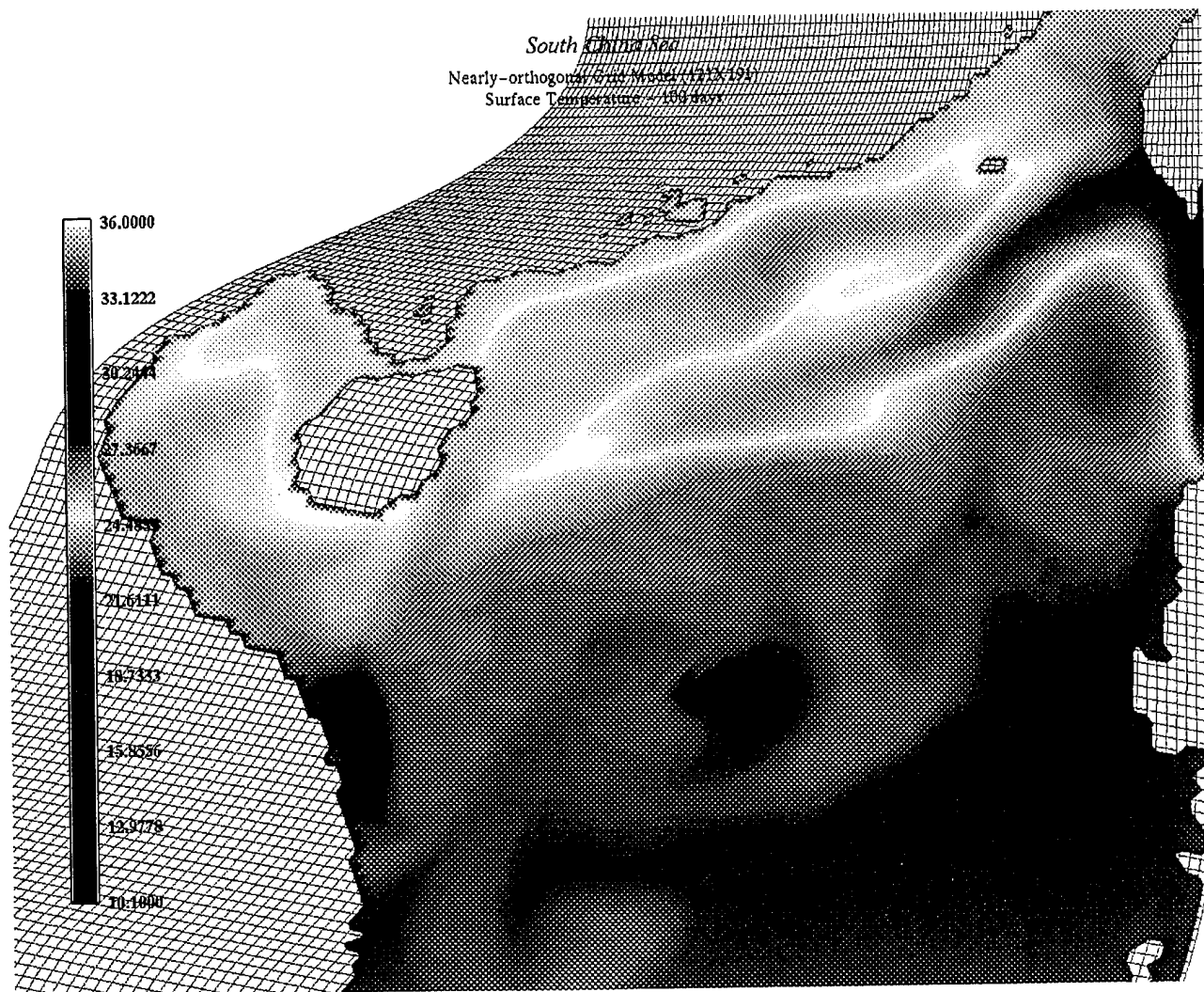


Figure B11: Grid2 - 100 days Surface Temperature

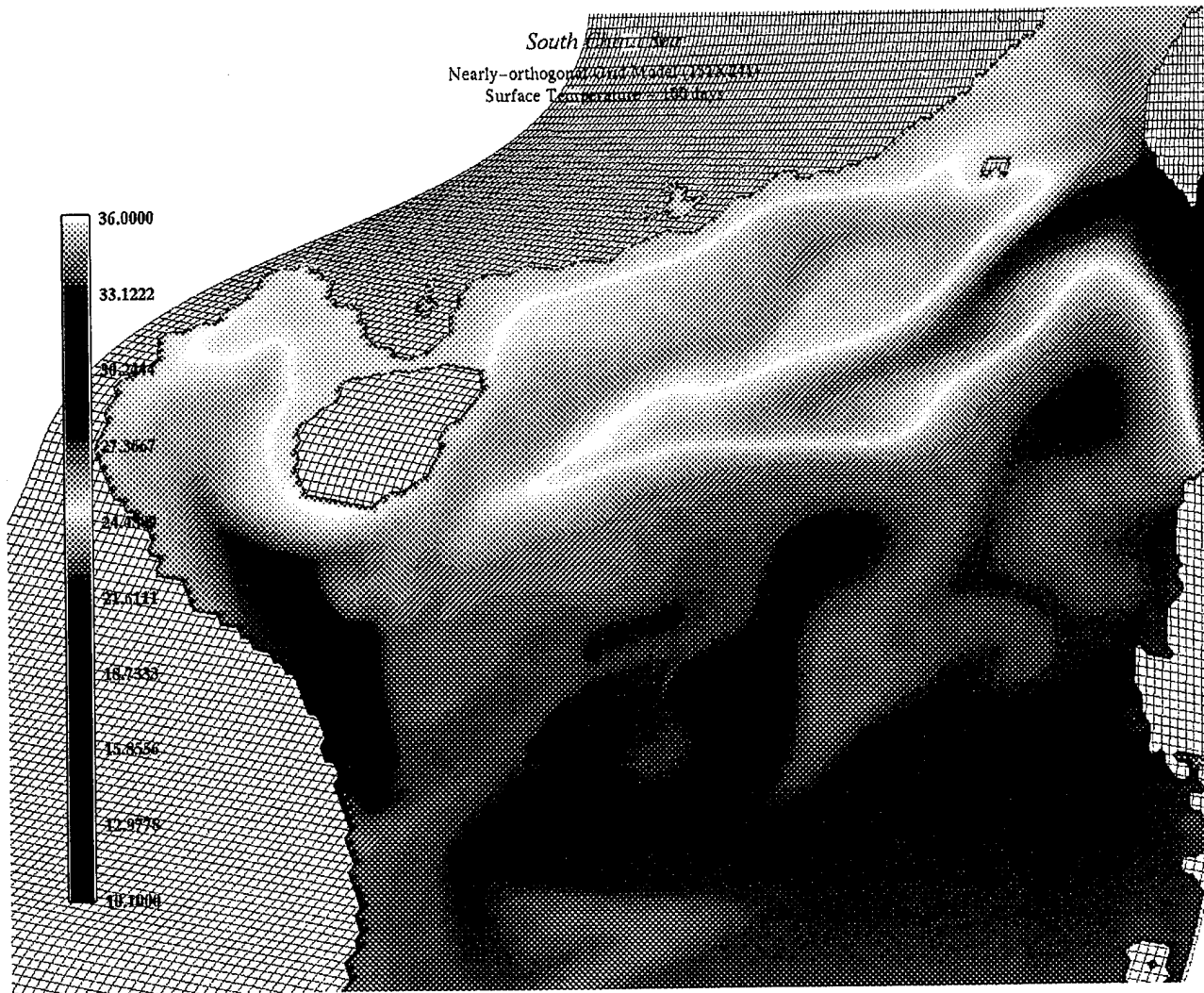


Figure B12: Grid3 - 100 days Surface Temperature

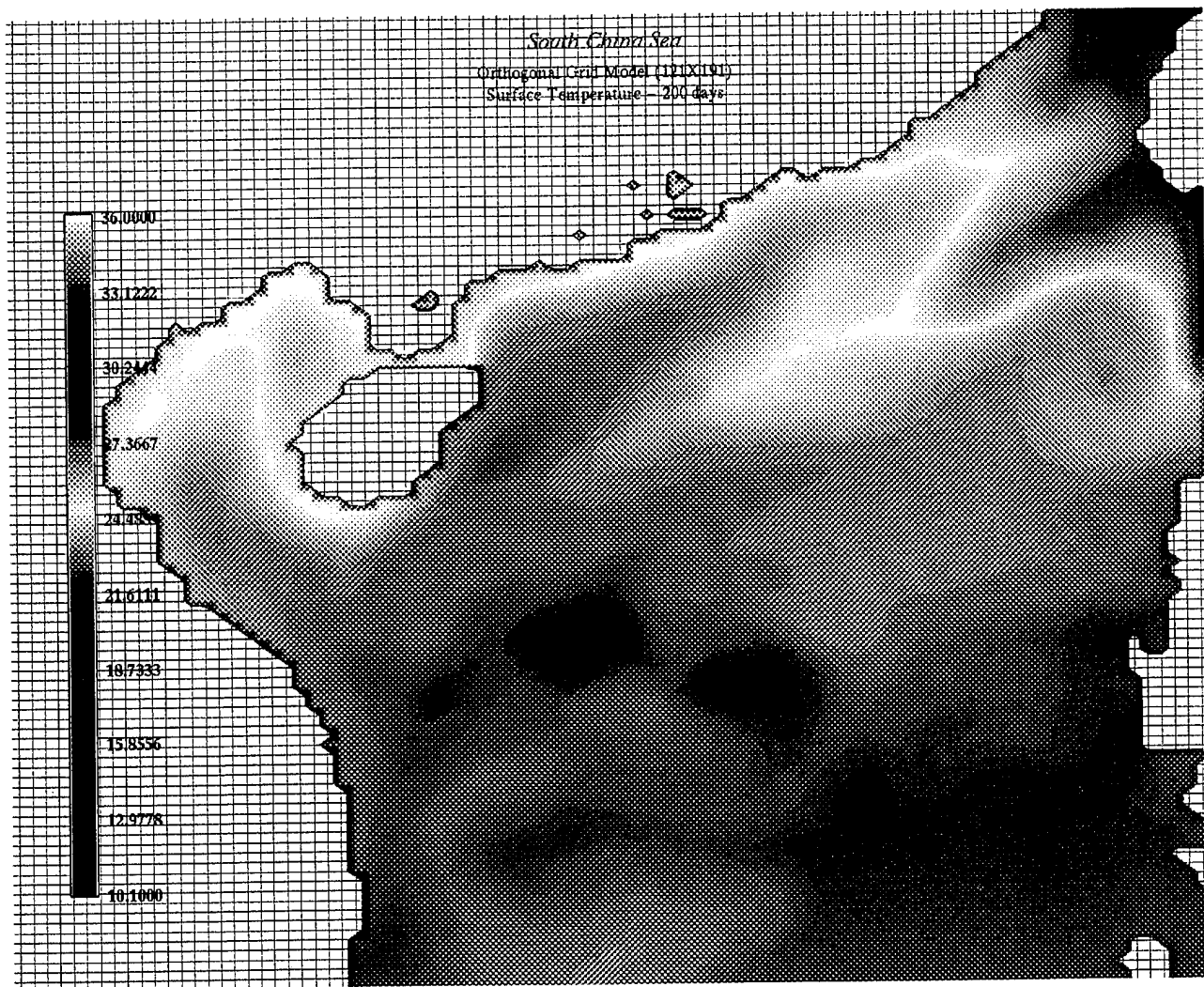


Figure B13: Grid1 - 200 days Surface Temperature

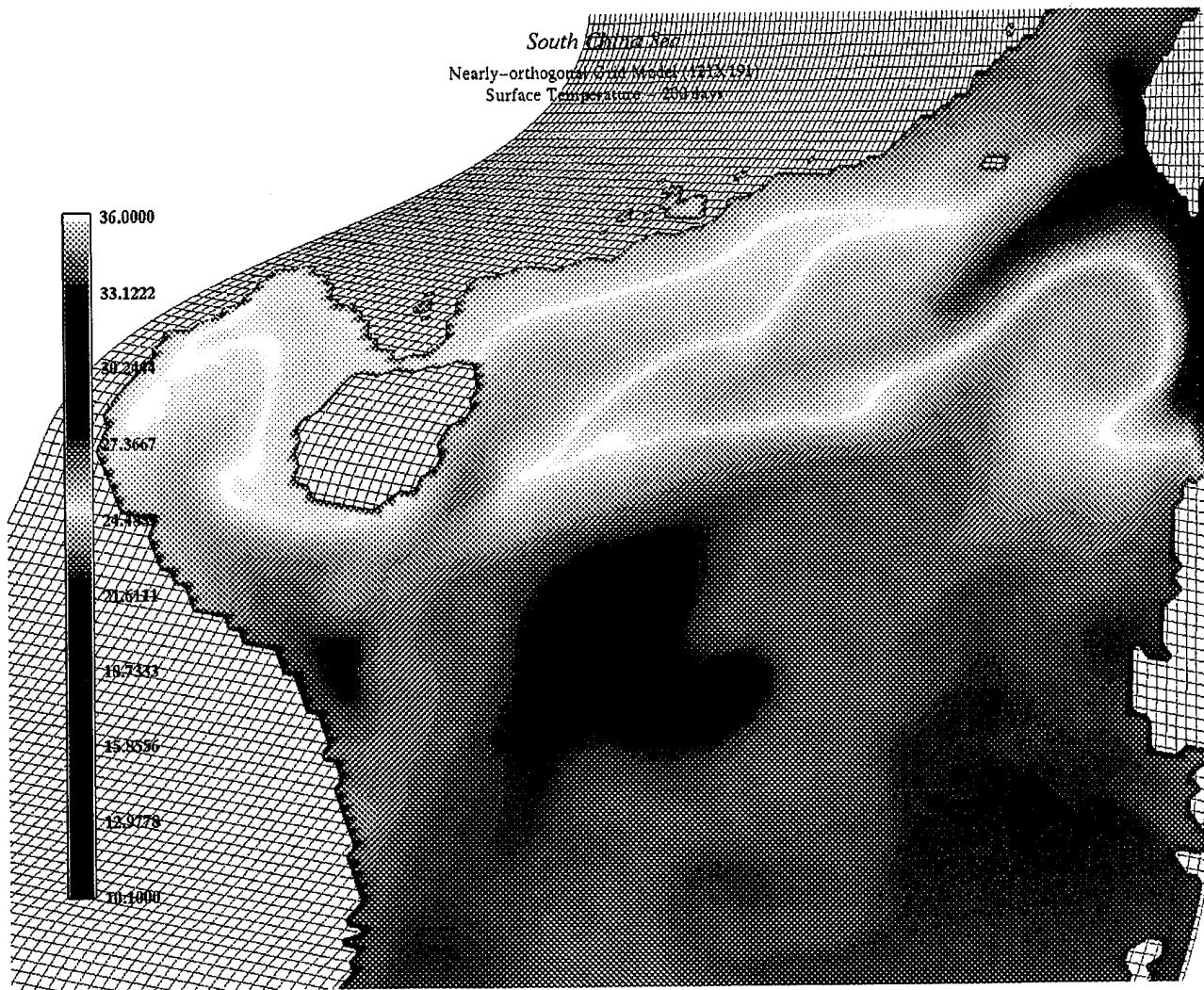


Figure B14: Grid2 - 200 days Surface Temperature

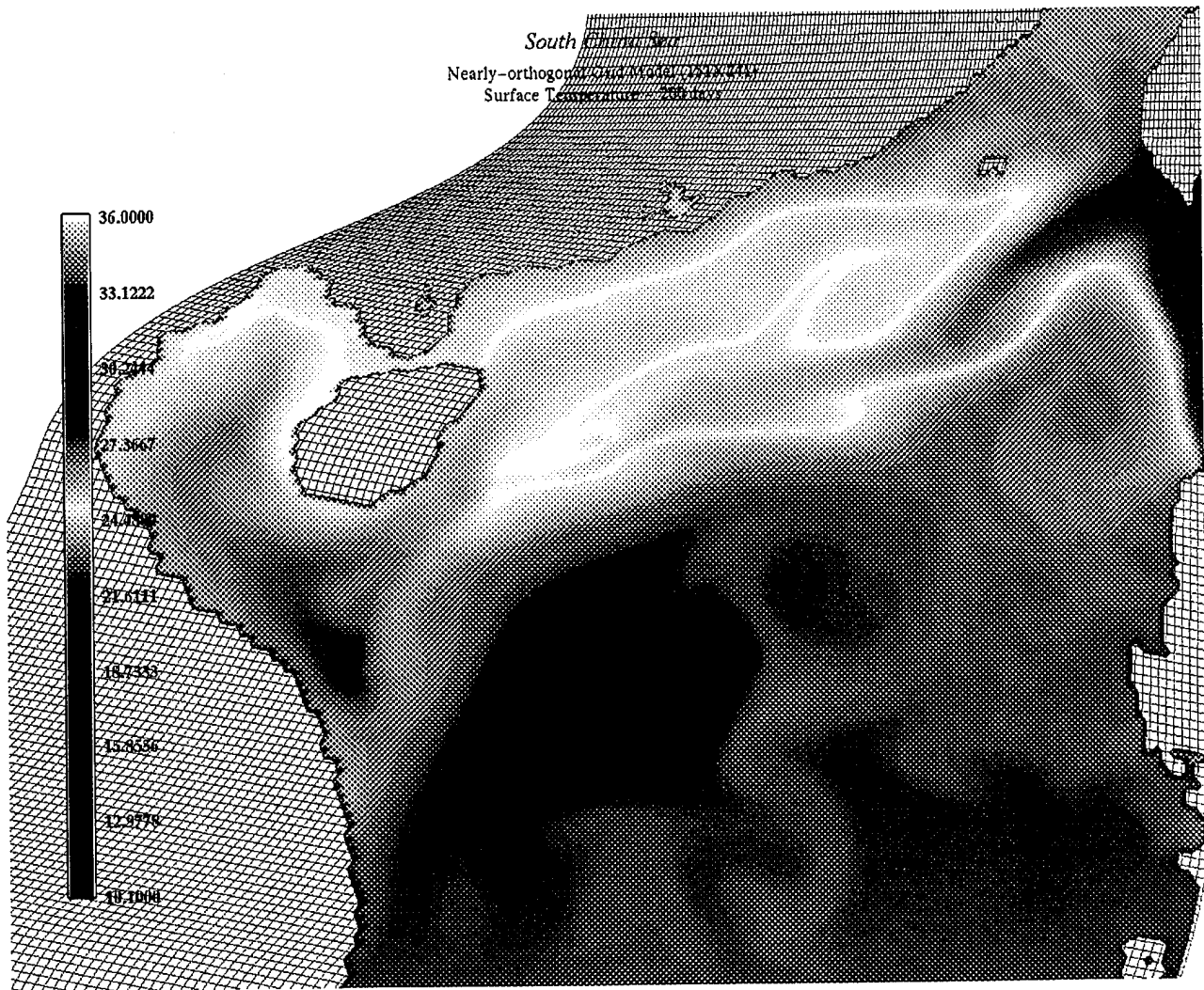


Figure B15: Grid3 - 200 days Surface Temperature

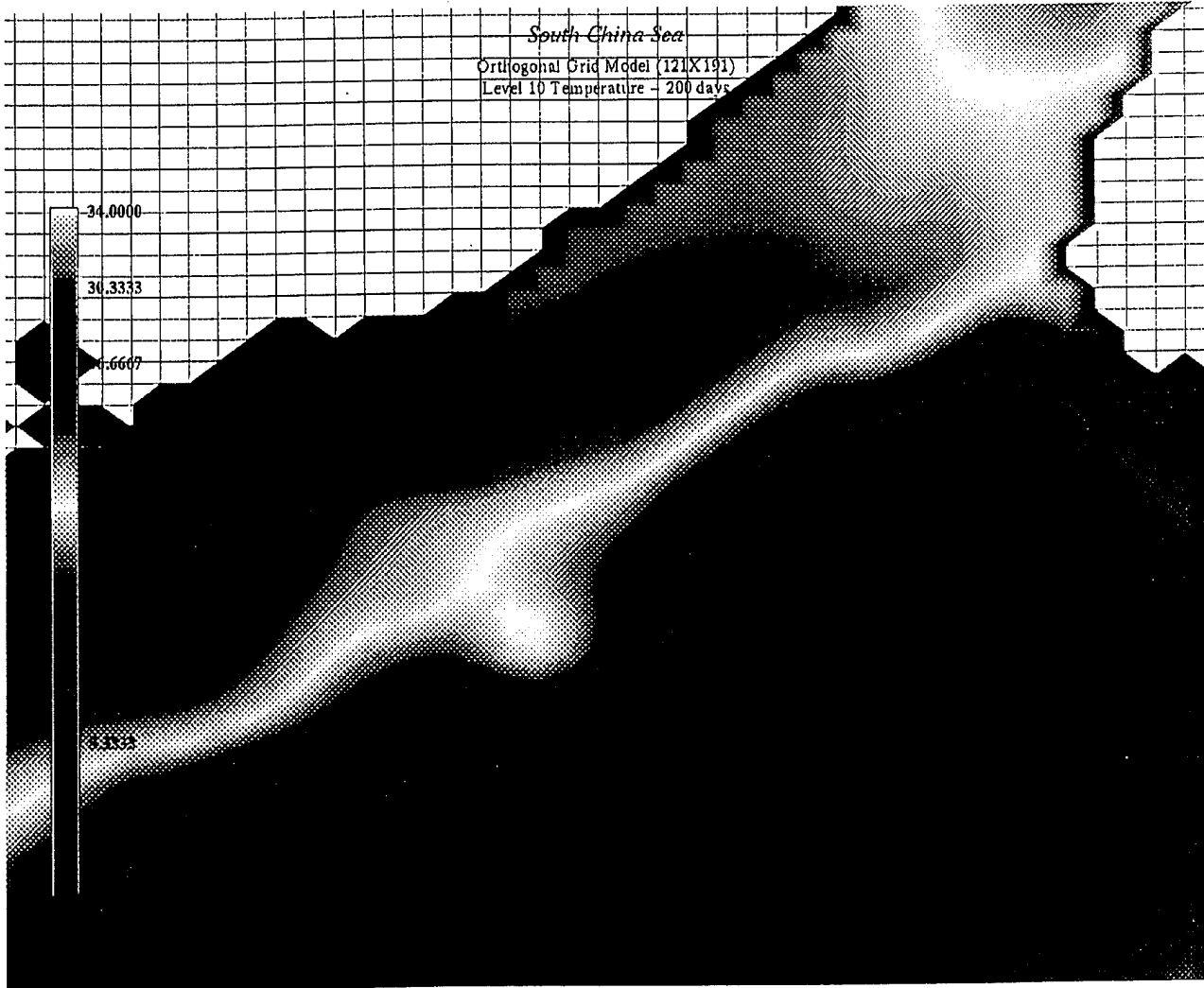


Figure B16: Grid1 - 200 days Level 10 Temperature

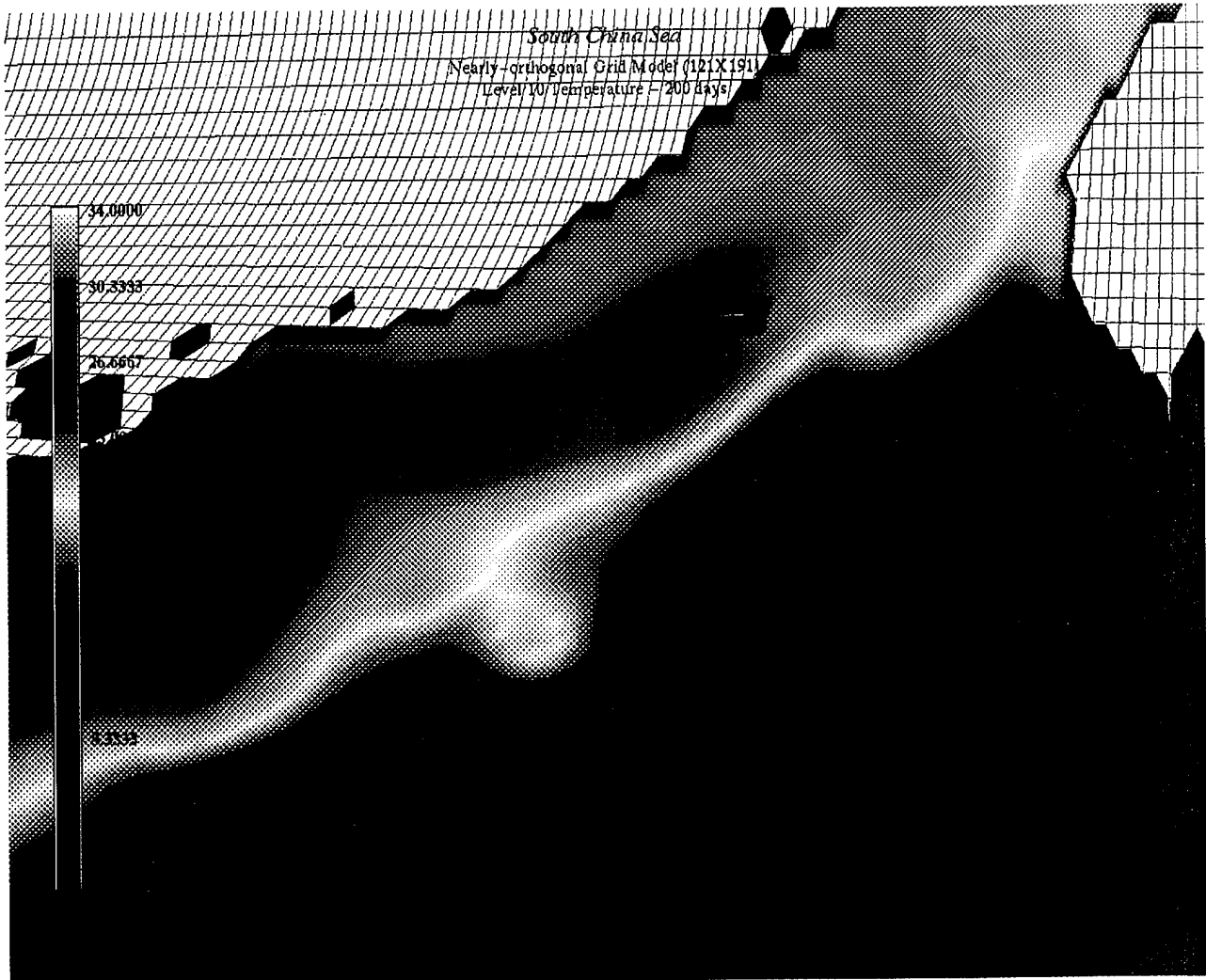


Figure B17: Grid2 - 200 days Level 10 Temperature

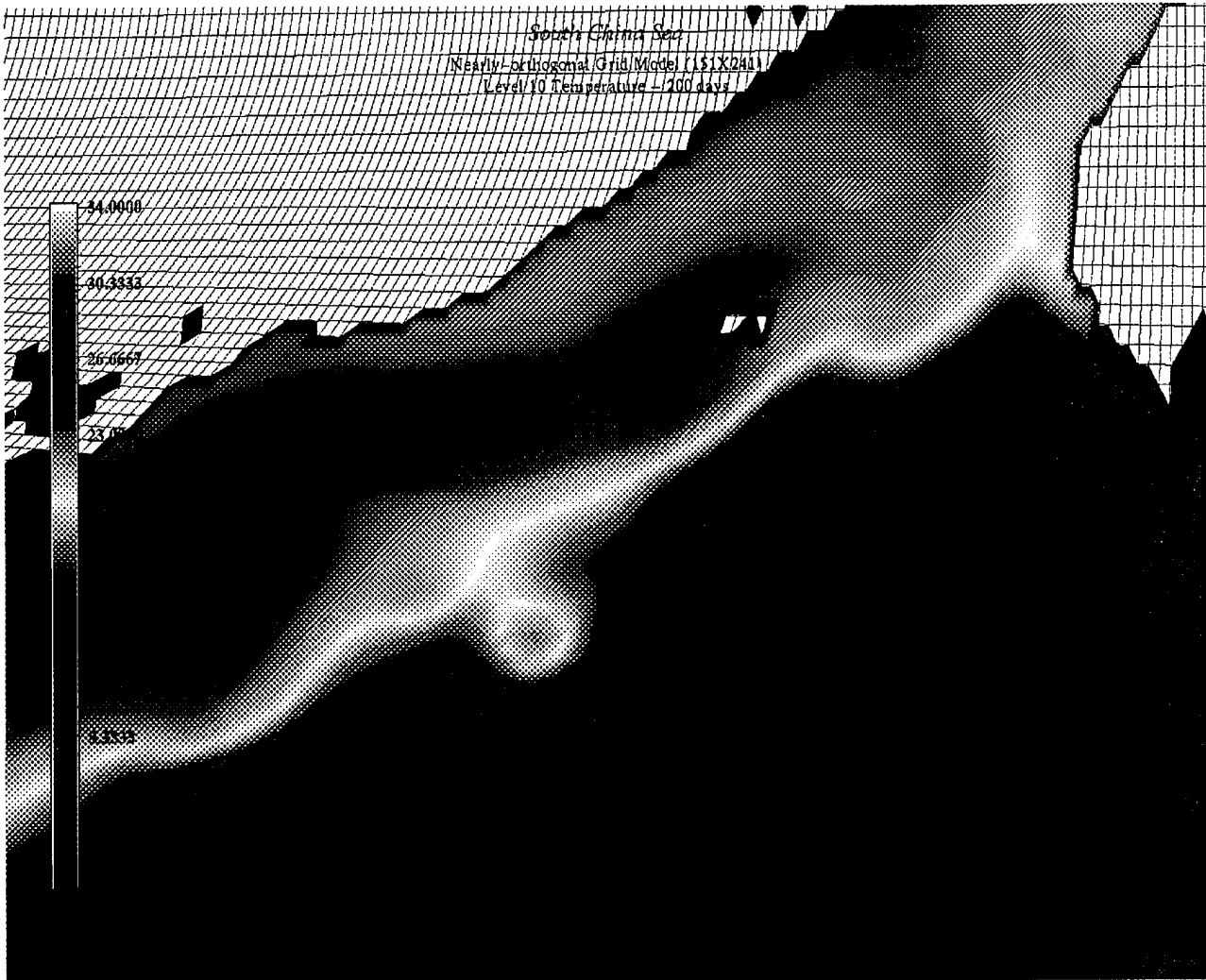


Figure B18: Grid3 - 200 days Level 10 Temperature

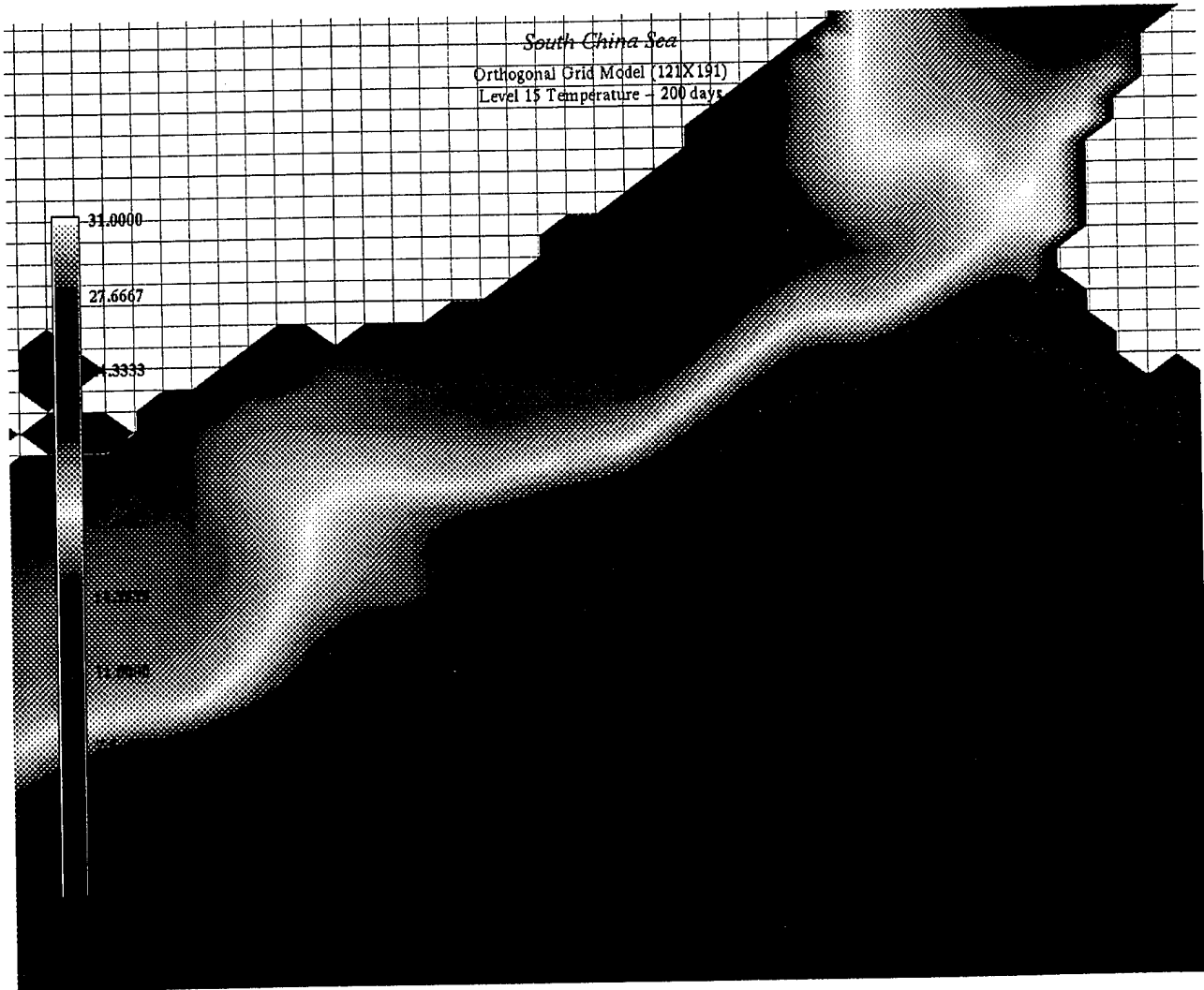


Figure B19: Grid1 - 200 days Level 15 Temperature

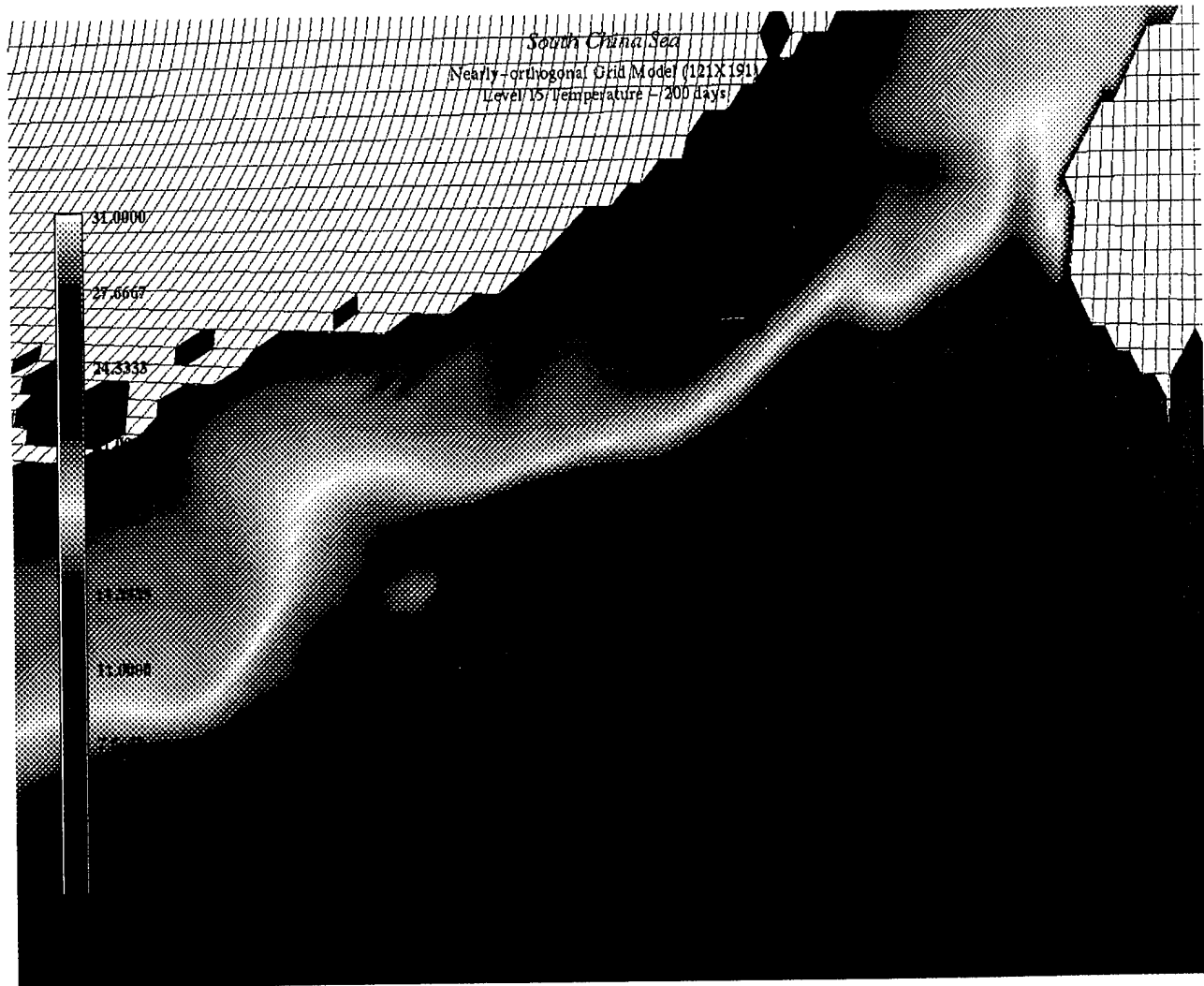


Figure B20: Grid2 - 200 days Level 15 Temperature

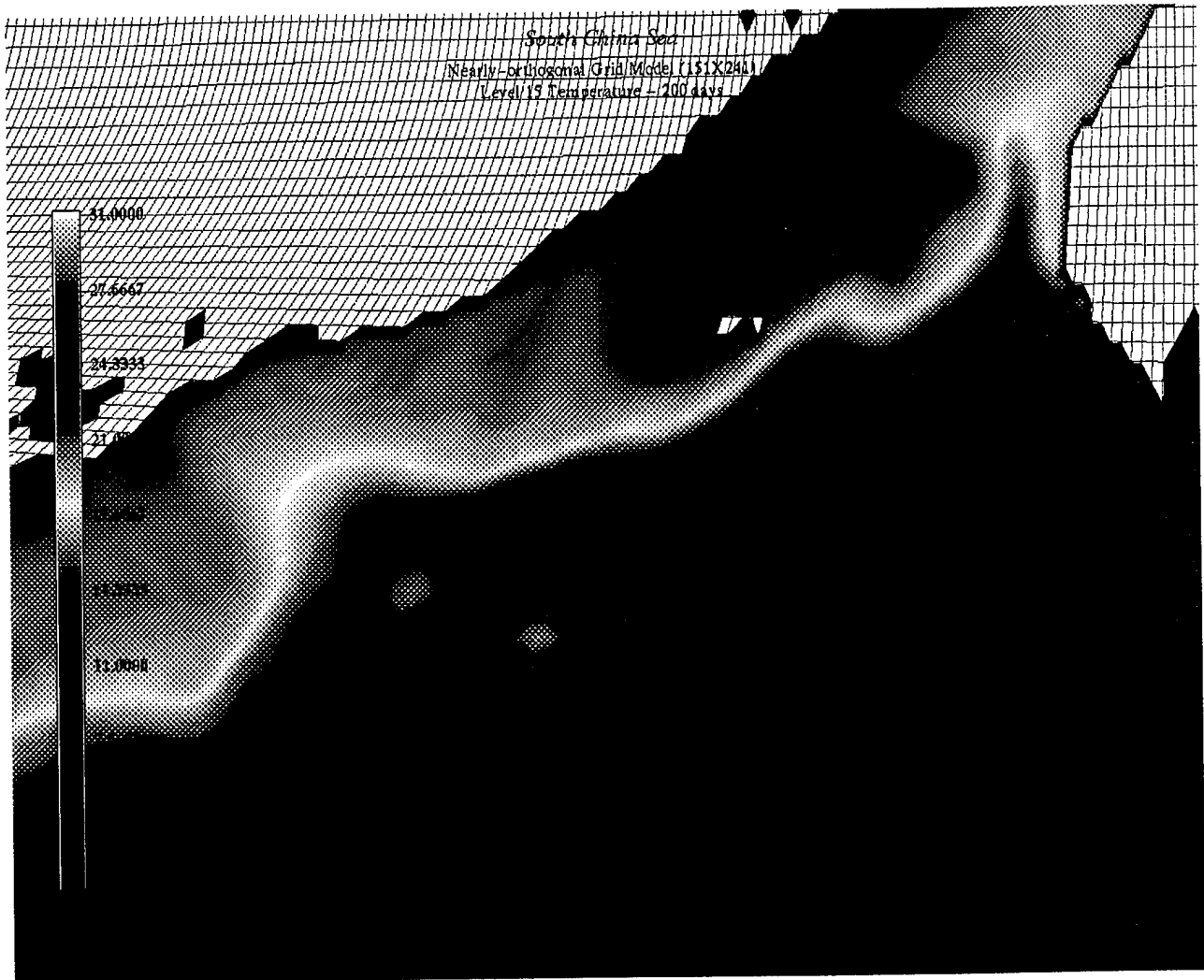


Figure B21: Grid3 - 200 days Level 15 Temperature

INITIAL DISTRIBUTION LIST

1. Defense Technical Information Center.....2
Cameron Station
Alexandria, VA 22304-6145
2. Library, Code 52.....2
Naval Postgraduate School
Monterey, CA 93943-5101
3. Dr. Daniel J. Collins1
Dept. of Aeronautics and Astronautics
AA/Co
Naval Postgraduate School
Monterey, California 93943-5000
4. Dr. Le N. Ly.....2
Dept. of Oceanography
OC/Le
Naval Postgraduate School
Monterey, CA 93943-5000
5. Dr. Max F. Platzer1
Dept. of Aeronautics and Astronautics
AA/PI
Naval Postgraduate School
Monterey, CA 93943-5000
6. Dr. Robert H. Bourke.....1
Dept. of Oceanography
OC/Bf
Naval Postgraduate School
Monterey, California 93943-5000
7. LT Vinh X. Tran1
Department Head Class 142
Surface Warfare Officer School Command
446 Cushing Road
Newport, RI 02841-1209